

2018

Synthesis and reactivity of paramagnetic late transition metal complexes supported by tris(oxazoliny)phenylborate

Regina Reinig
Iowa State University

Follow this and additional works at: <https://lib.dr.iastate.edu/etd>

 Part of the [Inorganic Chemistry Commons](#)

Recommended Citation

Reinig, Regina, "Synthesis and reactivity of paramagnetic late transition metal complexes supported by tris(oxazoliny)phenylborate" (2018). *Graduate Theses and Dissertations*. 16443.
<https://lib.dr.iastate.edu/etd/16443>

This Dissertation is brought to you for free and open access by the Iowa State University Capstones, Theses and Dissertations at Iowa State University Digital Repository. It has been accepted for inclusion in Graduate Theses and Dissertations by an authorized administrator of Iowa State University Digital Repository. For more information, please contact digirep@iastate.edu.

Synthesis and reactivity of paramagnetic late transition metal complexes supported by tris(oxazolinyl)phenylborate

by

Regina Rose Reinig

A dissertation submitted to the graduate faculty
in partial fulfillment of the requirements for the degree of

DOCTOR OF PHILOSOPHY

Major: Inorganic Chemistry

Program of Study Committee:
Aaron D. Sadow, Major Professor
Levi Stanley
Gordon Miller
Javier Vela
Theresa Windus

Iowa State University

Ames, IA

2018

Copyright © Regina Rose Reinig, 2018. All rights reserved.

DEDICATION

To Dr. Chin for inspiring me to pursue research in chemistry.

TABLE OF CONTENTS

	Page
ACKNOWLEDGEMENTS	vi
ABSTRACT	viii
CHAPTER 1 - INTRODUCTION	1
General Introduction	1
Dissertation Organization	4
References	6
CHAPTER 2 - SYNTHESIS AND OXIDATION CATALYSIS OF TRIS(OXAZOLINYL)BORATO COBALT(II) SCORPIONATES	8
Abstract	8
Introduction	9
Results and Discussion	11
Conclusion	29
Experimental Section	30
References	34
Supporting Information	38
CHAPTER 3 - RAPID AND ORDERED CARBONYLATION AND OXYGENATION OF A COBALT(II) METHYL	42
Abstract	42
Introduction	43

Results and Discussion	44
Conclusion	51
Experimental Section	52
References	53
CHAPTER 4 – CARBOXYLATES FROM REVERSIBLE CARBONYLATION FOLLOWED BY OXYGENATION OF A SERIES OF ORGANOCOBALT COMPOUNDS	56
Abstract	56
Introduction	57
Results and Discussion	60
Conclusion	89
Experimental Section	90
References	98
CHAPTER 5: SYNTHESIS, CHARACTERIZATION, AND REACTIVITY OF TRIS(OXAZOLINYL)BORATO IRON AND NICKEL COMPLEXES	102
Abstract	102
Introduction	103
Results and Discussion	105
Conclusion	115
Experimental Section	115
References	119

CHAPTER 6- EFFECTS OF BIRADICAL DEUTERATION ON THE
PERFORMANCE OF DNP: TOWARDS BETTER PERFORMING

POLARIZING AGENTS	121
Abstract	121
Introduction	122
Results and Discussion	124
Conclusion	130
Experimental Section	131
References	140
 CHAPTER 7 – CONCLUSION	 145
General Conclusions	145

ACKNOWLEDGEMENTS

I am grateful to so many inspiring and supportive individuals who guided me throughout my journey in graduate school. Firstly, thank you Dr. Aaron Sadow for being a graduate research adviser who was always excited to discuss research results, encouraged me to become a better chemist by challenging the way I thought, performed, and communicated my research, and always strived to maintain a positive, collaborative research environment. Thank you to each of my committee members, Dr. Levi Stanley, Dr. Javier Vela, Dr. Gordon Miller, Dr. Theresa Windus, and former member Dr. Jason Chen for your guidance, helpful discussions, and willingness to serve on my committee. Thank you to Dr. Sarah Cady for all of your instruction in EPR and patience with me as I learned this new technique....and sharing your wonderful cooking with us! Thank you to Dr. Arkady for always taking the time to collect the best crystal and solving the structures so quickly; hearing you say that you can indeed solve the crystal were some of my best days.

Thank you to all of the past and present Sadow group members all of whom I have learned so much from. Thank you especially Debabrata Mukherjee for serving as an excellent mentor when I first began conducting research in the Sadow lab and thank you Payel for making so many evenings in lab memorable by your delightful conversation. Thank you to Emma Barber, who was a wonderful mentee. And, thank you, Aradhana Das. I always treasured our time together in lab. Your positive energy helped sustain me in graduate school and I cherish all of our times together. A special thanks to Gina Roberts and Taiwo Dairo who I was so fortunate to get to know during my first summer of research, I cherish our lasting friendship!

Thank you to each of the individuals with whom I had the great privilege of collaborating with including Ellie Fought, Frédéric A. Perras, Weiwei Xie and Toshia Albright. The

collaborations with each one of you, which culminated in a manuscript, were highlights of my research experience.

Finally, thank you to my parents, siblings, and family who never questioned my choice of path. Through your actions, you have always taught me to be strong and never give up. And thank you, Travis, for being a loving, supportive, and caring husband. You have been the silver lining to my years in graduate school, and I can't imagine my life without you.

ABSTRACT

Our group previously developed the synthesis of main group Zn(II) and Mg(II) complexes supported by the To^M (tris(4,4-dimethyl-2-oxazoliny)phenylborate) ligand. The reactivity of these main group oxazoliny based complexes in oxygenation, hydrosilylation, and hydroboration reactions provided motivation for studying the reactivity of late first-row transition metals. This thesis focuses on the synthesis, characterization, and reactivity of late transition metal complexes based on iron, nickel and cobalt containing To^M as the ancillary as well as the synthesis and characterization of other paramagnetic molecules.

Salt metathesis reaction of $TiTo^M$ with $CoCl_2 \cdot THF$ (THF = tetrahydrofuran), $FeBr_2$, or $NiCl_2 \cdot DME$ (DME = dimethoxyethane) at room temperature in THF afforded To^MCoCl , To^MFeBr , and To^MNiCl , respectively. To^MCoCl , To^MFeBr , and To^MNiCl react with NaOAc to form the acetate complexes To^MCoOAc , To^MFeOAc , and To^MNiOAc , respectively. To^MCoOAc was studied in the oxidation of cyclohexane using meta-chloroperoxybenzoic acid (*m*CPBA) as the oxidant and found to selectively catalyze the formation of cyclohexanol over the over-oxidized products of cyclohexanone and ϵ -caprolactone.

Reaction of To^MCoCl , To^MFeBr , and To^MNiCl with alkylolithiums or potassium benzyl were attempted as a route to organometallic complexes. The nickel(II) alkyls were not identified under the reaction conditions attempted; however, To^MCoR (R = Me, Et, *n*Bu, CH_2SiMe_3 , Bn, and Ph) and To^MFeR (R = Bn) compounds were found to be isolable.

To^MCoR (R = Me, Et, *n*Bu, CH_2SiMe_3 , Bn, and Ph) complexes react with CO followed by O_2 to form the carboxylate compounds To^MCoO_2CR (R = Me, Et, *n*Bu, CH_2SiMe_3 , Bn, and Ph). The direct insertion of CO_2 into the Co-R bond is determined to be much slower, requiring several days to weeks depending upon the R group. To^MFeBn reacts with CO to form

To^MFe{C(O)Bn}(CO)₂, but sequential addition of O₂ does not provide the corresponding carboxylate compound suggesting the oxidative carbonylation reactivity is unique to cobalt.

Lastly, the expertise gained from the synthesis and characterization of paramagnetic complexes provided guidance for the synthesis and characterization of deuterated biradicals to be used as polarizing agents in dynamic nuclear polarization (DNP).

CHAPTER 1: INTRODUCTION

General Introduction

Late first-row transition metals iron, cobalt, and nickel have the advantage of being relatively economical and environmentally benign. The utility of late first-row transition metals has been demonstrated in commercially and biologically relevant reactions including oxygenation and polymerization reactions.

Iron, cobalt, and nickel complexes supported by the tris(pyrazolyl)borate (Tp) ligand are well established.¹ While TpM (M = Fe, Co or Ni) compounds have been very useful in catalytic transformations, a major general hindrance encountered in scorpionate chemistry is comproportionation reactions that result in, for example, Tp₂Fe.²⁻³ Tris(oxazoliny)phenylborate (To^M) has been reported to provide a more bowl-like steric environment suggesting it may support tetrahedral first-row transition metal complexes.⁴

A possible route to iron, cobalt, and nickel complexes supported by To^M is through salt metathesis reaction of TITo^M with metal halides. The suitability of TITo^M as a To^M transfer agent has been well-documented with examples including transfer of To^M from Tl to Zr, Zn, and Rh.⁵⁻⁷ The corresponding halide complexes, for example To^MCoCl, could be expected to be used as a precursor to more reactive ligands. The general route of salt metathesis may also be applicable to replacement of the chloride ligand, although reactions involving To^MZrCl₃ have demonstrated that this route can be complicated by the hard basic nature of the To^M ligand that often favors transmetalation to Mg or Li.⁵ Replacement of the chloride ligand with acetate is desirable given acetate complexes have been demonstrated as effective catalysts in oxidation reactions and the acetate moiety is commonly encountered in biological systems. An oxidation reaction of

primary interest is the oxidation of hydrocarbons where catalysts based upon metals such as Co(II) and Cu(II) serve as catalysts on an industrial scale.⁸ A major application is the use of cobalt carboxylates as the catalysts for the oxidation of *p*-xylene to terephthalic acid or dimethyl terephthalate which represents the largest industrial use of homogeneous catalysts.⁹ Cyclohexane is another common substrate for such oxidation reactions (Figure 1). Oxidation of cyclohexane typically provides a mixture of cyclohexanol and cyclohexanone which commercially can be used as precursors to caprolam and adipic acid which in turn are used to make nylon 6,6.¹⁰ However, the selective oxidation of cyclohexane is generally complicated by the over-oxidized products that so easily form.

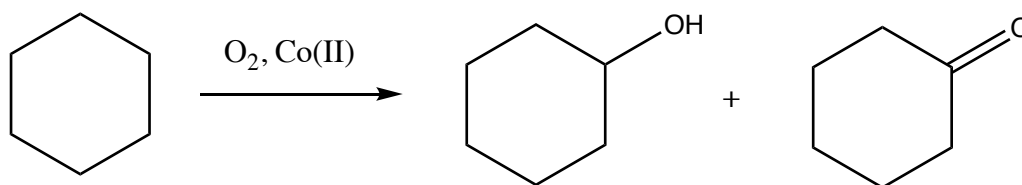


Figure 1. Oxidation of cyclohexane to cyclohexanol and cyclohexanone.

Iron, cobalt, and nickel complexes featuring an acetate coligand have been reported to serve as efficient catalysts for the oxidation of cyclohexane using *m*-CPBA as the terminal oxidant, thus demonstrating potential for further exploration of these late first-row transition metals.¹¹⁻¹⁴

Another reaction of interest related to cobalt is oxidative carbonylation. Traditionally, metals such as palladium, rhodium, and iridium are employed in these types of reactions.^{15,16} The utilization of more abundant late first-row transition metals in these processes is desirable. Precedence for cobalt as a suitable metal for such type of catalytic reactions can be found in nature where acetate formation is an important metabolic pathway in acetogens. The Wood-Ljungdahl pathway (Figure 2)¹⁷ proposes

reduction of CO₂ to CO followed by insertion of the CO into a Co-Me bond to form an acetyl group (Figure 2).¹⁷⁻¹⁹

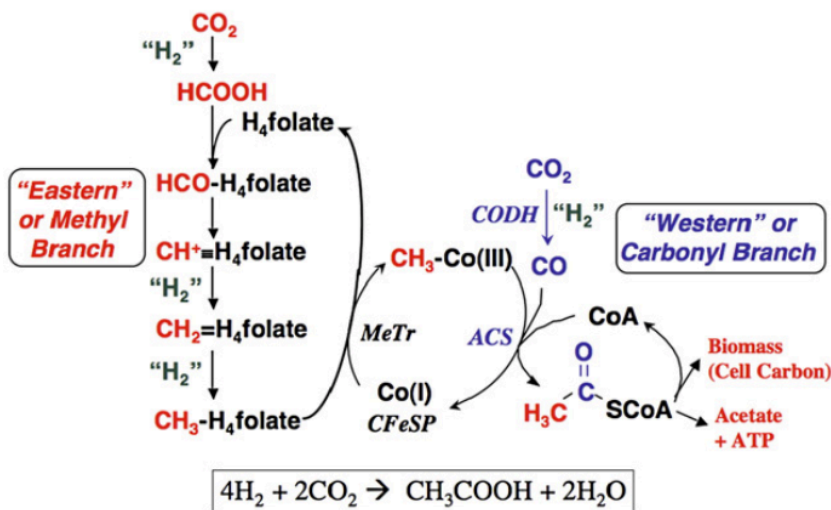


Figure 2. Western and Eastern Branch of the Wood-Ljungdahl Pathway.

Exploring the distinction between oxidative carbonylation, where CO₂ is the source of the carbonyl and O₂ is the oxidant, versus direct insertion of CO₂ to form carboxylates would provide insight into the synthesis of acetate and other carboxylate compounds. The synthesis of cobalt carboxylate compounds from cobalt alkyls could provide insight into rates and mechanisms for such processes.

This thesis contributes to the development of late first-row transition metals by demonstrating the reactivity of To^MCoOAc in the oxidation of cyclohexane and a series of cobalt alkyl compounds (To^MCoR; R = Me, Et, ⁿBu, CH₂SiMe₃, Bn, and Ph) that are reactive in oxidative carbonylation. In addition, the reactivity of To^MFeBn towards CO, O₂, and CO₂ is reported as well as the synthesis and characterization of To^MNiCl and To^MNiOAc. Finally, in theme with the paramagnetic nature of these complexes, a series of deuterated biradical polarizing agents were synthesized and demonstrated to be effective for obtaining improved dynamic nuclear polarization (DNP) enhancements.

Dissertation Organization

This thesis contains seven chapters. Chapter 1 provides a general introduction to the synthesis and study of late first-row transition metal complexes. Chapters 2, 3, and 6 are published journal papers that have been modified to provide coherency while chapters 4 and 5 consists of work that is not yet published, and thus are manuscripts in preparation for publication.

Chapter 2 describes the synthesis of tris(4,4-dimethyl-2-oxazoliny)phenylborato cobalt(II) chloride (To^MCoCl), which serves as a precursor to $To^MCoOtBu$ and To^MCoOAc . To^MCoOAc is demonstrated to selectively catalyze the oxidation of cyclohexane to cyclohexanol using *meta*-chloroperoxybenzoic acid (*mCPBA*) as the oxidant. Debabrata Mukherjee was the first member of our group to synthesize and obtain an X-ray quality crystal of To^MCoCl . Zachary B. Weinstein was responsible for the operation of the Chemspeed Technologies SWING-XL automated platform used for the oxidation catalysis as well as analysis of the oxidation catalysis results. Weiwei Xie was responsible for the X-ray powder diffraction analysis studies, Toshia Albright performed the EPR simulations, Sergey L. Bud'ko performed the magnetic susceptibility measurements, and previous experiments conducted by Benjamin Baird and Tristan S. Gray helped guide the synthesis reported in this chapter.

Chapter 3 presents the synthesis of To^MCoMe and detailed studies of the reactivity of To^MCoMe toward CO, O₂, and CO₂. The sequential addition of CO followed by O₂ to To^MCoMe affords To^MCoOAc . This oxidative carbonylation reactivity is explored in depth. Reaction of To^MCoMe with CO₂ also provides To^MCoOAc , but this reaction proceeds much more slowly than the two-step oxidative carbonylation pathway.

Ellie L. Fought carried out DFT, TDDFT, and DFT Hessian calculations of To^MCoMe , $To^MCoMe(CO)$, $To^MCo\{C(O)Me\}CO$, and To^MCoOAc .

Chapter 4 describes the synthesis of To^MCoR ($R = Me, Et, ^iBu, CH_2SiMe_3, Bn,$ and Ph) complexes to investigate the effect of the R group on the oxidative carbonylation reactivity observed for To^MCoMe . The results suggest that both alkyl and aryl groups provide similar reactivity, and that oxidative carbonylation is kinetically favored over direct CO_2 insertion into the Co-C bond. Ellie L. Fought conducted the DFT, TDDFT, and DFT Hessian calculations included in this chapter.

Chapter 5 reports the synthesis of To^MFeBr and To^MNiCl compounds. To^MFeBr and To^MNiCl readily react with NaOAc to form To^MFeOAc , and To^MNiOAc . To^MFeBr also serves as a precursor to the organometallic complex To^MFeBn . The reactivity of To^MFeBn is studied towards CO , O_2 , and CO_2 and compared with the reactivity observed for To^MCoBn .

Chapter 6 describes the synthesis and characterization of deuterated biradicals to be used as polarizing agents in dynamic nuclear polarization (DNP). This work was conducted in close collaboration with Frédéric A. Perras who was responsible for measuring the DNP enhancements for each of the biradicals studied.

Chapter 7 presents general conclusions. Dr. Arkady Ellern is credited for all of the X-ray data and solving of X-ray structures presented in this thesis.

References

- (1) E. Becker, S. Pavlik, and K. Kirchner, in *Advances in Organometallic Chemistry*, ed. Pedro J. Pérez, **2008**, pp. 155-321. I. R. Crossley, in *Advances in Organometallic Chemistry*, ed. Anthony Hill and Mark J. Fink, **2010**, pp. 109-208.
- (2) S. Trofimenko, *Chem. Rev.*, **1993**, *93*, 943-980.
- (3) S. Trofimenko, *Scorpionates: The Coordination Chemistry of Polypyrazolylborate Ligands*, Imperial College Press, London, 1999.
- (4) K. Wu, D. Mukherjee, A. Ellern, A. D. Sadow, W. E. Geiger, *New J. Chem.*, **2011**, *35*, 2169-2178.
- (5) J. F. Dunne, J. Su, A. Ellern, and A. D. Sadow, *Organometallics*, **2008**, *27*, 2399-2401.
- (6) D. Mukherjee, A. Ellern, and A. D. Sadow, *J. Am. Chem. Soc.*, **2010**, *132*, 7582-7583.
- (7) H.-A. Ho, T. S. Gray, B. Baird, A. Ellern, and A. D. Sadow, *Dalton Trans.*, **2011**, *40*, 6500-6514.
- (8) F. A. Chavez, J. M. Rowland, M. M. Olmstead, and P. K. Marscharak, *J. Am. Chem. Soc.*, **1998**, *120*, 9015-9027.
- (9) J. K. Beattie, J. A. Klepetko, A. F. Masters, and P. Turner, *Polyhedron*, **2003**, *22*, 947-965.
- (10) R. Pohorecki, W. Moniuk, and P. T. Wierzchowski, *Chemical Engineering Research and Design*, **2009**, *87*, 349-356.
- (11) T. Nagataki, Y. Tachi, and S. Itoh, *Chem. Commun.*, **2006**, 4016-4018.

- (12) S. Hikichi, K. Hanaue, T. Fujimura, H. Okuda, J. Nakazawa, Y. Ohzu, C. Kobayashi, and M. Akita, *Dalton Trans.*, **2013**, *43*, 3346-3356.
- (13) W. Nam, I. Kim, Y. Kim, and C. Kim, *Chem. Comm.*, **2001**, 1262-1263.
- (14) T. Nagataki, K. Ishii, Y. Tachi, and S. Itoh, *Dalton Trans.*, **2007**, 1120-1128.
- (15) Q. Liu, H. Zhang, and A. Lei, *Angew. Chem. Int. Ed.*, **2011**, *50*, 10788-10799.
- (16) D. J. Díaz, A. K. Darko, and L. McElwee-White, *Eur. J. Org. Chem.*, **2007**, 4453-4465.
- (17) S. W. Ragsdale, *Biofactors*, **1997**, *6*, 3-11.
- (18) S. W. Ragsdale, E. Pierce, *Biochimica et Biophysica Acta*, **2008**, *1784*, 1873-1898.
- (19) S. W. Ragsdale, *Ann. N. Y. Acad. Sci.*, **2008**, *1125*, 129-136.

**CHAPTER 2: SYNTHESIS AND OXIDATION CATALYSIS OF
TRI(OXAZOLINYL)BORATO COBALT(II) SCORPIONATES**

Modified from *European Journal of Inorganic Chemistry* **2016**, 2486-2494. Copyright ©
2016 Wiley-VCH Verlag GmbH & Co. KGaA.

Regina R. Reinig, Debabrata Mukherjee, Zachary B. Weinstein, Weiwei Xie, Toshia
Albright, Benjamin Baird, Tristan S. Gray, Arkady Ellern, Gordon J. Miller, Arthur H.
Winter, Sergey L. Bud'ko, and Aaron D. Sadow*

Abstract

The reaction of $\text{CoCl}_2 \cdot \text{THF}$ and thallium tris(4,4-dimethyl-2-oxazolinyl)phenylborate (TlTo^{M}) in tetrahydrofuran (THF) provides $\text{To}^{\text{M}}\text{CoCl}$ (**1**) in 95 % yield; however, appropriate solvents and starting materials are required to favor **1** over two other readily formed side-products, $(\text{To}^{\text{M}})_2\text{Co}$ (**2**) and $\{\text{HTo}^{\text{M}}\}\text{CoCl}_2$ (**3**). ESR, NMR, FTIR, and UV/Vis spectroscopy were used to distinguish these cobalt(II) products and probe their electronic and structural properties. Even after the structures indicated by these methods were confirmed by X-ray crystallography, the spectroscopic identification of trace contaminants in the material was challenging. The recognition of possible contaminants in the synthesis of $\text{To}^{\text{M}}\text{CoCl}$ in combination with the paramagnetic nature of these complexes provided impetus for the utilization of X-ray powder diffraction to measure the purity of the $\text{To}^{\text{M}}\text{CoCl}$ bulk powder. The X-ray powder diffraction results provide support for the bulk-phase purity of $\text{To}^{\text{M}}\text{CoCl}$ in preparations that avoid **2** and **3**. Thus, **1** is a precursor for new tris(oxazolinyl)borato cobalt chemistry, as exemplified by

its reactions with $\text{KO}t\text{Bu}$ and NaOAc to give $\text{To}^{\text{M}}\text{CoO}t\text{Bu}$ (**4**) and $\text{To}^{\text{M}}\text{CoOAc}$ (**5**), respectively. Compound **5** is a catalyst for the oxidation of cyclohexane with *meta*-chloroperoxybenzoic acid (*m*CPBA), and the rate constants and selectivity for cyclohexanol versus cyclohexanone and ϵ -caprolactone were assessed.

Introduction

Tridentate *fac*-coordinating monoanionic scorpionate-type ligands¹ support and stabilize first-row metal centers bonded to reactive moieties including hydrides,² alkyl groups containing β -hydrogen atoms,³ imido and oxido ligands,⁴ azides,⁵ and oxidizing moieties such as peroxides.⁶ In addition, 3d metal compounds coordinated by scorpionate ligands have served as models for metal sites in enzymes and provided motivation to study their spectroscopic and structural features in detail.⁷ Typically, sterically encumbered scorpionates are required to support reactive species such as peroxides and superoxides.

Variation of the steric and electronic properties of the ancillary scorpionate donors can greatly influence the stability of reactive moieties and the reactivity of the complexes. For example, the steric encumbrance of tris(3-*tert*-butyl-5-methylpyrazolyl)borate ($\text{Tp}^{\text{tBu,Me}}$), known as the tetrahedral enforcer, stabilizes reactive groups such as alkyl peroxides.⁸ However, it also may limit the well-known catalytic oxidation chemistry of scorpionate peroxide complexes of first-row transition metals.^{6,9} The smaller parent tris(pyrazolyl)borate (Tp) or tris(3,5-dimethyl-pyrazolyl)borate (Tp*) ligands, which might provide more accessible metal centers, instead form octahedral $\{\kappa^3\text{-Tp}\}_2\text{M}$ compounds.¹⁰ Even the bulkier tris(3-phenyl-5-methyl-pyrazolyl)borate

(Tp^{tBu,Me}) ligand forms octahedral (Tp^{tBu,Me})₂Co upon isomerization of a pyrazole ring.¹¹ Thus, the steric properties of non-pyrazolyl-based scorpionate ligands, such as those involving nonplanar oxazoline donors, may sufficiently stabilize reactive moieties and also allow new metal-centered reactivity that involves switching between four- and five-coordinate species in a way not accessible with Tp^{tBu}-based compounds.

Recently, we discovered that tris(4,4-dimethyl-2-oxazoliny)phenylborate (To^M) supports reactive main-group complexes of mononuclear and tetrahedral zinc(II) and magnesium(II). For example, a catalytically active mononuclear zinc hydride was readily synthesized by the reaction of To^MZnOtBu and PhSiH₃.¹² The To^MZnX system also supports and stabilizes alkylperoxides, such that To^MZnOOEt is thermally persistent even at temperatures above 100 °C.¹³ Moreover, To^MZnEt is sufficiently reactive to undergo selective oxidation upon treatment with O₂. To^M gives a more open geometry and bowl-like steric profile, in contrast to the tetrahedral enforcer Tp^{tBu,Me} that typically stabilizes reactive moieties.

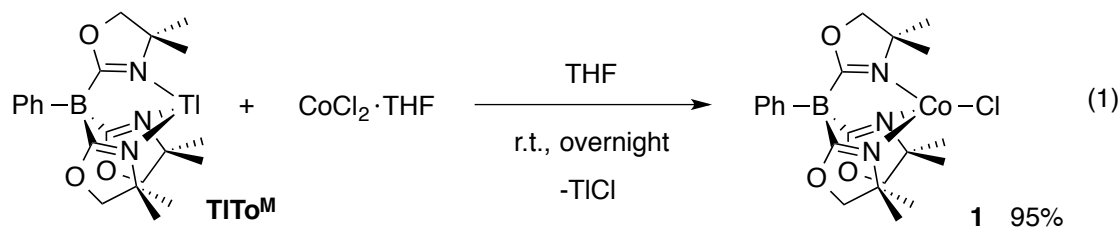
These examples provide motivation for studying the synthesis and reactivity of tetrahedral first-row transition-metal centers supported by To^M, in which redox-active metal centers could lead to new chemistry and catalysis. In particular, the electron-donating properties and bowl-like steric environment¹⁴ provided by the coordination pocket of To^M could stabilize reactive groups bonded to metal centers with accessible d electrons to facilitate catalytic chemistry. Moreover, a series of optically active tris(4-R-2-oxazoliny)phenylborate ligands are also available for imposing chiral environments on tetrahedrally coordinated first-row transition metal sites.¹⁵

The present study describes the synthesis and characterization of $\text{To}^{\text{M}}\text{CoCl}$ (**1**) as a precursor to reactive complexes. We also provide syntheses and characterization data of $(\text{To}^{\text{M}})_2\text{Co}$ (**2**) and $\{\text{HTo}^{\text{M}}\}\text{CoCl}_2$ (**3**), which are side-products discovered during exploratory syntheses toward **1**. The open steric profile of the To^{M} ligand results in additional synthetic challenges compared with syntheses of sterically encumbered tris(pyrazolyl)borate based first-row metal compounds, in terms of controlling the formation of **1**, **2**, and **3**. The chlorido ligand in **1** may be substituted through salt-metathesis reactions to give $\text{To}^{\text{M}}\text{CoOtBu}$ (**4**) and $\text{To}^{\text{M}}\text{CoOAc}$ (**5**) without To^{M} transmetalation or ligand redistribution demonstrating that **1** is a viable synthetic precursor for new cobalt(II) compounds. Complex **5** was studied as a catalyst for the oxidation of cyclohexane. Although the selective oxidation of cyclohexane remains a challenge, cobalt complexes have shown great promise in this area.^{9d}

Results and Discussion

The reaction of TlTo^{M} and $\text{CoCl}_2 \cdot \text{THF}$ (THF = tetrahydrofuran) affords $\text{To}^{\text{M}}\text{CoCl}$ (**1**) as a bright blue solid in excellent yield (equation (1)). $\text{To}^{\text{M}}\text{CoCl}$ is paramagnetic, and its identity as a pseudotetrahedral d^7 center is supported by a host of characterization data including ^1H and ^{11}B NMR spectroscopy, IR spectroscopy, UV/Vis spectroscopy, ESR spectroscopy, X-ray diffraction studies, elemental analysis, and magnetic measurements that included both magnetometry and the Evans method. Many of these tools were needed initially to interpret the spectroscopic data, as the identities of the paramagnetic products were challenging to establish, and later to demonstrate the purities of the isolated materials. As outlined below, the ratio of $\text{TlTo}^{\text{M}}/\text{CoCl}_2$, the use of $\text{CoCl}_2 \cdot \text{THF}$,

and the choice of solvent are crucial to the high-yielding synthesis of **1** without contamination with the readily formed side-products $(\text{To}^{\text{M}})_2\text{Co}$ (**2**) and $\{\text{HTo}^{\text{M}}\}\text{CoCl}_2$ (**3**).



The signals in the ^1H NMR spectrum of $\text{To}^{\text{M}}\text{CoCl}$ dissolved in benzene- d_6 were broad and dispersed over a large chemical shift range, as expected for a paramagnetic compound. Despite these spectroscopic effects, the number of ^1H NMR signals and their integrated ratio provided characteristic data associated with a pseudo- C_{3v} -symmetric oxazolinylborate species. Broad resonances at $\delta = 8.38$ (18 H) and 24.88 ppm (6 H) were assigned to the methyl and methylene groups, respectively, of equivalent oxazoline rings in the To^{M} ligand. The equivalence of the rings suggested the tridentate coordination of the To^{M} ligand to the cobalt center. A ^{11}B NMR signal at $\delta = -29$ ppm was shifted significantly from the isotropic value observed for the To^{M} ligand in diamagnetic environments (e.g., the ^{11}B NMR chemical shift of TlTo^{M} is $\delta = -16$ ppm). This paramagnetically shifted ^{11}B NMR resonance further indicated the successful conversion of diamagnetic TlTo^{M} to a new species, and we note that the ^{11}B NMR spectrum is useful for counting the number of To^{M} species in the reaction mixture.¹⁶

The infrared spectrum contained a band at 1598 cm^{-1} (KBr), which was assigned to the C=N stretching mode (ν_{CN}) of the oxazoline groups. Typically, higher-energy ν_{CN} bands ($> 1615\text{ cm}^{-1}$) are observed for dissociated oxazoline moieties in oxazolinylborate ligands; therefore, this data further supports tridentate ligand coordination. In addition, the observation of only a single peak from the symmetric mode (the asymmetric ν_{CN} band

had low intensity) in the solid-state and solution IR spectra (1586 cm^{-1}) suggested a similar configuration in the two phases. The tetrahedral geometry of **1** was also supported by the electronic absorption spectrum (Figure 1), which contained a band from $\lambda \approx 550$ to 700 nm with λ_{max} at 568 ($\epsilon = 362\text{ M}^{-1}\text{cm}^{-1}$) and 635 nm ($\epsilon = 641\text{ M}^{-1}\text{cm}^{-1}$). The larger peak was sandwiched by shoulders at $\lambda \approx 600$ and 660 nm . The spectra of high-spin pseudotetrahedral cobalt(II) complexes show peaks in this range, and these signals are likely related to the many-featured ν_3 band [${}^4T_1(P) \leftarrow {}^4A_2(F)$] observed for $[\text{CoCl}_4]^{2-}$.¹⁷ The To^MCoCl spectrum is also similar to the spectra of related tris(pyrazolyl)borate (Tp) cobalt(II) complexes such as $\text{Tp}^{i\text{Bu,Me}}\text{CoCl}$ with maxima at $\lambda = 526, 602, 636,$ and 660 nm ¹⁸ or $\text{Tp}^{i\text{Pr}}_2\text{CoEt}$, which exhibited maxima at $\lambda = 580, 610,$ and 690 nm .¹⁹ For tetrahedral Co^{II} complexes, two lower-energy transitions [${}^4T_1(F) \leftarrow {}^4A_2(F)$ and ${}^4T_2(F) \leftarrow {}^4A_2(F)$] are also expected. Indeed, a weak absorption was also observed at $\lambda \approx 1000\text{ nm}$.

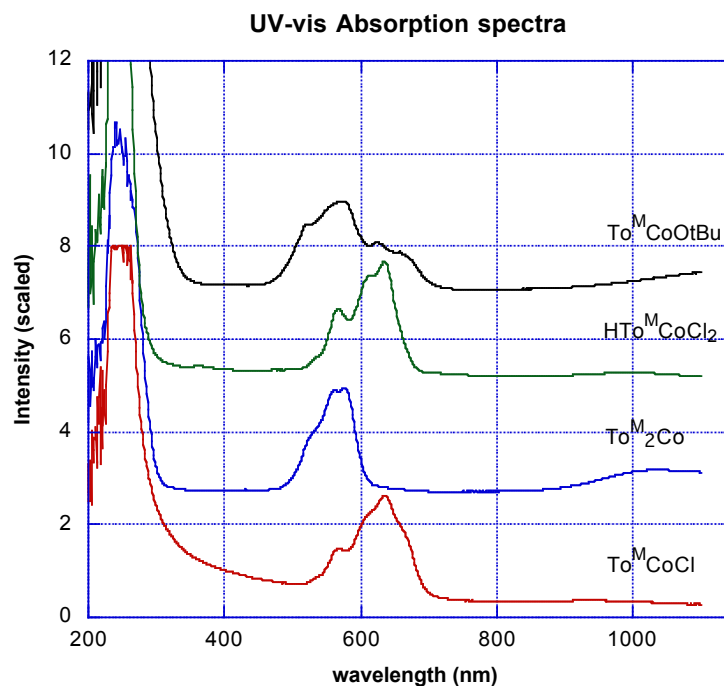


Figure 1. UV/Vis spectra of To^MCoCl (**1**), $(\text{To}^M)_2\text{Co}$ (**2**), $\{\text{HTo}^M\}\text{CoCl}_2$ (**3**), and To^MCoOtBu (**4**).

The paramagnetic nature of **1** was further investigated by magnetic susceptibility measurements and ESR spectroscopy. The Evans method revealed a solution magnetic moment of $4.5(2) \mu_B$. This data is consistent with a high-spin cobalt(II) complex ($S = 3/2$, for which spin-only $\mu_{\text{eff}} = 3.9 \mu_B$) with the 4A_2 ground state, as discussed above. This electronic configuration was maintained at low temperature according to magnetometry measurements, which showed $\mu_{\text{eff}} = 4.3(1) \mu_B$ at 10.3 K. The ESR spectrum (X-band, 10 K) of a neat point sample revealed the low, rhombic site symmetry. The ESR spectrum was simulated for an $S = 3/2$ spin system with anisotropic g values of $g_x = 5.96(2)$, $g_y = 3.50(2)$, and $g_z = 2.10(2)$.²⁰ Similar g values have been reported for other pseudotetrahedral cobalt(II) complexes featuring rhombic symmetry.^{21,22} Hyperfine coupling to ^{59}Co ($I = 7/2$) was not detected under these conditions.²¹

Blue crystals of **1**, obtained from a saturated toluene solution cooled to -38°C , were determined to be $\text{To}^{\text{M}}\text{CoCl}$ through an X-ray diffraction study (Figure 2). The X-ray crystal structure revealed a pseudotetrahedral cobalt center coordinated by the tridentate tris(oxazolinyl)borate ligand. Compound **1** and $\text{To}^{\text{M}}\text{ZnCl}^{23}$ have similar structural features. For example, the Co–N and Zn–N bond lengths range from 2.0091(9) to 2.040(1) Å; the zinc complex has both the highest and the lowest values, and the cobalt compound has intermediate bond lengths. The N–M–Cl angles range from 115.33(4) to 130.82(4)° for the two compounds, and the cobalt compound has the extreme angles. In addition, the B–M–Cl angles of 170.99(3) and 174.27(2)° for the cobalt and zinc complexes, respectively, show a slight displacement of the Cl atom from the anticipated position in a pseudo- C_{3v} structure, and this distortion is slightly larger for the cobalt complex. The structural similarity of diamagnetic zinc(II) and paramagnetic cobalt(II)

compounds suggests that these distortions are sterically controlled rather than the result of electronic influences. The Co1–Cl1 bond length of 2.2025(4) Å in **1** is similar to that observed in other four-coordinate cobalt(II) scorpionate complexes (e.g., $\text{Tp}^{\text{Ph,Me}}\text{CoCl}$, 2.2004(9) Å; $\text{Tp}^{\text{iBu,H}}\text{CoCl}$, 2.216(2) Å; and $\text{Tp}^{\text{iBu,Me}}\text{CoCl}$, 2.2204(9) Å).^{18,24}

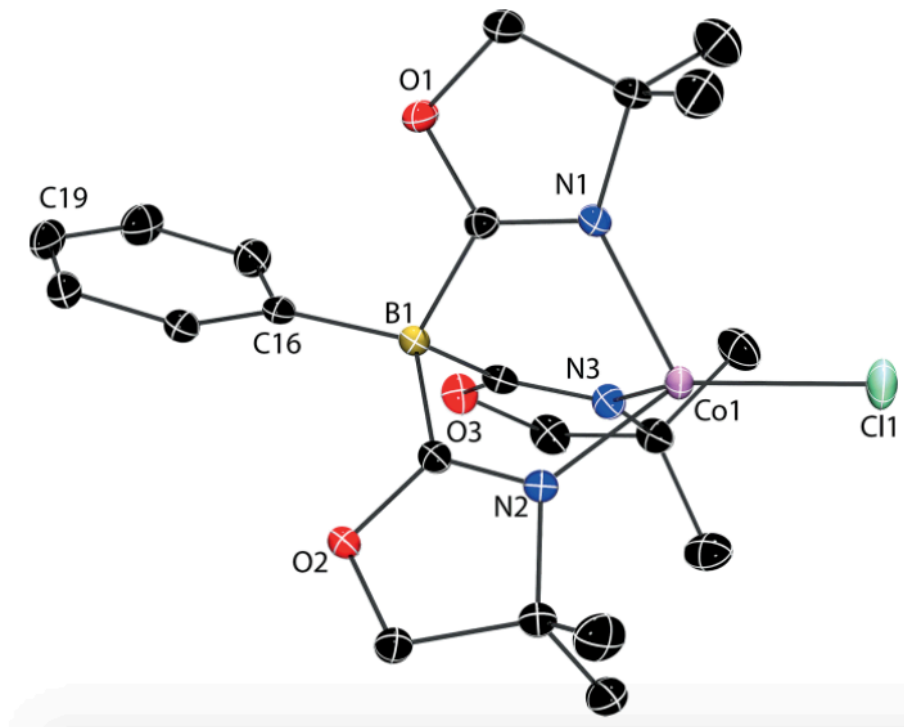


Figure 2. Thermal ellipsoid plot of $\text{To}^{\text{M}}\text{CoCl}$ (**1**). Ellipsoids are plotted at 50 % probability. H atoms are omitted for clarity. Selected bond lengths (Å) and angles (°): Co1–Cl1 2.2026(5), Co1–N1 2.011(1), Co1–N2 2.030(1), Co1–N3 2.026(1); Cl1–Co1–N1 115.31(4), Cl1–Co1–N2 130.80(4), Cl1–Co1–N3 121.73(4), B1–Co1–Cl1 170.99(3).

Although the reaction of TiTo^{M} and $\text{CoCl}_2 \cdot \text{THF}$ is reproducible, the choice of $\text{CoCl}_2 \cdot \text{THF}$ is critical to a successful and high yielding synthesis. In micromolar-scale reactions, equimolar amounts of TiTo^{M} and $\text{CoCl}_2 \cdot \text{THF}$ provide **1** quantitatively. Excess $\text{CoCl}_2 \cdot \text{THF}$ (1.5 equiv.) is needed in larger-scale preparations to optimize the $\text{To}^{\text{M}}\text{CoCl}$ yield (calculated with respect to TiTo^{M}), because the separation of $\text{To}^{\text{M}}\text{CoCl}$ from

CoCl₂·THF is easier than that from (To^M)₂Co (**2**). In contrast, the reaction of anhydrous CoCl₂ and TlTo^M in THF provides a purple mixture of **1** and **2**. During our initial synthetic studies, the appearance of two sets of signals in the ¹H NMR spectra and the formation of purple material in these reactions made the isolation and characterization of pure To^MCoCl challenging. The ¹H NMR spectrum of the purple reaction mixture contained signals at δ = 15.1 and 12.5 ppm as well as the resonances later assigned to **1**. The formation of two paramagnetic To^MCo species was also suggested by the two ¹¹B NMR signals at δ = -29 and 42 ppm; the former was assigned to To^MCoCl, and the latter was assigned to (To^M)₂Co on the basis of a single-crystal X-ray diffraction study and its independent synthesis, which is described below. Repeated recrystallizations from saturated toluene solutions at -38 °C yielded purple X-ray-quality crystals, and a single-crystal diffraction study revealed that the substance was (To^M)₂Co (**2**; Figure 3).

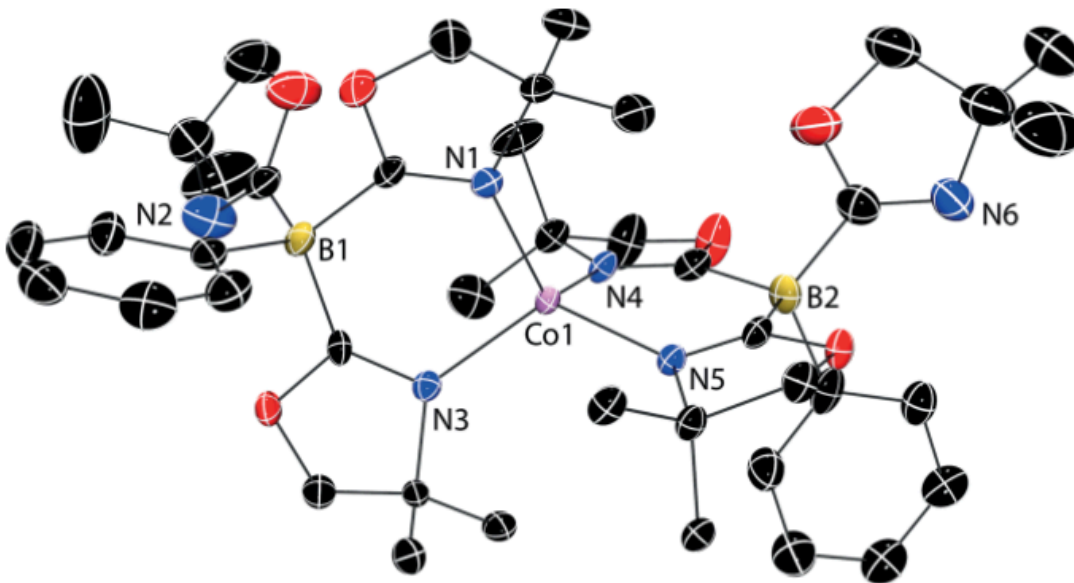
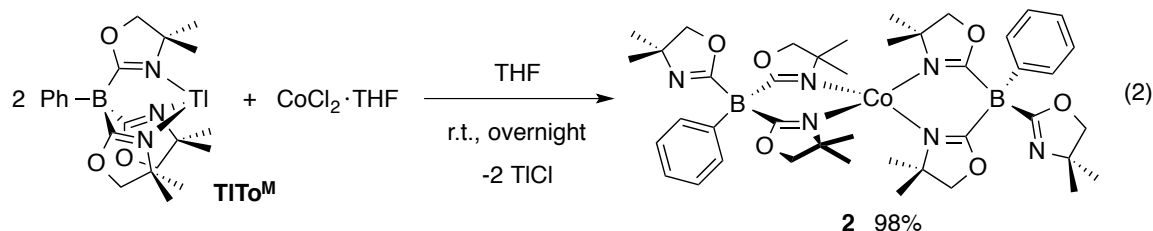


Figure 3. Thermal ellipsoid plot of (To^M)₂Co (**2**) with ellipsoids at 35% probability. H atoms and two cocrystallized toluene molecules are omitted for clarity. Selected bond lengths (Å) and angles (°): Co1–N1 2.010(4), Co1–N3 2.003(4), Co1–N4 2.013(4), Co1–N5 2.000(4); N1–Co1–N3 97.2(2), N4–Co1–N5 97.8(2), N1–Co1–N4 114.2(2), N3–Co1–N4 116.4(2), N5–Co1–N3 116.4(2), N5–Co1–N1 116.0(2).

The cobalt center in **2**, as in **1**, has a distorted tetrahedral geometry. Each of the tris(oxazolinyl)borate ligands in **2** is bidentate with one non-coordinated oxazoline ring, and the structure is similar to the solid-state structures of $(\text{To}^{\text{M}})_2\text{Mg}$ and $(\text{To}^{\text{M}})_2\text{Zn}$.^{13,25} Although the $(\kappa^2\text{-To}^{\text{M}})_2\text{Co}$ structure forms readily, the To^{M} ligand apparently does not support six-coordinate pseudo-sandwich-type first-row metal compounds, in contrast to $(\kappa^3\text{-Tp}^*)_2\text{M}$ compounds.²⁶ Moreover, we have not observed disproportionation of $\text{To}^{\text{M}}\text{CoCl}$ into $(\text{To}^{\text{M}})_2\text{Co}$ and CoCl_2 ; therefore, $\text{To}^{\text{M}}\text{CoCl}$ may be a suitable precursor for the synthesis of new inorganic compounds through chloride substitution. The crystallographic data show that the metal centers are sterically protected by the oxazoline methyl groups, and this likely prevents the formation of the six-coordinate structure. Compound **2** has shorter Co–N interatomic distances than **1**, and all of the N–Co–N angles in **2** are larger than those in **1**. The interatomic distances and angles of **2** fall between those of $(\text{To}^{\text{M}})_2\text{Mg}$ and $(\text{To}^{\text{M}})_2\text{Zn}$ and bear greater resemblance to those of the latter. For example, the Co–N bonds in **2** are shorter than those in $(\text{To}^{\text{M}})_2\text{Mg}$ by ca. 0.05 Å but are equivalent within error to the Zn–N bonds encountered in $(\text{To}^{\text{M}})_2\text{Zn}$.

Unfortunately, purification by crystallization is not effective for preparative-scale separations of mixtures of $(\text{To}^{\text{M}})_2\text{Co}$ and $\text{To}^{\text{M}}\text{CoCl}$. Moreover, the ^1H NMR spectrum of the reaction mixture did not contain features that easily identified inequivalent oxazoline rings in the bidentate coordinated structure. We prepared **2** independently to confirm that the unidentified signals in the ^1H NMR spectrum of the mixture of cobalt species corresponded to **2**. The reaction of CoCl_2 and 2 equiv. of TiTo^{M} affords purple $(\text{To}^{\text{M}})_2\text{Co}$ in excellent yield (equation (2)). $(\text{To}^{\text{M}})_2\text{Co}$ and $\text{To}^{\text{M}}\text{CoCl}$ are similarly soluble in

benzene, toluene, diethyl ether, THF, and dichloromethane, and this similarity likely causes the difficulties with the separation of mixtures of the two compounds.



The ^1H and ^{11}B NMR spectra of isolated **2** contained signals that matched those detected in the crude mixture with **1**; therefore, $(\text{To}^{\text{M}})_2\text{Co}$ is indeed the second product obtained when anhydrous CoCl_2 is the starting material. However, these NMR spectroscopic data did not allow the direct quantitative estimation of the purity and offered few further structural insights. In contrast, the ν_{CN} bands at 1603 and 1554 (KBr) or 1609 and 1555 cm^{-1} (CH_2Cl_2) in the infrared spectrum of **2** were structurally informative. These signals were assigned to the ν_{CN} modes of non-coordinated and coordinated oxazoline groups, respectively, consistent with the bidentate bonding mode determined by X-ray crystallography.

Furthermore, the d–d transitions in the UV/Vis spectrum of **2** again appeared in the expected region for a high-spin tetrahedral Co^{II} complex at $\lambda_{\text{max}} = 562$ ($\epsilon = 539 \text{ M}^{-1} \text{ cm}^{-1}$) and 576 nm ($\epsilon = 552 \text{ M}^{-1} \text{ cm}^{-1}$). These signals were similar to those observed for the four-coordinate C_2 -symmetric Bp_2Co species ($\text{Bp} = \text{H}_2\text{B}(\text{C}_3\text{N}_2\text{H}_3)_2$).^{10a} The center of gravity of this band was blueshifted with respect to that for the related transition in **1** (see the absorption spectra in Figure 1). Note that a similar relationship was described between Bp_2Co and TpCoCl , in terms of a blueshifted absorption for the $^4\text{T}_1(\text{P}) \leftarrow ^4\text{A}_2(\text{F})$ transition (for the tetrahedral site).¹⁸ A second, lower-energy band was observed at $\lambda \approx$

1040 nm ($\epsilon = 120 \text{ M}^{-1} \text{ cm}^{-1}$), and this band was redshifted and more intense than the band for the transition in $\text{To}^{\text{M}}\text{CoCl}$. The high-spin nature of **2** was further supported by the solution magnetic moment of $4.2(2) \mu_{\text{B}}$ (measured by the Evans method), which was slightly smaller than that of Bp_2Co but significantly reduced in comparison with that of six-coordinate Tp_2Co .^{10a} The high-spin state of **2** at low temperature was confirmed by magnetometry experiments, which revealed $\mu_{\text{eff}} = 3.9(1) \mu_{\text{B}}$ at 12.5 K. An ESR spectrum of **2** acquired at 5 K as a point sample or as a glassed solution in 2-methyltetrahydrofuran contained only weak signals. One of the signals for the point sample showed evidence of the hyperfine coupling of the cobalt center in the form of a seven-line pattern. The discrepancy from the expected eight-line pattern for $I = 7/2$ was presumably caused by the broadness at the onset of the peak. In addition, the spectrum was consistent with a low-symmetry species.

Compound **1** and TlTo^{M} react overnight to give **2**, and this conversion occurs more rapidly than the reaction of TlTo^{M} and CoCl_2 under equivalent conditions. In the attempted synthesis of **1** from anhydrous CoCl_2 , the poor selectivity is hypothesized to come from the relative rates of transmetalation for CoCl_2 versus **1**, and these rates are likely influenced by the heterogeneous nature of the reaction mixture. This contrasts with the reactivity of bulky tris(pyrazolyl)borato cobalt compounds. For example, $\text{Tp}^{\text{Ph,Me}}\text{CoCl}$ and $\text{Tp}^{\text{Ph,Me}}\text{Tl}$ do not afford $(\text{Tp}^{\text{Ph,Me}})_2\text{Co}$.¹¹

In the course of our studies of the selective preparation of **1**, polar solvents were tested to give a monophasic reaction (i.e., to improve the kinetics). In fact, the reaction of TlTo^{M} and CoCl_2 in methanol gives a blue material, which was initially attributed to $\text{To}^{\text{M}}\text{CoCl}$ on the basis of its color and ^1H NMR spectrum in benzene- d_6 , as a result of the

presence of **1** in the mixture. Moreover, the electronic absorption spectra of **1** and the substance obtained from the reaction in methanol are similar (see Figure 1). However, this material is less soluble in benzene than **1**, and the XRD powder pattern of this material did not match that expected for **1** (see Figure 5 below). The recrystallization of this material from dichloromethane afforded blue X-ray-quality crystals, and a diffraction study proved that this product is the protonated oxazoline derivative of **1**, namely, $\{\text{HTo}^{\text{M}}\}\text{CoCl}_2$ (**3**, Figure 4).

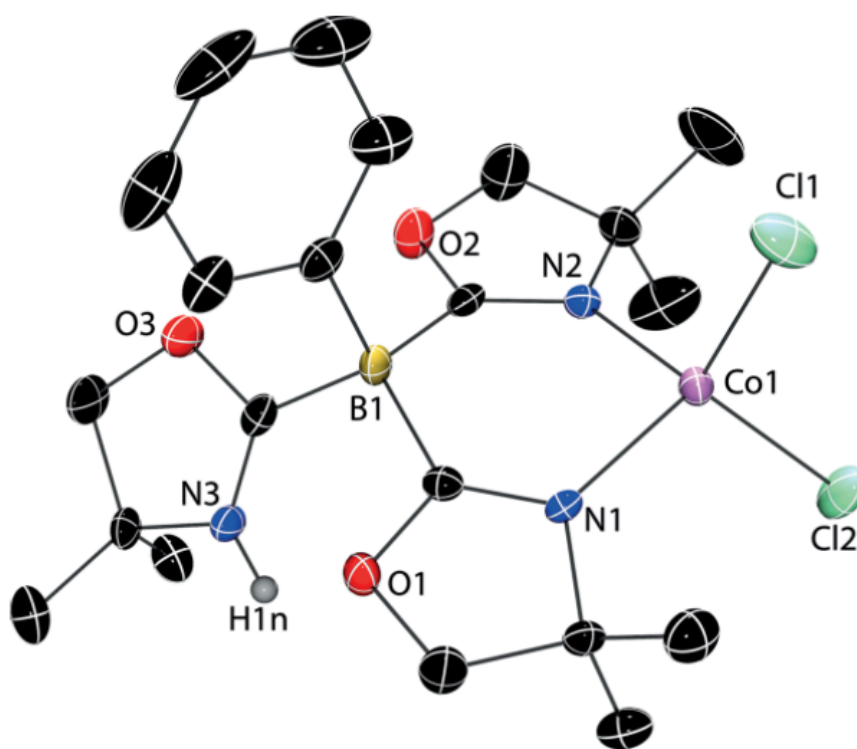
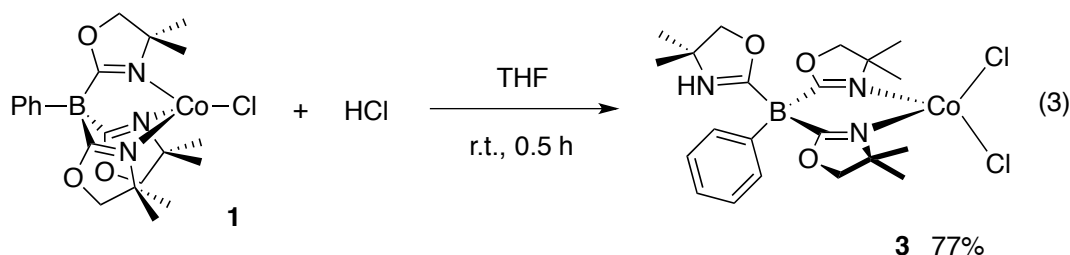


Figure 4. Thermal ellipsoid plot of $\{\text{HTo}^{\text{M}}\}\text{CoCl}_2$ (**3**) plotted at 50 % probability. H atoms, with the exception of H1n, are omitted for clarity. Selected bond lengths (Å) and angles (°): Co1–N1 2.006(3), Co1–N2 2.005(4), Co1–Cl1 2.237(3), Co1–Cl2 2.261(2); N1–Co1–N2 96.2(1), N2–Co1–Cl1 109.77(9), N1–Co1–Cl1 115.18(9), N2–Co1–Cl2 111.68(9), N1–Co1–Cl2 110.6(1), Cl1–Co1–Cl2 112.40(9).

The crystal structure of **3** shows a tetrahedral cobalt center featuring two chlorido ligands and a bidentate To^{M} –cobalt interaction. The third oxazoline ring is protonated, and HTo^{M} may be viewed as an overall charge-neutral ligand coordinated to CoCl_2 . Thus,

$\{\text{HTo}^{\text{M}}\} \text{CoCl}_2$ differs from **1** and **2** by its zwitterionic nature. Related iridium and rhodium compounds of protonated or methylated tris(oxazolinyl)borate complexes have been reported, as have zwitterionic cobalt(II) complexes stabilized by bulky tris(carbene)borate ligands.^{16,27} Compared with **1**, compound **3** features slightly longer Co–Cl bonds (by more than 0.034 Å) and shorter Co–N bonds (by more than 0.025 Å).

The reaction of **1** and (HOEt₂)Cl provides an independent synthesis of **3** (equation (3)). Alternatively, LiTo^M and CoCl₂ react in wet dichloromethane to provide crystals of **3** directly from the reaction mixture.



Compound **3** is highly soluble in dichloromethane and methanol but poorly soluble in benzene, toluene, tetrahydrofuran, and diethyl ether. The poor solubility of **3** and the high solubility of **1** in benzene-*d*₆ can result in erroneous interpretation of the purity of To^MCoCl on the basis of the NMR spectra of crude reactions mixtures. Thus, dry dichloromethane-*d*₂ is the best solvent for unambiguous NMR analysis of the purity of these compounds. The ¹H NMR spectrum of **3** in dichloromethane showed paramagnetically shifted ¹H NMR signals that were unassignable yet characteristic. The ¹¹B NMR signal appeared at $\delta = -7.5$ ppm, and this peak was much less shifted from the diamagnetic range than those of **1** and **2**. The infrared spectrum was consistent with the crystallographically determined structure and provided structural insights. The bands at

1588 and 1598 cm^{-1} were assigned to ν_{CN} of cobalt-coordinated oxazoline and protonated oxazoline, respectively. Compound **3** was also a high-spin Co^{II} species, on the basis of magnetometry experiments that indicated a μ_{eff} of 4.2(1) μ_{B} at 5 K.

As all three compounds were formed from the same starting materials and ^1H NMR spectroscopy provided ambiguous results during the course of these synthetic studies, we instead utilized powder XRD measurements to characterize the bulk compositions of the samples. These experiments, along with solution and solid-state IR spectroscopy, provide a connection between the solid-state and molecular structures that usually relies on solution-phase NMR spectroscopy (which was structurally uninformative for these (oxazolinyborato)cobalt(II) compounds). Powder XRD is an appealing alternative characterization technique, because it is not complicated by the electronic structure or unpaired electrons and probes the composition of the crystalline component of the bulk powder.

The experimental powder XRD patterns matched the corresponding XRD patterns calculated from single-crystal data for samples of **1**, **2**, and **3**. These results provided additional confidence that the single-crystal diffraction experiments corresponded to structures that describe the bulk samples. For example, the powder XRD experiments indicated that the preparation from $\text{CoCl}_2 \cdot \text{THF}$ gives a reproducible and high-yielding route to **1** (Figure 5).

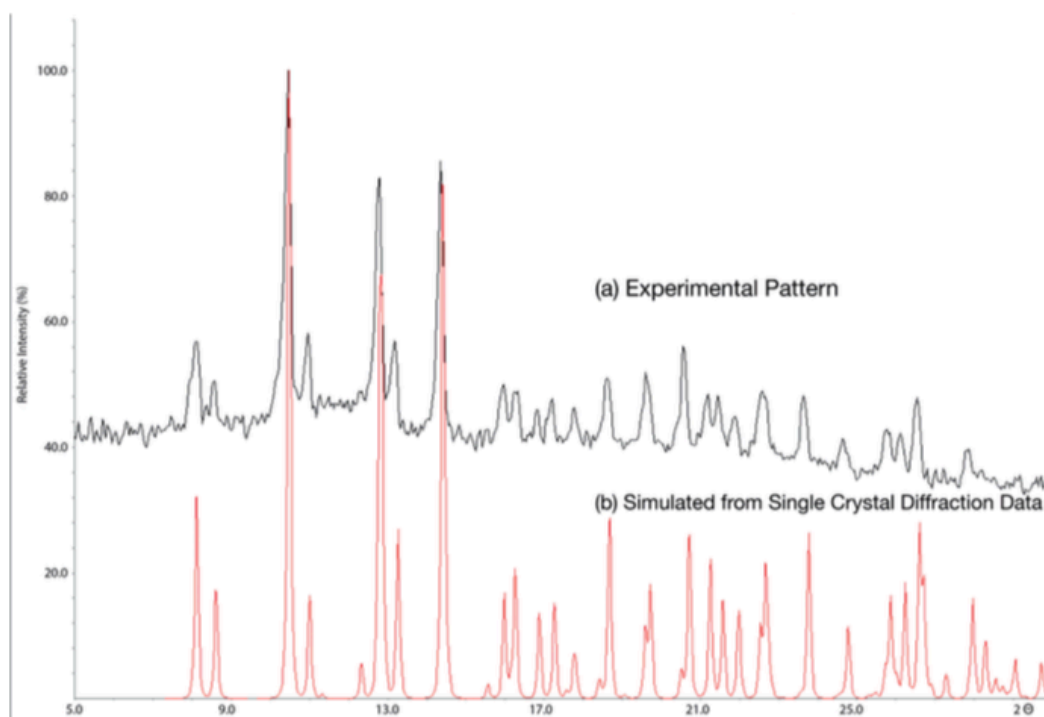
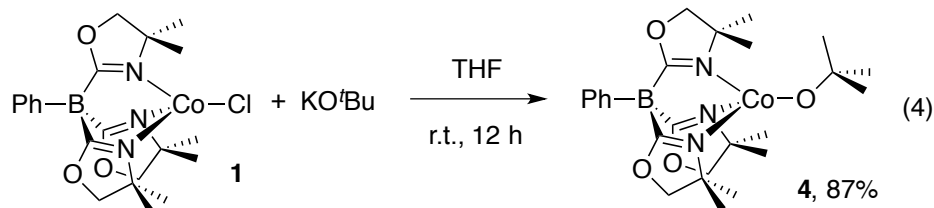


Figure 5. X-ray powder diffraction pattern of $\text{To}^{\text{M}}\text{CoCl}$ (**1**) at 293 K with $\text{Cu-K}\alpha$ radiation. The observed pattern (A) is shown in black, and the calculated intensity pattern (B) is indicated by red solid lines.

The viability of this method for the measurement of the purity was further tested with analytically pure **3/1** in a 50:50 ratio. The XRD pattern of this mixture matched the expected powder pattern and verified that the presence of the two products could be identified by the diffraction method.

We also attempted to synthesize $\text{To}^{\text{M}}\text{CoX}$ compounds using cobalt acetate as the starting material. However, the reaction of cobalt acetate and TlTo^{M} generated a mixture of **2** and another species, which was later identified as $\text{To}^{\text{M}}\text{CoOAc}$ (see below). Thus, $\text{CoCl}_2 \cdot \text{THF}$ is the preferred starting material for the entry into the cobalt(II) chemistry of tris(oxazolinyl)borate ligands.

With isolable, fully characterized, and spectroscopically and analytically pure $\text{To}^{\text{M}}\text{CoCl}$ in hand, we tested its reactivity in halide substitutions to prepare $\text{To}^{\text{M}}\text{CoOtBu}$ (**4**) and $\text{To}^{\text{M}}\text{CoOAc}$ (**5**). The reaction of $\text{To}^{\text{M}}\text{CoCl}$ and $\text{KO}t\text{Bu}$ in tetrahydrofuran readily provides $\text{To}^{\text{M}}\text{CoOtBu}$ (equation (4)).



In the ^1H NMR spectrum of **4**, all of the signals were readily assigned by integration, including a new signal at $\delta = 11.16$ ppm that integrated to 9 H relative to the To^{M} signals. This resonance was assigned to the OtBu group. Moreover, a new ^{11}B NMR signal was detected at $\delta = 73$ ppm, which was further downfield than those of the other cobalt complexes. The paramagnetically shifted ^{11}B NMR spectrum rules out the transmetalation of the To^{M} ligand to K.

Unlike blue $\text{To}^{\text{M}}\text{CoCl}$, compound **4** is purple. Accordingly, the UV/Vis absorption spectrum of **4** contained a broad peak with a blueshifted onset edge at $\lambda \approx 500$ nm, as might be expected owing to the replacement of the weak-field chlorido ligand with a *tert*-butoxide ligand. The tridentate coordination of the tris(oxazolonyl)borate ligand to the cobalt center was suggested by a single strong IR band at 1590 cm^{-1} , which was assigned to the oxazoline ν_{CN} mode. Compound **4** is a high-spin cobalt(II) complex from room temperature to 36 K, as determined by magnetometry measurements ($\mu_{\text{eff}} = 4.6(1)\ \mu_{\text{B}}$ at 36 K). Unlike compounds **1–3**, $\text{To}^{\text{M}}\text{CoOtBu}$ undergoes a broad, thermally induced spin transition, and μ_{eff} is $1.3(1)\ \mu_{\text{B}}$ at 2.5 K, consistent with a low-spin state ($S = 1/2$).

The recrystallization of **4** from toluene at $-35\text{ }^{\circ}\text{C}$ provided X-ray-quality crystals, and a single-crystal X-ray diffraction study confirmed the identity of **4** as $\text{To}^{\text{M}}\text{CoOtBu}$ (Figure 6). The Co–N bonds in **4** are longer than those in **1**. In addition, the B1–Co1–O4 angle in **4** is smaller than the B1–Co1–Cl1 angle in **1**. The Co1–O4–C22 angle in **4** is smaller than the B1–Co1–Cl1 angle in **1**. The Co1–O4–C22 angle is $134.2(2)^{\circ}$, and this angle wedges the *t*Bu group between the methyl groups of the N2 and N3 oxazolines.

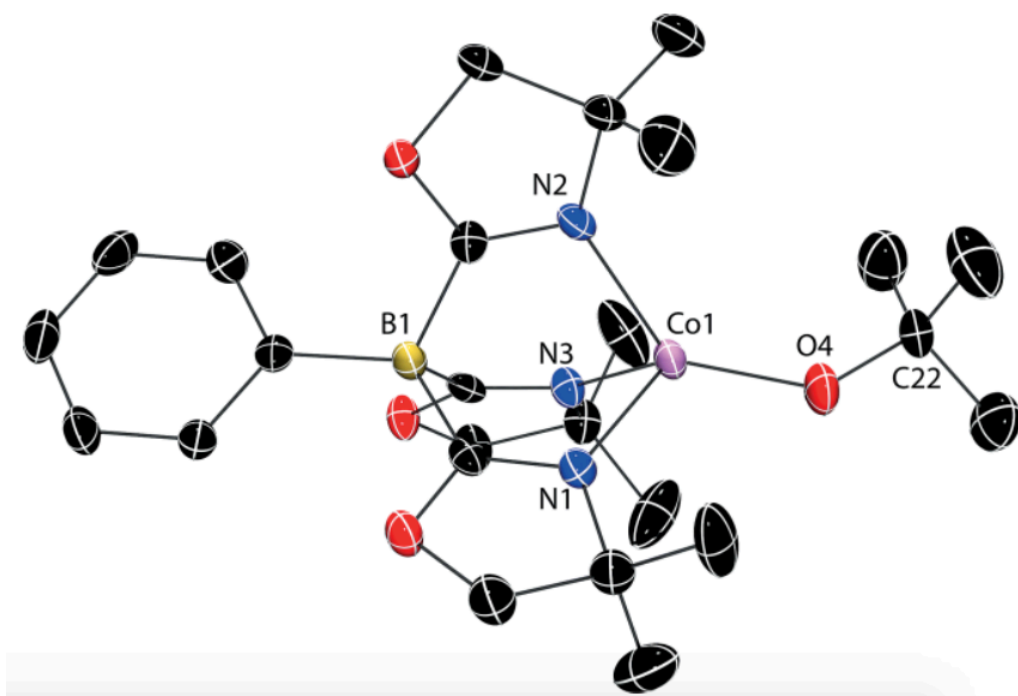
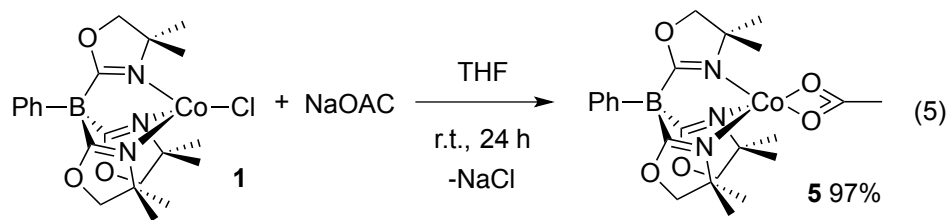


Figure 6. Thermal ellipsoid plot of $\text{To}^{\text{M}}\text{CoOtBu}$ (**4**). Ellipsoids are plotted at 50 % probability. H atoms are omitted for clarity. Selected bond lengths (\AA) and angles ($^{\circ}$): Co1–O4 1.821(2), Co1–N1 2.049(3), Co1–N2 2.055(3), Co1–N3 2.026(2); O4–Co1–N1 111.2(1), O4–Co1–N2 128.0(1), O4–Co1–N3 131.0(1), B1–Co1–O4 166.2(1), Co1–O4–C22 134.2(2).

The reaction of $\text{To}^{\text{M}}\text{CoCl}$ and NaOAc in THF provides $\text{To}^{\text{M}}\text{CoOAc}$ (**5**) as a light purple solid in high isolated yield (97%; Equation (5)). Compound **5** was characterized by ^1H and ^{11}B NMR spectroscopy. The ^1H NMR spectrum contained new tris(oxazoliny)phenylborate signals, and the acetate signal appeared far downfield ($\delta =$

171.25 ppm). The ^{11}B NMR signal of **5** appeared at 95 ppm, which is downfield relative to the signals for **1** and **4**.



In the IR spectrum, a single band corresponding to the oxazoline ν_{CN} stretching mode was observed at 1591 cm^{-1} . Compound **5** is high spin ($\mu_{\text{eff}} = 4.8(2)\ \mu_{\text{B}}$), as determined by the Evans method. X-ray-quality crystals were obtained by recrystallization from pentane at $-35\text{ }^{\circ}\text{C}$ (Figure 7). The Co–O bonds (2.098(2) and 2.089(2) Å) are longer than the Co–O bond in **4** (1.821(2) Å), and the Co–N bonds are also longer than those in **1** and **4**.

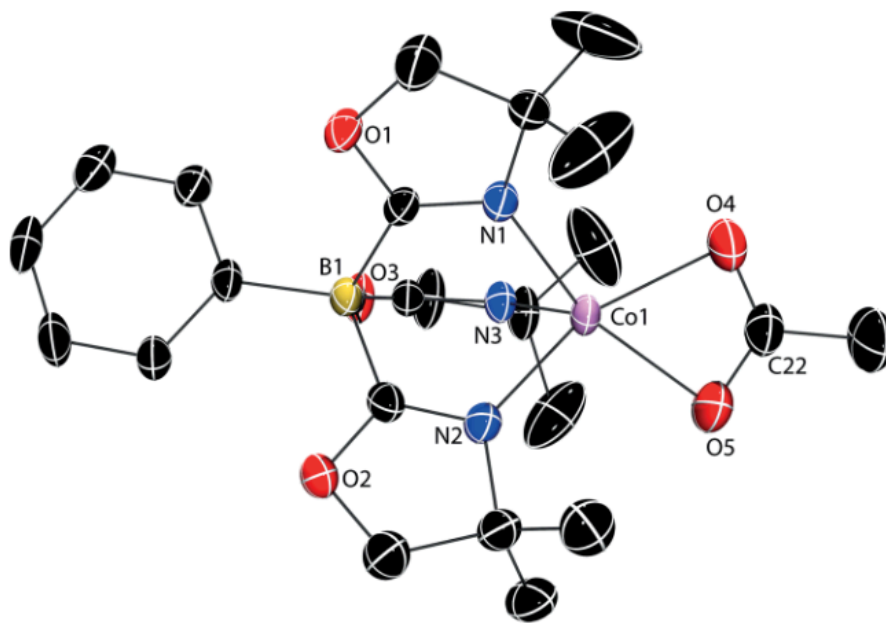


Figure 7. Thermal ellipsoid plot of $\text{To}^{\text{M}}\text{CoOAc}$ (**5**). Ellipsoids are plotted at 50 % probability. H atoms are omitted for clarity. Selected bond lengths (Å) and angles ($^{\circ}$): Co1–O4 2.098(2), Co1–O5 2.089(1), Co1–N1 2.065(2), Co1–N2 2.064(2), Co1–N3 2.026(2); O5–Co1–N1 154.5(1), O5–Co1–N2 100.2(1), O5–Co1–N3 112.4(1), O5–Co1–O4 61.8(1).

Cobalt(II) acetate is used as an industrial catalyst in the oxidation of *p*-xylene to terephthalic acid,²⁸ and nitrogen-ligand-based cobalt compounds have also been studied in cyclohexane oxidation to cyclohexanol.^{9d} In this oxidation catalysis, selectivity for a single oxidation to cyclohexanol, rather than over-oxidation to cyclohexanone or ϵ -caprolactone, is desired. Despite the important role of cobalt in oxidation chemistry, TpCoX-based compounds are reported as not effective for cyclohexane oxidation,²⁹ so a study of $\text{To}^{\text{M}}\text{CoOAc}$ as an oxidation catalyst provides a comparison with the pyrazolylborate analogues.

Complex **5** catalyzes the oxidation of cyclohexane to cyclohexanol with *meta*-chloroperoxybenzoic acid (*m*CPBA) as the terminal oxidant and affords 536 equiv. of cyclohexanol per 1 equiv. of catalyst after 7 h. At the early stages of the reaction (3 h), the product ratio for cyclohexanol/cyclohexanone/ ϵ -caprolactone is 20:1.5:1 with 337 equiv. of cyclohexanol formed per 1 equiv. of **5**. This selectivity decreases as the reaction proceeds, and ϵ -caprolactone is formed from the reaction of *m*CPBA and cyclohexanone. Cumene hydroperoxide and *tert*-butyl hydroperoxide were tested as oxidants for this catalytic transformation, but only *m*CPBA afforded the desired conversion. A control experiment, in which cyclohexane and *m*CPBA were mixed at room temperature, did not provide detectable quantities of cyclohexanol, cyclohexanone, or ϵ -caprolactone. Furthermore, anhydrous CoCl_2 or anhydrous $\text{Co}(\text{OAc})_2$ (as $\text{Co}_4(\text{OAc})_7\text{OH}$) are poorly soluble under these reaction conditions, and this limits comparisons with **5**. However, the partially soluble suspended materials give lower activities and poorer selectivities than **5** under comparable conditions.

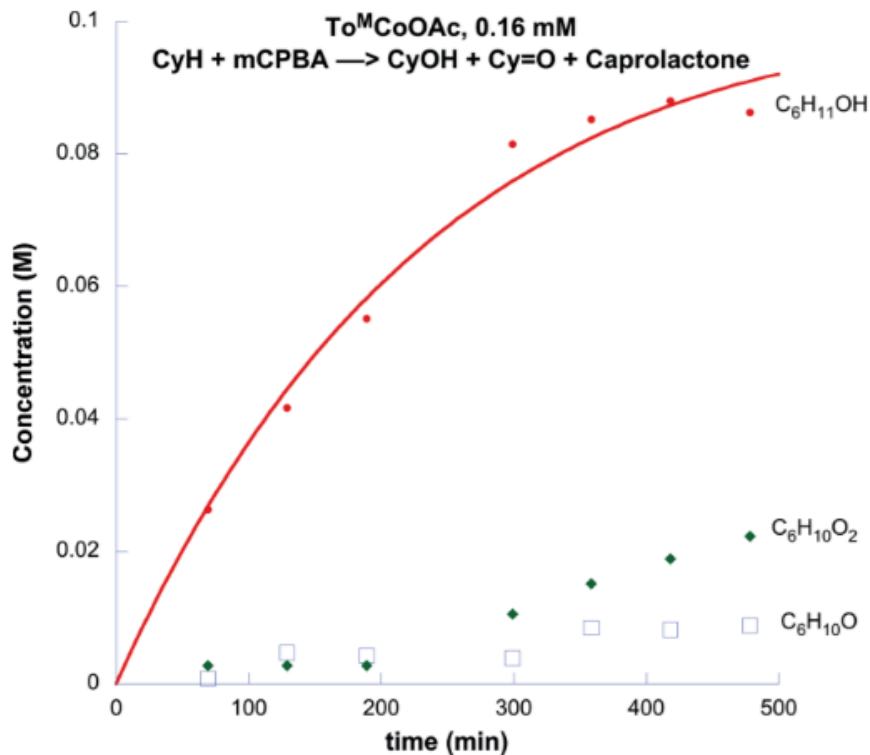


Figure 8. Concentration versus time plots for the products of cyclohexane oxidation with *m*CPBA. The experiment was performed four times.

To better identify the parameters associated with the oxidation process, the reaction mixture was monitored by GC to determine the concentrations of cyclohexanol, cyclohexanone, and ϵ -caprolactone. In a reaction with 0.16 mM **5**, the concentration of cyclohexanol reaches a steady state after ca. 300 min. The plot of [cyclohexanol] versus time in Figure 8 can be fitted with a nonlinear least-squares regression ($R = 0.98$) to Equation (6).³⁰

From this analysis, the observed rate constant for the oxidation of cyclohexane to cyclohexanol (k_1) is $1.69(8) \times 10^{-4} \text{ s}^{-1}$, and that for the oxidation of cyclohexanol is $3.9(1) \times 10^{-3} \text{ s}^{-1}$ (average of four experiments, see the Supporting Information below for individual curves). Thus, the selectivity for cyclohexanol production comes largely from the high initial $[\text{C}_6\text{H}_{12}]$. On the basis of these results, we are currently studying reaction

conditions (temperature, solvent polarity, and reagent concentrations) and catalyst structures that favor higher k_1 values and smaller k_2 values.

Conclusion

The synthesis of **1** from TiTo^{M} and $\text{CoCl}_2 \cdot \text{THF}$ provides an entry point into tris(oxazolinyl)borato cobalt chemistry. Like zinc and magnesium compounds, four-coordinate pseudotetrahedral cobalt complexes are supported by the tris(oxazolinyl)borate ligand, despite its reduced steric profile with respect to that of the highly bulky *tert*-butyl-substituted tris(pyrazolyl)borate scorpionates. The starting materials and reaction conditions are critical for obtaining **1**, rather than **2** or **3**. However, these other two compounds can be prepared by using 2 equiv. of TiTo^{M} or polar protic solvents, respectively. Once the paramagnetic compounds were fully characterized by X-ray diffraction as well as IR, NMR, and UV/Vis spectroscopy, the characteristic spectroscopic signatures in the ^{11}B NMR spectra, ^1H NMR spectra, and powder XRD patterns are useful for establishing the synthetic reproducibility and product identities as well as the purities of the materials.

$\text{To}^{\text{M}}\text{CoCl}$ is reactive with $\text{KO}t\text{Bu}$ and NaOAc in salt-metathesis reactions. In this context, we are currently working to synthesize, characterize, and study the reactivity of alkylcobalt(II) compounds supported by tris(oxazolinyl)borate ligands. $\text{To}^{\text{M}}\text{CoOAc}$ is a catalyst for the selective oxidation of cyclohexane, in contrast to tris(pyrazolyl)borato cobalt compounds. We are currently preparing optically active analogues to study enantioselective C–H bond functionalization.

Experimental Section

General Experimental Methods: All reactions were performed by standard Schlenk techniques under dry argon. Tetrahydrofuran, diethyl ether, and toluene were dried and deoxygenated with an IT PureSolv system. Benzene- d_6 was heated under reflux over Na/K alloy and vacuum-transferred. CoCl_2 (Strem) was used to prepare $\text{CoCl}_2 \cdot \text{THF}$ by Soxhlet extraction of CoCl_2 with THF. TlTo^{M} was synthesized according to reported procedures.^{16, 31} **Caution!** *Thallium salts are highly toxic, and thallium-containing compounds and waste should be handled appropriately.* KOtBu was purified by sublimation. $m\text{CPBA}$ was purified by washing with $\text{K}_2\text{HPO}_4/\text{KH}_2\text{PO}_4$ buffer solution (pH 7.5).³² The ^1H and ^{11}B NMR spectra were recorded with a Bruker Avance III 600 spectrometer. The ^{11}B NMR spectra were referenced to an external sample of $\text{BF}_3 \cdot \text{Et}_2\text{O}$. The infrared spectra were measured with a Bruker Vertex 80 FTIR spectrometer. The electron paramagnetic resonance (EPR) spectra were obtained with an X-band Eleksys 580 FT-EPR spectrometer in continuous-wave mode, and the spectra were simulated with XSophe. The direct current (DC) magnetization was measured with a Quantum Design MPMS-5 superconducting quantum interference device (SQUID) magnetometer. The UV/Vis spectra were recorded with an Agilent 8453 UV/Vis spectrophotometer with the analyte (2 mM) in dichloromethane. Elemental analyses were performed with a Perkin–Elmer 2400 Series II CHN/S analyzer. The catalytic cyclohexane oxidation experiments and the kinetic studies were performed with a Chemspeed Technologies SWING-XL automated platform. GC–MS was performed with Agilent 7890A GC and Agilent 5975C MS instruments equipped with an HP-5MS column. The powder XRD patterns were collected with a STOE WinXPOW powder diffractometer. The single-crystal X-ray

diffraction data were collected with an APEX II diffractometer. CCDC 1433255 (for **1**), 1433256 (for **2**), 1433257 (for **3**), 1433258 (for **4**), and 1457506 (for **5**) contain the supplementary crystallographic data. These data can be obtained free of charge from The Cambridge Crystallographic Data Centre.

To^MCoCl (1): TITo^M (2.015 g, 3.43 mmol) was dissolved in THF (75 mL), and the solution was added dropwise to a stirred suspension of CoCl₂·THF (1.01 g, 5.11 mmol) in THF (75 mL). The reaction mixture was stirred overnight, and then the solvent was evaporated to give a blue residue. The product was extracted with benzene (100 mL) and dried under vacuum to afford To^MCoCl (**1**) as a bright blue solid (1.55 g, 3.25 mmol, 94.8 % based on TITo^M). Recrystallization from toluene gave analytically pure To^MCoCl. ¹H NMR (benzene-*d*₆, 600 MHz): δ = 24.88 (s, 6 H, CNCMe₂CH₂O), 8.38 (s, 18 H, CNCMe₂CH₂O), 4.77 (s, 2 H, C₆H₅), 4.25 (s, 1 H, *p*-C₆H₅), -0.41 (s, 2 H, C₆H₅) ppm. ¹¹B NMR (benzene-*d*₆, 128 MHz): δ = -29.6 ppm. IR (KBr): ν 2969 (m), 2930 (m), 2898 (m), 2871 (m), 1588 (s, ν_{CN}), 1461 (m), 1388 (m), 1369 (m), 1351 (m), 1273 (m), 1193 (m), 1162 (m), 1107 (m), 988 (s) cm⁻¹. UV/Vis (CH₂Cl₂): λ_{max} (ϵ) = 568 (362), 635 (641), 940 (92 M⁻¹cm⁻¹) nm. Evans method: μ_{eff} (C₆D₆) = 4.5(2) μ_{B} . C₂₁H₂₉BClCoN₃O₃ (476.7): calcd. C 52.91, H 6.13, N 8.82; found C 53.26, H 6.20, N 9.03. M.p. 194–196 °C (dec.).

(To^M)₂Co (2): TITo^M (0.102 g, 0.173 mmol) and CoCl₂·THF (0.0169 g, 0.0855 mmol) were stirred in THF (5 mL) for 1 d. The reaction mixture changed gradually from blue to purple. The reaction mixture was filtered, and the solvent was evaporated to afford (To^M)₂Co (**2**) as a purple solid (0.0689 g, 0.0837 mmol, 97.8 %). Recrystallization from toluene afforded analytically pure X-ray-quality single crystals of (To^M)₂Co. ¹H NMR (benzene-*d*₆, 600 MHz): δ = 15.04, 12.41, 2.63 ppm. ¹¹B NMR (benzene-*d*₆, 128 MHz): δ

= 42.3 ppm. IR (KBr): ν 2965 (m), 2928 (m), 2888 (m), 1602 (m, ν_{CN}), 1554 (s, ν_{CN}), 1463 (m), 1369 (m), 1279 (m), 1261 (m), 1198 (m) 1153 (m), 1100 (m), 1002 (m), 969 (m). UV/Vis (CH_2Cl_2): λ_{max} (ϵ) = 562 (539), 576 (552), 1042 ($120 \text{ M}^{-1}\text{cm}^{-1}$) nm. Evans method: μ_{eff} (C_6D_6) = 4.2(2) μ_{B} . $\text{C}_{42}\text{H}_{58}\text{B}_2\text{CoN}_6\text{O}_6$ (823.5): calcd. C 61.26, H 7.10, N 10.21; found C 61.21, H 7.20, N 9.78. M.p. 121–123 °C (dec.).

{HTo^M}CoCl₂ (3): Complex **1** (0.199 g, 0.417 mmol) was dissolved in THF (30 mL), and the solution was added dropwise to a solution of HCl in diethyl ether (210 μL , 0.420 mmol). The blue solution was stirred overnight, and the volatiles were removed in vacuo to afford {HTo^M}CoCl₂ (**3**) as a bright blue solid (0.144 g, 0.281 mmol, 67.4 %).

Recrystallization from dichloromethane afforded analytically pure {HTo^M}CoCl₂. ¹H NMR (dichloromethane-*d*₂, 600 MHz): δ = 17.3, 14.3, 9.9, 8.6, 7.0, 6.6, -21.4, -23.3 ppm. ¹¹B NMR (dichloromethane-*d*₂, 128 MHz): δ = -7.5 ppm. IR (KBr): ν 3270 (m, ν_{NH}), 2976 (m), 2932 (m), 2984 (m), 1598 (s, ν_{CN}), 1588 (s, ν_{CN}), 1462 (m), 1424 (m), 1371 (m), 1306 (m), 1274 (m), 1194 (m) 1171 (m), 965 (m), 937 (m) cm^{-1} . UV/Vis (CH_2Cl_2): λ_{max} (ϵ) = 567 (360), 614 (479), 635 (528), 999 ($130 \text{ M}^{-1}\text{cm}^{-1}$) nm. μ_{eff} (CD_2Cl_2) = 4.0(2) μ_{B} . $\text{C}_{21}\text{H}_{30}\text{BCl}_2\text{CoN}_3\text{O}_3$ (513.1): calcd. C 49.16, H 5.89, N 8.19; found C 49.35, H 6.16, N 7.72. M.p. 218–221 °C (dec.).

To^MCoOtBu (4): Complex **1** (0.202 g, 0.423 mmol) was dissolved in THF (10 mL), and the solution was added to KOtBu (0.053 g, 0.472 mmol) to instantly afford a purple solution. The reaction mixture was stirred overnight, and then KCl was removed by filtration. The volatiles were evaporated in vacuo to afford a bright purple solid. The purple solid was washed with pentane (3 \times 5 mL) and then dried under vacuum to yield To^MCoOtBu (0.189 g, 0.367 mmol, 86.8%). X-ray-quality crystals were obtained from

pentane at $-40\text{ }^{\circ}\text{C}$. ^1H NMR (benzene- d_6 , 600 MHz): $\delta = 15.54$ (s, 6 H, $\text{CNCMe}_2\text{CH}_2\text{O}$), 11.33 (s, 2 H, C_6H_5), 11.16 (s, 9 H, CoOCMe_3), 9.51 (s, 2 H, C_6H_5), 8.00 (s, 1 H, p - C_6H_5), -6.26 (s, 18 H, $\text{CNCMe}_2\text{CH}_2\text{O}$) ppm. ^{11}B NMR (benzene- d_6 , 128 MHz): $\delta = 72.9$ ppm. IR (KBr): ν 2966 (m), 2930 (m), 2889 (m), 1590 (s, ν_{CN}), 1465 (m), 1433 (m), 1386 (m), 1364 (m), 1278 (m), 1251 (m), 1193 (s), 1158 (m), 1002 (m), 966 (m), 928 (m) cm^{-1} . UV/Vis (CH_2Cl_2): λ_{max} (ϵ) = 524 (245), 575 (327), 624 (179), 657 ($148\text{ M}^{-1}\text{cm}^{-1}$) nm. $\text{C}_{25}\text{H}_{38}\text{BCoN}_3\text{O}_4$ (514.3): calcd. C 58.38, H 7.45, N 8.17; found C 58.04, H 7.48, N 8.29. M.p. 233–235 $^{\circ}\text{C}$ (dec.).

To^MCoOAc (5): Complex **1** (0.101 g, 0.211 mmol) was dissolved in THF (5 mL), and the solution was added to NaOAc (0.017 g, 0.212 mmol). The reaction mixture was stirred for 24 h to afford a purple solution and a white precipitate. The NaCl precipitate was removed by filtration, and the volatiles were evaporated in vacuo to afford a light purple solid. The resulting purple solid was washed with pentane (3×5 mL) and dried under vacuum to yield To^MCoOAc (0.102 g, 0.204 mmol, 96.7 %). X-ray-quality crystals were obtained from pentane at $-40\text{ }^{\circ}\text{C}$. ^1H NMR (benzene- d_6 , 600 MHz): $\delta = 171.25$ (s, 3 H, O_2CMe), 33.36 (s, 2 H, C_6H_5), 17.86 (s, 2 H, C_6H_5), 15.06 (s, 1 H, p - C_6H_5), 12.40 (s, 6 H, $\text{CNCMe}_2\text{CH}_2\text{O}$), 42.84 (s, 18 H, $\text{CNCMe}_2\text{CH}_2\text{O}$) ppm. ^{11}B NMR (benzene- d_6 , 128 MHz): $\delta = 95.3$ ppm. IR (KBr): ν 2964 (m), 2930 (m), 2894 (m), 1591 (s, ν_{CN}), 1563 (m), 1463 (m), 1442 (m), 1368 (m), 1351 (m), 1275 (m), 1197 (m), 1162 (m), 1098 (m), 1024 (m) 960 (m) cm^{-1} . UV/Vis (CH_2Cl_2) λ_{max} (ϵ) = 486 (51), 585 ($104\text{ M}^{-1}\text{cm}^{-1}$) nm. Evans method: $\mu_{\text{eff}}(\text{C}_6\text{D}_6) = 4.8(2)\ \mu_{\text{B}}$. $\text{C}_{23}\text{H}_{32}\text{BCo}_3\text{NO}_5$ (500.3): calcd. C 55.22, H 6.45, N 8.40; found C 55.21, H 6.58, N 7.79. M.p. 161–164 $^{\circ}\text{C}$ (dec.).

To^MCoOAc-Catalyzed Oxidation of Cyclohexane: The oxidation of cyclohexane was performed under conditions similar to those previously reported by Hikichi et al.^[9d] A reaction flask was charged with cyclohexane (1.6 mL, 15 mmol, 2.45 M) and To^MCoOAc (1 μmol, 0.16 mM) dissolved in dichloromethane/acetonitrile (95 %, 1 mL). Upon the addition of 1,2-dichloroethane/acetonitrile (3.5 mL, 97.5 %) containing *m*CPBA (345 mg, 2.0 mmol) and nitrobenzene (30 μL, 300 μmol), the reaction was initiated and maintained at 25 °C. At each time point, an aliquot (0.2 mL) was removed and quenched with triphenylphosphine (10 mg, 38.1 μmol). The organic products were identified and quantified by GC–MS through the integration of the peak areas with respect to a known amount of the nitrobenzene standard. In this analysis, the quenched reaction product (10 μL) was added to dichloromethane (1.5 mL) and analyzed by GC–MS. Each chromatogram was obtained under the following conditions: split, 25:1; inlet temperature, 250 °C; initial oven temperature, 45 °C; temperature ramp, 15 °C min⁻¹ to 150 °C. From this data, the concentration of cyclohexanol versus time was analyzed with a nonlinear least-squares regression.

References

- (1) S. Trofimenko, *Scorpionates: The Coordination Chemistry of Polypyrazolylborate Ligands*, Imperial College Press, London, **1999**.
- (2) a) J. D. Jewson, L. M. Liable-Sands, G. P. A. Yap, A. L. Rheingold, K. H. Theopold, *Organometallics*, **1999**, *18*, 300–305; b) R. Han, I. B. Gorrell, A. G. Looney, G. Parkin, *J. Chem. Soc., Chem. Commun.*, **1991**, 717–719; c) J. L. Kisko, T. Hascall, G. Parkin, *J. Am. Chem. Soc.*, **1998**, *120*, 10561–10562.

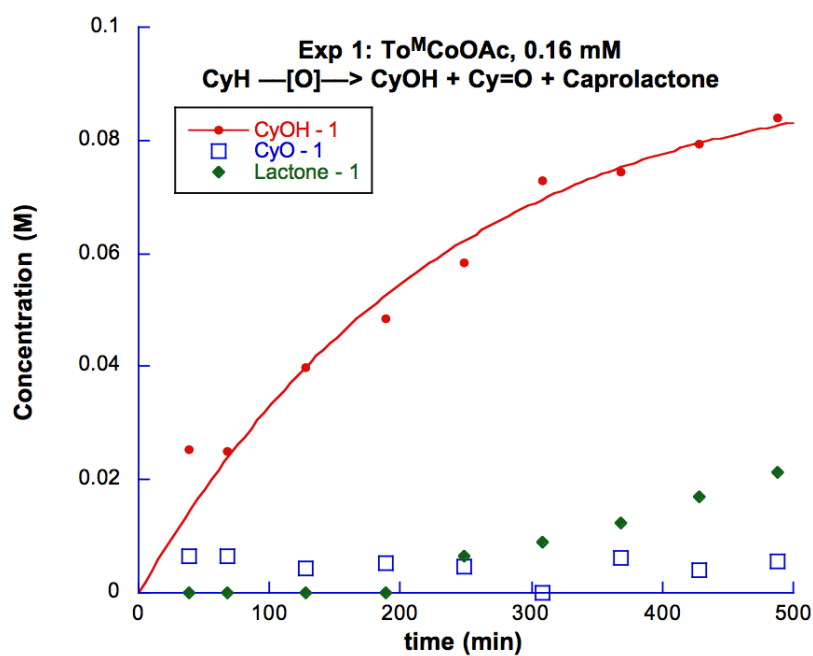
- (3) a) A. Kunishita, T. L. Gianetti, J. Arnold, *Organometallics*, **2012**, *31*, 372–380; b) N. Shirasawa, M. Akita, S. Hikichi, Y. Moro-oka, *Chem. Commun.*, **1999**, 417–418; c) F. A. Jové, C. Pariya, M. Scoblete, G. P. A. Yap, K. H. Theopold, *Chem. Eur. J.*, **2011**, *17*, 1310–1318.
- (4) a) D. M. Jenkins, T. A. Betley, J. C. Peters, *J. Am. Chem. Soc.*, **2002**, *124*, 11238–11239; b) R. E. Cowley, R. P. Bontchev, J. Sorrell, O. Sarracino, Y. Feng, H. Wang, J. M. Smith, *J. Am. Chem. Soc.*, **2007**, *129*, 2424–2425.
- (5) C. E. MacBeth, J. C. Thomas, T. A. Betley, J. C. Peters, *Inorg. Chem.*, **2004**, *43*, 4645–4662.
- (6) S. Hikichi, H. Komatsuzaki, M. Akita, Y. Moro-oka, *J. Am. Chem. Soc.*, **1998**, *120*, 4699–4710.
- (7) a) N. Kitajima, W. B. Tolman, *Prog. Inorg. Chem.* **1995**, *43*, 419–531; b) G. Parkin, *Chem. Rev.*, **2004**, *104*, 699–767.
- (8) J. W. Egan, B. S. Haggerty, A. L. Rheingold, S. C. Sendlinger, K. H. Theopold, *J. Am. Chem. Soc.*, **1990**, *112*, 2445–2446.
- (9) a) G. Strukul, *Catalytic Oxidations with Hydrogen Peroxide as Oxidant*, Kluwer Academic Publishers, Boston, **1992**; b) S. Hikichi, M. Akita, Y. Moro-oka, *Coord. Chem. Rev.*, **2000**, *198*, 61–87; c) T. Nagataki, Y. Tachi, S. Itoh, *Chem. Commun.*, **2006**, 4016–4018; d) J. Nakazawa, A. Yata, T. Hori, T. D. P. Stack, Y. Naruta, S. Hikichi, *Chem. Lett.*, **2013**, *42*, 1197–1199.
- (10) a) J. P. Jesson, S. Trofimenko, D. R. Eaton, *J. Am. Chem. Soc.*, **1967**, *89*, 3148–3158; b) A. L. Rheingold, L. M. Liable-Sands, S. Trofimenko, *Inorg. Chem.*, **2001**, *40*, 6509–6513.

- (11) A. L. Rheingold, R. L. Ostrander, B. S. Haggerty, S. Trofimenko, *Inorg. Chem.*, **1994**, *33*, 3666–3676.
- (12) D. Mukherjee, R. R. Thompson, A. Ellern, A. D. Sadow, *ACS Catal.*, **2011**, *1*, 698–702.
- (13) D. Mukherjee, A. Ellern, A. D. Sadow, *J. Am. Chem. Soc.*, **2012**, *134*, 13018–13026.
- (14) K. Wu, D. Mukherjee, A. Ellern, A. D. Sadow, W. E. Geiger, *New J. Chem.*, **2011**, *35*, 2169–2178.
- (15) a) B. Baird, A. V. Pawlikowski, J. Su, J. W. Wiench, M. Pruski, A. D. Sadow, *Inorg. Chem.*, **2008**, *47*, 10208–10210; b) S. R. Neal, A. Ellern, A. D. Sadow, *J. Organomet. Chem.*, **2011**, *696*, 228–234; c) S. Xu, Y. Magoon, R. R. Reinig, B. M. Schmidt, A. Ellern, A. D. Sadow, *Organometallics*, **2015**, *34*, 3508–3519.
- (16) H.-A. Ho, J. F. Dunne, A. Ellern, A. D. Sadow, *Organometallics*, **2010**, *29*, 4105–4114.
- (17) F. A. Cotton, D. M. L. Goodgame, M. Goodgame, *J. Am. Chem. Soc.*, **1961**, *83*, 4690–4699.
- (18) J. Krzystek, D. C. Swenson, S. A. Zvyagin, D. Smirnov, A. Ozarowski, J. Telsler, *J. Am. Chem. Soc.*, **2010**, *132*, 5241–5253.
- (19) N. Shirasawa, T. T. Nguyet, S. Hikichi, Y. Moro-oka, M. Akita, *Organometallics*, **2001**, *20*, 3582–3598.
- (20) G. R. Hanson, K. E. Gates, C. J. Noble, M. Griffin, A. Mitchell, S. Benson, *J. Inorg. Biochem.*, **2004**, *98*, 903–916.

- (21) H. Drulis, K. Dyrek, K. P. Hoffmann, S. K. Hoffmann, A. Weselucha-Birczynska, *Inorg. Chem.*, **1985**, *24*, 4009–4012.
- (22) a) A. Bencini, C. Benelli, D. Gatteschi, C. Zanchini, *Inorg. Chem.*, **1979**, *18*, 2137–2140; b) A. Romerosa, C. Saraiba-Bello, M. Serrano-Ruiz, A. Caneschi, V. McKee, M. Peruzzini, L. Sorace, F. Zanobini, *Dalton Trans.*, **2003**, 3233–3239; c) J. M. Zadrozny, J. Liu, N. A. Piro, C. J. Chang, S. Hill, J. R. Long, *Chem. Commun.*, **2012**, *48*, 3927–3929.
- (23) D. Mukherjee, A. Ellern, A. D. Sadow, *J. Am. Chem. Soc.*, **2010**, *132*, 7582–7583.
- (24) a) K. Uehara, S. Hikichi, M. Akita, *J. Chem. Soc., Dalton Trans.*, **2002**, 3529–3538; b) I. B. Gorrell, G. Parkin, *Inorg. Chem.*, **1990**, *29*, 2452–2456.
- (25) J. F. Dunne, D. B. Fulton, A. Ellern, A. D. Sadow, *J. Am. Chem. Soc.*, **2010**, *132*, 17680–17683.
- (26) S. Trofimenko, *J. Am. Chem. Soc.*, **1967**, *89*, 6288–6294.
- (27) a) A. V. Pawlikowski, T. S. Gray, G. Schoendorff, B. Baird, A. Ellern, T. L. Windus, A. D. Sadow, *Inorg. Chim. Acta*, **2009**, *362*, 4517–4525; b) R. E. Cowley, R. P. Bontchev, E. N. Duesler, J. M. Smith, *Inorg. Chem.*, **2006**, *45*, 9771–9779.
- (28) a) R. A. F. Tomás, J. C. M. Bordado, J. F. P. Gomes, *Chem. Rev.* **2013**, *113*, 7421–7469; b) J. K. Beattie, J. A. Klepetko, A. F. Masters, P. Turner, *Polyhedron*, **2003**, *22*, 947–965.
- (29) S. Hikichi, K. Hanaue, T. Fujimura, H. Okuda, J. Nakazawa, Y. Ohzu, C. Kobayashi, M. Akita, *Dalton Trans.*, **2013**, *42*, 3346–3356.

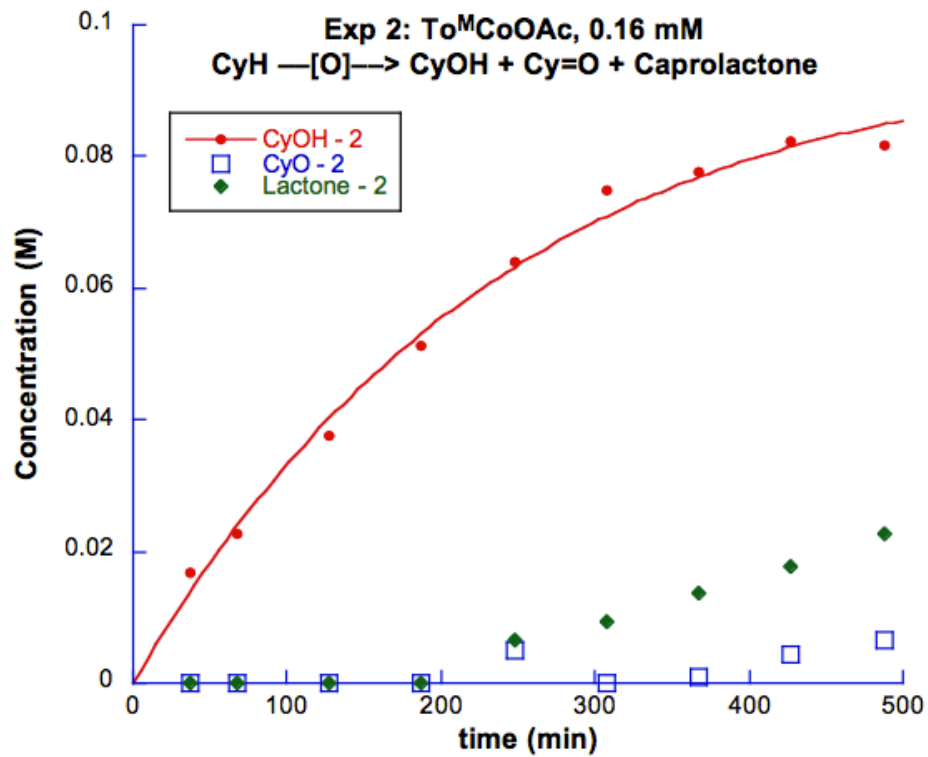
- (30) J. H. Espenson, *Chemical Kinetics and Reaction Mechanisms*, 2nd ed., McGraw-Hill, New York, **1995**.
- (31) J. F. Dunne, J. Su, A. Ellern, A. D. Sadow, *Organometallics*, **2008**, *27*, 2399–2401.
- (32) V. K. Aggarwal, Z. Gultekin, R. S. Grainger, H. Adams, P. L. Spargo, *J. Chem. Soc. Perkin Trans. 1*, **1998**, 2771–2782.

Supporting Information



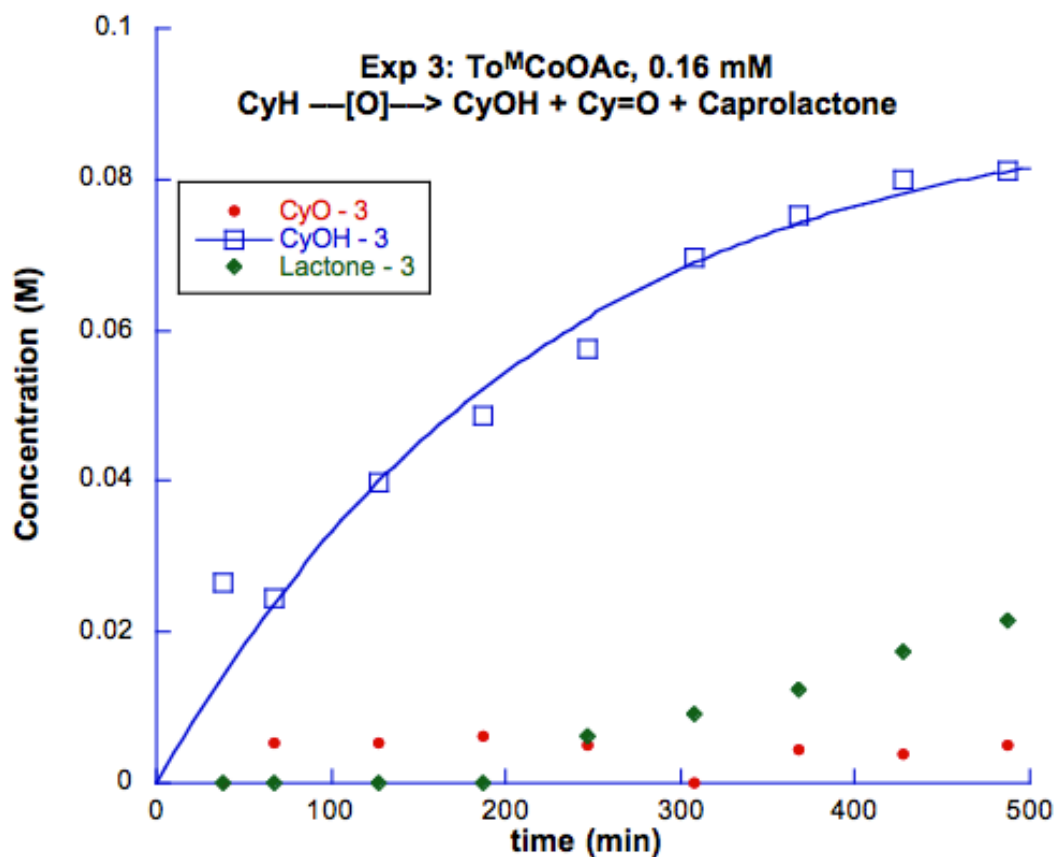
2.45*M2/(M3-M2)*(exp(-M2*x)-exp(-M3*x))		
	Value	Error
m2 = k1	0.0001641	1.646E-5
m3 = k2	0.003948	0.0007014
Chisq	0.000163	NA
R	0.9803	NA

Figure S1. Concentration vs. time plots for the oxidation of cyclohexane by To^MCoOAc (**5**) (0.16 mM) with mCBPA performed on a Chemspeed SwingXL Catalysis Platform. Figures S1-4 show reproducibility of the oxidation experiments. Species were quantified using GC-MS based on calibration to a nitrobenzene standard.



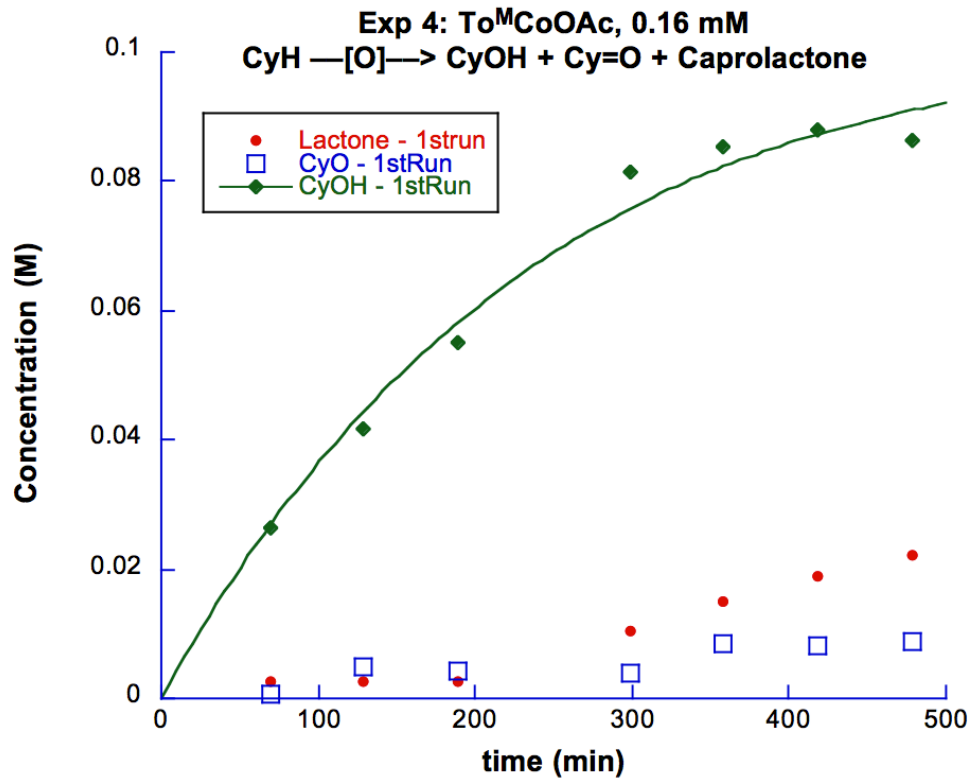
$2.45 \cdot M2 / (M3 - M2) \cdot (\exp(-M2 \cdot x) - \exp(-M3 \cdot x))$		
	Value	Error
$m2 = k1$	0.0001645	8.794E-6
$m3 = k2$	0.003803	0.000369
Chisq	4.821E-5	NA
R	0.9954	NA

Figure S2. Concentration vs. time plots for the oxidation of cyclohexane by $\text{To}^{\text{M}}\text{CoOAc}$ (5) (0.16 mM) with mCBPA performed on a Chemspeed SwingXL Catalysis Platform. Figures S1- S4 show reproducibility of the oxidation experiments. Species were quantified using GC-MS based on calibration to a nitrobenzene standard.



2.45*M2/(M3-M2)*(exp(-M2*x)-exp(-M3*x))		
	Value	Error
m2 = k1	0.0001668	1.813E-5
m3 = k2	0.004147	0.0007742
Chisq	0.0001862	NA
R	0.9761	NA

Figure S3. Concentration vs. time plots for the oxidation of cyclohexane by To^MCoOAc (5) (0.16 mM) with mCBPA performed on a Chemspeed SwingXL Catalysis Platform. Figures S1- S4 show reproducibility of the oxidation experiments. Species were quantified using GC-MS based on calibration to a nitrobenzene standard.



y = 2.45*M2/(M3-M2)*(exp(-M2...		
	Value	Error
m2	0.0001809	1.515E-5
m3	0.003891	0.000571
Chisq	7.912E-5	NA
R	0.9895	NA

Figure S4. Concentration vs. time plots for the oxidation of cyclohexane by To^MCoOAc (5) (0.16 mM) with mCBPA performed on a Chemspeed SwingXL Catalysis Platform. Figures S1- S4 show reproducibility of the oxidation experiments. Species were quantified using GC-MS based on calibration to a nitrobenzene standard.

**CHAPTER 3: RAPID AND ORDERED CARBONYLATION AND
OXYGENATION OF A COBALT(II) METHYL**

Modified from *Chemical Communications* **2017**, 53, 11020-11023. [‡] Copyright © 2017

The Royal Society of Chemistry.

Regina R. Reinig, Ellie L. Fought, Arkady Ellern, Theresa L. Windus, and

Aaron D. Sadow*

*Department of Chemistry, U.S. DOE Ames Laboratory, Iowa State University, Ames IA
50011-3111*

Abstract

The oxidative carbonylation of $\text{To}^{\text{M}}\text{CoMe}$ (**1**; To^{M} = tris(4,4-dimethyl-2-oxazolanyl)phenylborate) involves its rapid, reversible reaction with CO to form $\text{To}^{\text{M}}\text{Co}\{\text{C}(\text{O})\text{Me}\}\text{CO}$ (**2**) followed by rapid reaction with O_2 yielding $\text{To}^{\text{M}}\text{CoOAc}$ (**3**), in contrast to the slow direct carboxylation of $\text{To}^{\text{M}}\text{CoMe}$ by CO_2 .

Other Author's contributions

Ellie L. Fought: Responsible for DFT calculations, TDDFT calculations, and DFT Hessian calculations of $\text{To}^{\text{M}}\text{CoMe}$, $\text{To}^{\text{M}}\text{CoMe}(\text{CO})$, $\text{To}^{\text{M}}\text{Co}\{\text{C}(\text{O})\text{Me}\}\text{CO}$, and $\text{To}^{\text{M}}\text{CoOAc}$.

Introduction

Catalytic oxidative carbonylation reactions are generally proposed to involve metal-based oxidations.^{1,2} Consider, for example, catalytic production of benzoic acid from benzene, CO, and an oxidant. Palladium(II) mediates the combination of the arene, CO and water to afford benzoic acid, with palladium(0) generated as a byproduct. Then, the suggested catalytic cycle is completed by metal-based oxidation, rather than oxygenation of an acylpalladium intermediate. Interestingly, the proposed biosynthesis of the energy-carriers acetate or acetyl-CoA follows a conceptually similar outline, involving insertion of CO into a metal-methyl bond followed by metal-based oxidation and thiolysis (reductive elimination of the C–S bond) to form acetyl-CoA.^{3,4}

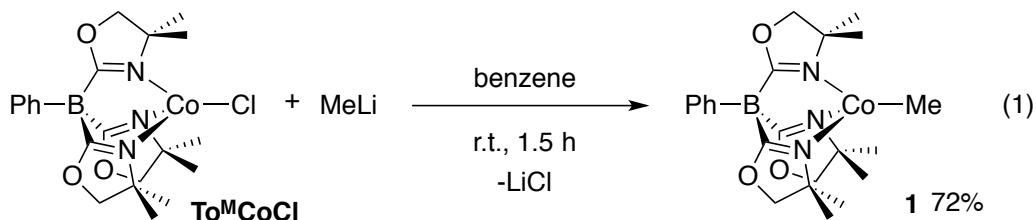
Oxygenation of metal-carbon bonds (or the reductive coupling followed by oxidation pathway) is key to many hydrocarbon functionalization schemes. On the other hand, acetate may be derived directly from CO₂ and methyl transition metal compounds. Although CO₂ is a substrate for acetogenesis, it is reduced by carbon monoxide dehydrogenase (CODH) to CO prior to its interaction with the metal-methyl.⁴ Likewise, oxidative carbonylation yields are sometimes improved under CO₂, yet CO is the ultimate source of carbonyl in the transformation. The distinction between CO/[O] in oxidative carbonylation versus CO₂ in carboxylation, in terms of their kinetic and thermodynamic parameters, is critical for the development of sustainable processes that utilize C₁ starting materials, such as methane, carbon monoxide, or carbon dioxide, because the processes must balance atom and energy economy with rate, yield, and selectivity to be viable.

Four-coordinate organocobalt(II) species are expected to be reactive toward CO, O₂ and CO₂ based on studies of bulky Tp^{*t*-Bu,Me}, Tp^{*i*Pr}, Tp^{*i*Pr₂}, and [PhTt^{*t*Bu}] (Tp^{R,R'} =

HB(3R,5R'-N₂C₃HR₂)₃; PhTt^{tBu} = PhB(CH₂S^tBu)₃).⁵⁻¹⁰ These reactions give either reduction or carbonylation products, oxidation or oxygenation, or carboxylation, respectively. CO affects one-electron reductions to give Tp^{tBu}CoCO or Tp^{iPr,Me}Co(CO)₂,^{6, 11} while carbonylation to cobalt(II) acyl species is also reported.^{7, 8} Oxygenation of organocobalt(II) to a cobalt alkyl peroxide could follow our observations for related zinc compounds, where kinetics of zinc alkyl oxygenation to alkylperoxides or alkoxides are consistent with a turnover-limiting bimolecular substitution of zinc alkyl with alkylperoxy radical (S_H2).¹² This oxygenation pathway avoids metal-centered oxidation. Indeed, alkylperoxy and acylperoxy metal compounds are intermediates in oxygenation reactions.^{13, 14} In the present work, a comparison of oxygenation, carbonylation and oxygenation, and carboxylation of To^MCoMe (**1**; To^M = tris(4,4-dimethyl-2-oxazolinyl)phenylborate) reveals that the kinetically favored pathway selectively produces acetate through an ordered, multistep sequence.

Results and Discussion

The reaction of To^MCoCl¹⁵ and MeLi at room temperature affords To^MCoMe (**1**) as a deep aquamarine solid (equation (1)).



The ¹H NMR spectrum of **1** showed signals at 15.44 and -12.05 ppm assigned to the oxazoline's methylene and methyl groups, respectively, on the basis of integration.

These signals were shifted downfield compared to $\text{To}^{\text{M}}\text{CoCl}$ (24.88 and 8.38 ppm, respectively). A resonance for the methyl ligand was not detected. The ^{11}B signal at 100 ppm was significantly shifted in comparison to the peak of $\text{To}^{\text{M}}\text{CoCl}$ (-29 ppm). A single ν_{CN} band at 1594 cm^{-1} in the IR spectrum suggested tridentate $\text{To}^{\text{M}}\text{Co}$ coordination. The UV-Vis spectrum of **1** (in Et_2O) revealed intense absorptions at 346 (ϵ : $1412\text{ M}^{-1}\text{cm}^{-1}$) and 697 (ϵ : $1078\text{ M}^{-1}\text{cm}^{-1}$) assigned to charge transfer transitions associated with the alkyl ligand on the basis of their large molar absorptivities ($>1000\text{ M}^{-1}\text{cm}^{-1}$) and the lack of similar signals in $\text{To}^{\text{M}}\text{CoCl}$. Weaker absorptions at 581 (ϵ : $388\text{ M}^{-1}\text{cm}^{-1}$) and 617 (ϵ : $424\text{ M}^{-1}\text{cm}^{-1}$) were attributed to $d\leftarrow d$ transitions. The effective magnetic moment of **1** ($4.2(2)\ \mu_{\text{B}}$), determined by Evans method, is consistent with a high-spin cobalt(II) ($S = 3/2$). The EPR spectrum of **1**, acquired at 5 K in glassed toluene, showed a rhombic spectrum with hyperfine coupling to the ^{59}Co center ($I = 7/2$) in a characteristic eight-line pattern.

The identity of **1** as the cobalt(II) methyl is unambiguously established by X-ray diffraction (Figure 1). The compound is slightly distorted from the C_{3v} symmetry suggested by solution-phase spectroscopy, with the C22 (methyl) displaced from the B-Co vector ($\angle\text{B-Co-Me}$: 172.83°). The Co1-C22 distance in $\text{To}^{\text{M}}\text{CoMe}$ ($1.994(2)\ \text{\AA}$) is within the range of similar pseudotetrahedral methylcobalt(II) species, which vary from 1.9 to $2.1\ \text{\AA}$.^{5,6,d,16,10, 17}

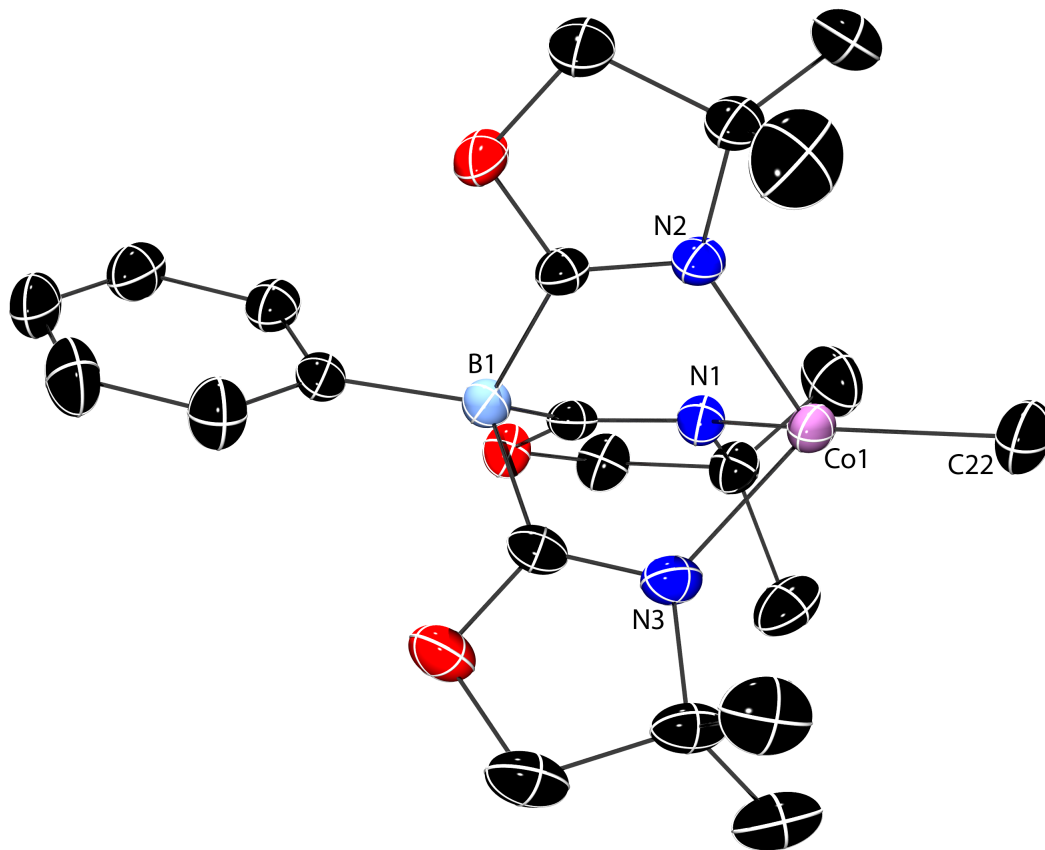


Figure 1. Rendered thermal ellipsoid diagram of $To^M CoMe$ (**1**) with ellipsoids plotted at 50% probability. H atoms are omitted for clarity.

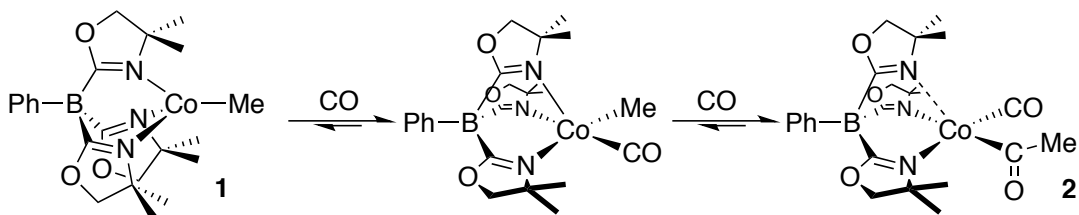
DFT calculations show that the quartet state ($S = 3/2$) is lowest energy and 49 kcal/mol lower than the doublet state. A TDDFT-calculated electronic transition at 310 nm (using implicit solvation) allows the experimental band at 346 nm to be classified as LMCT. This transition involves occupied orbitals mostly on the methyl carbon to unoccupied orbitals delocalized over Co, B, and the unsaturated C in the To^M ligand. Additional peaks at 602 nm, 740 nm and 743 nm, found both in $To^M CoMe$ and $To^M CoCl$ calculations, support the assignment of the weaker signals in the experimental spectra as $d \leftarrow d$ transitions. The strong, experimentally observed band at 697 nm was not evident, which may be due to the single configuration approach of TDDFT.

$\text{To}^{\text{M}}\text{CoMe}$ and CO (1 atm) rapidly react in benzene- d_6 or THF at room temperature, as evidenced by an immediate color change from blue to orange. The possible products of $\text{To}^{\text{M}}\text{CoMe}$ and CO include reduced $\text{To}^{\text{M}}\text{CoCO}$ or $\text{To}^{\text{M}}\text{Co}(\text{CO})_2$ species, $\text{To}^{\text{M}}\text{Co}(\text{Me})\text{CO}$ or its inserted isomer $\text{To}^{\text{M}}\text{CoC}(\text{O})\text{Me}$, $\text{To}^{\text{M}}\text{Co}\{\text{C}(\text{O})\text{Me}\}\text{CO}$, or $\text{To}^{\text{M}}\text{Co}\{\text{C}(\text{O})\text{Me}\}(\text{CO})_2$. A single ^{11}B NMR signal at -4 ppm, shifted upfield by 104 ppm from the value for **1**, suggested the formation of a single $\text{To}^{\text{M}}\text{Co}$ -containing product (**2**). The ^1H and ^{11}B NMR spectra did not vary from room temperature to -80 °C.

Evaporation of a solution of **2** to dryness overnight gives **1** as the only detectable $\text{To}^{\text{M}}\text{Co}$ -containing species, indicating that the reaction of **1** and CO is reversible. This reversibility hampers the isolation of **2**. Compound **2** persists in partially degassed solutions, while evaporation of all solvent and immediate redissolution affords a mixture of **1** and **2**. The reversible interaction of **1** and CO rules out formation of $\text{To}^{\text{M}}\text{CoCO}$ because the byproducts of $1 e^-$ reduction of **1** are unlikely to persist in a form that could re-methylate **2**.

An in situ IR spectrum of the orange THF solution, collected on a ZnSe ATR crystal, revealed bands at 1984, 1886, 1687, and 1655 cm^{-1} . The two higher energy peaks were assigned to coordinated CO ligands, with the higher energy peak at 1984 cm^{-1} significantly more intense. The lower energy absorptions were assigned to rotamers of the cobalt acyl group, and the signal at 1655 cm^{-1} was notably non-Gaussian shaped with a shoulder tailing toward the red. On the basis of DFT calculations (see below), we assign this shoulder to the ν_{CN} of a weakly or non-coordinated oxazoline, which typically appears at 1630 cm^{-1} .¹⁵ In addition, a peak at 1590 cm^{-1} , corresponding to the ν_{CN} of cobalt-coordinated oxazoline, was red-shifted by $\sim 4 \text{ cm}^{-1}$ in comparison to the $\text{To}^{\text{M}}\text{CoMe}$

starting material. For comparison, the IR spectrum of isolated $\text{Tp}^{i\text{Pr}_2}\text{Co}\{\text{C}(\text{O})\text{Et}\}\text{CO}$ contained a single CO band at 1999 cm^{-1} and an acyl peak at 1636 cm^{-1} .⁷ The IR spectrum of $\text{PhTt}^{i\text{Bu}}\text{Co}(\text{C}(\text{O})\text{Me})\text{CO}$ contained carbonyl ν_{CO} at 1993 cm^{-1} and acyl ν_{CO} at 1684 and 1663 cm^{-1} (assigned to rotomers).¹⁰ Thus, the interaction of $\text{To}^{\text{M}}\text{CoMe}$ and CO affords a mixture of $\text{To}^{\text{M}}\text{Co}\{\text{C}(\text{O})\text{Me}\}\text{CO}$ (**2**; major, 1984 , 1687 , and 1655 cm^{-1}) and $\text{To}^{\text{M}}\text{Co}(\text{Me})\text{CO}$ (minor, 1886 cm^{-1} ; Scheme 1).



Scheme 1. Reversible reaction of $\text{To}^{\text{M}}\text{CoMe}$ (**1**) and CO.

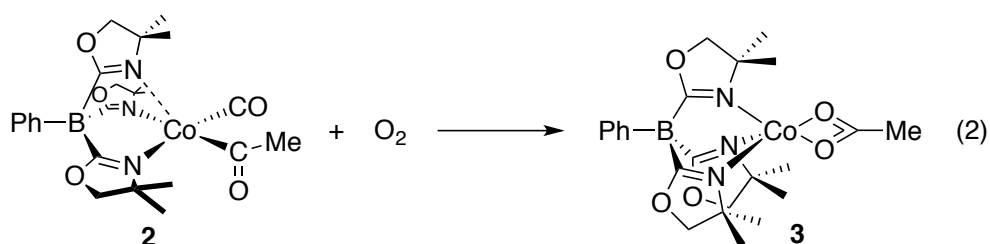
The effective magnetic moment of **2** is $2.7(1)\ \mu_{\text{B}}$ (determined by Evans method). This value is reduced with respect to high spin $\text{To}^{\text{M}}\text{CoMe}$ and is distinct from that of low-spin acyls $\text{PhTt}^{i\text{Bu}}\text{Co}\{\text{C}(\text{O})\text{R}\}\text{CO}$ ($\text{R} = \text{Me}, \text{Et}, \text{Ph}$; $\mu_{\text{eff}} = 1.9 - 2.1\ \mu_{\text{B}}$).¹⁰ The result for **2** does not fit the spin-only μ_{eff} for low spin $\text{Co}(\text{II})$ ($S = 1/2$ is $1.73\ \mu_{\text{B}}$). While high spin $\text{Co}(\text{I})$ ($S = 1$) would give a spin-only value of $2.83\ \mu_{\text{B}}$ (e.g., for $\text{Tp}^{\text{Np}}\text{CoCO}$ and $\text{Tp}^{i\text{Pr},\text{Me}}\text{CoCO}$, $\mu_{\text{eff}} = 3.1(1)\ \mu_{\text{B}}$), this type of product is ruled out above.^{11, 18} Instead, the effective magnetic moment of **2** is rationalized by a square pyramidal structure with a long axial $\text{Co}-\text{N}$ interaction on the basis of the typical moments for square planar cobalt(II) complexes.¹⁹⁻²¹ While a trigonal bipyramidal structure is also consistent with the magnetic moment, DFT calculations (described below) are more consistent with the square pyramidal geometry. A room temperature isotropic signal ($g_{\text{iso}} \approx 2.1$) in the EPR spectrum of **2** further supported the low spin assignment.^{22, 23} The UV-vis spectrum of **2**

was distinct from **1** and contained a broad, weak band from 760 to 1100 nm with a λ_{max} at 885 nm (ϵ : 305 M⁻¹cm⁻¹). In addition, a strong absorption tails from 200 to 600 nm.

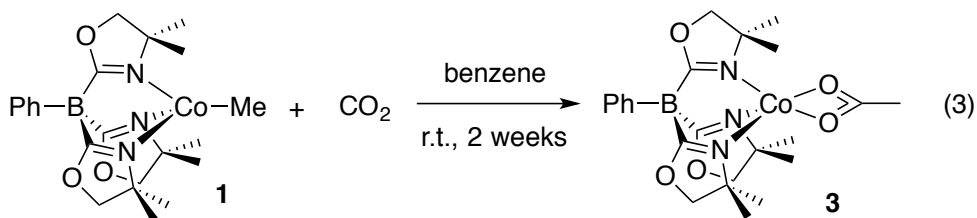
DFT calculations of To^MCo{C(O)Me}CO suggest a square pyramidal geometry for the optimized structure. The low spin state is 33 kcal/mol lower in energy than the high spin state. A TDDFT calculation with implicit solvation finds strong electronic transitions at 448 and 462 nm, with multiple smaller contributing transitions between 300 nm and 400 nm, consistent with experimental findings. In a DFT Hessian calculation, the frequency corresponding to the acyl carbonyl stretching mode is found at 1731 cm⁻¹ and the terminal carbonyl stretching is located at 2117 cm⁻¹. In addition, the calculated ν_{CN} stretches occur at 1636, 1667, and 1693 cm⁻¹ with the highest energy ν_{CN} being associated with the non-coordinated oxazoline. DFT calculations also suggest a square pyramidal geometry for the optimized structure of To^MCo(Me)CO. The low spin state is found to be 30 kcal/mol lower in energy than the high spin state. TDDFT calculations identify electronic transitions at 386 nm and 395 nm, which could be obscured by the multiple excitations found with the To^MCo{C(O)Me}CO species. The calculated frequency for the CO stretch at 2030 cm⁻¹ is lower energy than in To^MCo{C(O)Me}CO, providing support for the assignment of the experimental spectrum.

The orange carbonylated cobalt **2** rapidly reacts with O₂ to give purple To^MCoOAc (**3**, equation (2)), identified by comparison with an authentic sample's electronic spectrum (λ_{max} = 486 and 585 nm), ¹H and ¹¹B NMR spectra, and X-ray diffraction pattern.¹⁵ This reaction is sufficiently rapid and selective (and To^MCoOAc is easily crystallized) that this product is typically isolated from attempted crystallizations of the monocarbonyl acyl complex at -80 °C due to trace O₂ impurities. In situ-

generated **2** reacts with O₂ to afford **3** under a range of conditions, including 1 atm of O₂ at room temperature (analyzed by ¹H and ¹¹B NMR spectroscopy) or addition of O₂ as a THF solution (5 – 20 equiv. O₂, with or without excess CO, analyzed by UV-vis spectroscopy) at room temperature. Also, addition of a solution of O₂ (10-20 equiv.) to **2** at –100 °C provides an intermediate ($\lambda_{\text{max}} = 511, 550, \text{ and } 585 \text{ nm}$) that converts into **3** upon warming to room temperature. That is, the transformation of equation (2) is fairly robust.



also sluggishly provides $\text{To}^{\text{M}}\text{CoOAc}$ at room temperature over ~ 2 weeks. Thus, while CO_2 insertion is possible, carbonylation and oxygenation by O_2 is the kinetically favored pathway.



These three sets of experiments provide considerable insight into the oxidative carbonylation sequence. First, a pathway from **2** to **3** involving **1** as an intermediate via initial decarbonylation steps is unlikely because decarbonylation appears to be slow as indicated by the long drying times needed to fully convert **2** to **1**. Second, catalytic oxidation of CO to CO_2 by $\text{To}^{\text{M}}\text{Co}^{\text{II}}/\text{O}_2$ followed by carboxylation is ruled out as kinetically unfeasible by the experiment of equation (3).

Conclusion

We conclude that the sequence involving carbonylation of **1** to produce **2** followed by oxygenation to form **3** is kinetically favored. These results suggest that strategies for utilization of CO_2 involving carboxylation of organic compounds could benefit from an enzyme-inspired approach involving initial reduction to CO , CO migratory insertion, and finally oxidation rather than a direct, one-step carboxylation. At least in this case, a multistep compulsory-ordered pathway is considerably faster (and more selective) than random addition or direct insertion. Because acetate is important as a privileged ligand in oxidation catalysis and in CH activation pathways, the oxidative carbonylation studied here may be useful as part of selective hydrocarbon

functionalization schemes. We are currently investigating related cobalt(II) alkyl and aryl compounds in pursuit of catalytic conversions.

Experimental Section

General Procedures. All reactions were performed using standard Schlenk techniques under an atmosphere of dry argon. Benzene and diethyl ether were dried and deoxygenated using an IT PureSolv system. Benzene- d_6 was degassed with freeze-pump-thaw cycles, heated to reflux over a Na/K alloy, and then vacuum transferred. To^MCoCl and To^MCoOAc (**3**) were synthesized following the reported procedure.⁶ 1H and ^{11}B NMR spectra were collected on a Bruker Avance III 600 spectrometer. ^{11}B NMR spectra were referenced to an external sample of $BF_3 \cdot Et_2O$. Infrared spectra were measured on a Bruker Vertex 80 FTIR spectrometer. EPR were obtained on an X-band Elecsys 580 FT-EPR spectrometer in continuous wave mode. UV-Vis spectra were recorded on an Agilent 8453 UV-vis spectrophotometer. The electronic spectrum of To^MCoOAc was not previously disclosed and is reported here. Elemental analyses were performed using a Perkin-Elmer 2400 Series II CHN/S. Single crystal X-ray diffraction data was collected on an APEX II.

To^MCoMe (1). Methylolithium (1.6 M in diethyl ether, 1.00 mL, 1.6 mmol) was added to a solution of To^MCoCl (0.510 g, 1.07 mmol) in benzene (50 mL). The green reaction mixture was stirred for 1.5 h, the salt byproduct was removed by filtration, and the solvent was evaporated to afford To^MCoMe as a dark aquamarine solid (0.353 g, 0.773 mmol, 72%). X-ray quality crystals were obtained from pentane at -40 °C. 1H NMR (benzene- d_6 , 600 MHz): δ 15.44 (s, 6 H, $CNCMe_2CH_2O$), 14.18 (s, 2 H, C_6H_5), 10.61 (s, 2 H, C_6H_5), 8.88 (s, 1 H, $p-C_6H_5$), -12.05 (s, 18 H, $CNCMe_2CH_2O$). ^{11}B NMR (benzene-

d_6 , 128 MHz): δ 100.3. IR (KBr, cm^{-1}): ν 2967 (m), 2925 (m), 2897 (m), 2861 (m), 1594 (s, ν_{CN}), 1462 (m), 1386 (m), 1352 (m), 1269 (m), 1194 (m), 1160 (m), 960 (m). UV-vis (Et_2O) $\lambda_{\text{max}} = 346$ (ϵ : $1412 \text{ M}^{-1}\text{cm}^{-1}$), 581 (ϵ : $388 \text{ M}^{-1}\text{cm}^{-1}$), 617 (ϵ : $424 \text{ M}^{-1}\text{cm}^{-1}$), 697 (ϵ : $1078 \text{ M}^{-1}\text{cm}^{-1}$). $\mu_{\text{eff}}(\text{C}_6\text{D}_6) = 4.2(2) \mu_{\text{B}}$ as determined by the Evans method. Anal. Calcd. for $\text{C}_{22}\text{H}_{32}\text{BCoN}_3\text{O}_3$: C, 57.91; H, 7.07; N, 9.21 Found: C, 57.93; H, 7.18; N, 9.20. Mp. 235-237 °C, dec.

References

- (1) B. Gabriele, G. Salerno and M. Costa, in *Catalytic Carbonylation Reactions*, ed. M. Beller, Springer Berlin Heidelberg, Berlin, Heidelberg, **2006**, pp. 239-272.
- (2) D. J. Díaz, A. K. Darko and L. McElwee-White, *Eur. J. Org. Chem.*, **2007**, 4453-4465.
- (3) P. A. Lindahl, *J. Biol. Inorg. Chem.*, **2004**, *9*, 516-524.
- (4) S. W. Ragsdale and E. Pierce, *Biochim. Biophys. Acta, Proteins Proteomics*, **2008**, *1784*, 1873-1898.
- (5) A. Kunishita, T. L. Gianetti and J. Arnold, *Organometallics*, **2012**, *31*, 372-380.
- (6) J. D. Jewson, L. M. Liable-Sands, G. P. A. Yap, A. L. Rheingold and K. H. Theopold, *Organometallics*, **1999**, *18*, 300-305.
- (7) N. Shirasawa, M. Akita, S. Hikichi and Y. Moro-oka, *Chem. Commun.*, **1999**, 417-418.
- (8) N. Shirasawa, T. T. Nguyet, S. Hikichi, Y. Moro-oka and M. Akita, *Organometallics*, **2001**, *20*, 3582-3598.

- (9) S. Yoshimitsu, S. Hikichi and M. Akita, *Organometallics*, **2002**, *21*, 3762-3773.
- (10) J. A. DuPont, M. B. Coxey, P. J. Schebler, C. D. Incarvito, W. G. Dougherty, G. P. A. Yap, A. L. Rheingold and C. G. Riordan, *Organometallics*, **2007**, *26*, 971-979.
- (11) J. L. Detrich, O. M. Reinaud, A. L. Rheingold and K. H. Theopold, *J. Am. Chem. Soc.*, **1995**, *117*, 11745-11748.
- (12) D. Mukherjee, A. Ellern and A. D. Sadow, *J. Am. Chem. Soc.*, **2012**, *134*, 13018-13026.
- (13) S. Hikichi, H. Komatsuzaki, M. Akita and Y. Moro-oka, *J. Am. Chem. Soc.*, **1998**, *120*, 4699-4710.
- (14) S. Hikichi, K. Hanaue, T. Fujimura, H. Okuda, J. Nakazawa, Y. Ohzu, C. Kobayashi and M. Akita, *Dalton Trans.*, **2013**, *42*, 3346-3356.
- (15) R. R. Reinig, D. Mukherjee, Z. B. Weinstein, W. Xie, T. Albright, B. Baird, T. S. Gray, A. Ellern, G. J. Miller, A. H. Winter, S. L. Bud'ko and A. D. Sadow, *Eur. J. Inorg. Chem.*, **2016**, 2486-2494.
- (16) R. E. Cowley, R. P. Bontchev, E. N. Duesler and J. M. Smith, *Inorg. Chem.*, **2006**, *45*, 9771-9779.
- (17) P. J. Schebler, B. S. Mandimutsira, C. G. Riordan, L. M. Liabe-Sands, C. D. Incarvito and A. L. Rheingold, *J. Am. Chem. Soc.*, **2001**, *123*, 331-332.
- (18) J. L. Detrich, R. Konečný, W. M. Vetter, D. Doren, A. L. Rheingold and K. H. Theopold, *J. Am. Chem. Soc.*, **1996**, *118*, 1703-1712.

- (19) E. K. Barefield, D. H. Busch and S. M. Nelson, *Q. Rev. Chem. Soc.*, **1968**, 22, 457-498.
- (20) R. Poli, *Chem. Rev.*, **1996**, 96, 2135-2204.
- (21) M. Cibian and G. S. Hanan, *Chem. Eur. J.*, **2015**, 21, 9474-9481.
- (22) P. H. Haffner and J. E. Coleman, *J. Biol. Chem.*, **1973**, 248, 6630-6636.
- (23) D. M. Jenkins, A. J. Di Bilio, M. J. Allen, T. A. Betley and J. C. Peters, *J. Am. Chem. Soc.*, **2002**, 124, 15336-15350.

**CHAPTER 4: CARBOXYLATES FROM REVERSIBLE CARBONYLATION
FOLLOWED BY OXYGENATION OF A SERIES OF ORGANOCOBALT
COMPOUNDS**

Modified from a paper to be submitted to a journal

Regina R. Reinig, Ellie L. Fought, Arkady Ellern, Theresa L. Windus, Aaron D. Sadow*

Abstract

The organocobalt scorpionate compounds To^MCoR ($To^M = \text{tris}(4,4\text{-dimethyl-2-oxazolinyl})\text{phenylborate}$; $R = \text{Bn}$, **1**; CH_2SiMe_3 , **2**; Ph , **3**; Et , **4**; ^nBu , **5**; Me , **6**) are synthesized to investigate the impact of the organometallic moiety in carbonylation, oxidation, and carboxylation reactions. The compounds are prepared by reaction of To^MCoCl with the corresponding organolithium or organopotassium reagents. Compounds **1** – **6** were characterized by 8-line hyperfine coupling to cobalt in EPR spectra and solution phase magnetic measurements ($\mu_{\text{eff}} = 4 - 5 \mu_B$) as containing a high-spin cobalt(II) center. The UV-Vis spectra revealed a diagnostic band at ca. 700 nm ($\epsilon > 1000 \text{ M}^{-1}\text{cm}^{-1}$) associated with the tetrahedral organocobalt(II) center and assigned to a $d \leftarrow d$ transition on the basis of configuration interaction (CI) calculations. Complexes **1** – **6** react rapidly with CO to form equilibrating mixtures of the low spin organocobalt carbonyl $To^MCo(R)CO$, acyl $To^MCoC(=O)R$, and acyl carbonyl $To^MCo\{C(O)R\}CO$. The ^1H and ^{11}B NMR spectra contained only one set of signals for the CO-treated solutions, whereas the solution-phase IR spectra contained up to two ν_{CO} and three $\nu_{\{C(=O)R\}}$ signals with intensities varying depending on the R group ($R = \text{Bn}$, **7**; CH_2SiMe_3 , **8**; Ph , **9**; Et , **10**; ^nBu , **11**; Me , **12**). Single crystal X-ray diffraction of $To^MCo\{C(O)Et\}CO$ (**10**) supported its assignment as a square pyramidal cobalt(II) acyl carbonyl complex. Upon evaporation

of volatiles, solutions of **8** – **12** revert to the CO-free organocobalt starting materials **2** – **6**, whereas attempts to isolate benzyl-derived **7** affords an unusual alkoxy ketone species, characterized by single crystal X-ray diffraction. Despite these differences observed in the carbonylation of **1** – **6** as a result of varying the R group, compounds **7** – **12** all react rapidly with O₂ through an oxygenation pathway to afford the corresponding carboxylate compounds To^MCoO₂CR (R = Bn, **13**; CH₂SiMe₃, **14**; Ph, **15**; Et, **16**; ⁿBu, **17**; Me, **18**). In contrast, the insertion of CO₂ into the Co–C bond in **7** – **12** requires several days to weeks.

Introduction

Oxidative carbonylation, an organotransition metal-mediated route to carboxylates, typically proceeds by a sequence in which a metal hydrocarbyl reacts with CO to form an acyl, followed by hydrolysis and reductive elimination. Under catalytic conditions, oxidation and metalation completes the cycle to generate a new metal hydrocarbyl. This kind of pathway has been proposed for palladium-catalyzed oxidative carbonylation of arenes as well as catalytic carboxylations of amides to give carbamates and ureas.^{1,2} Remarkably, the biological synthesis of acetate also involves carbonylation of an organometallic nickel methyl to give an acetyl group that is transferred to acetyl Co-A to form a thioacetate and subsequently hydrolyzed.³⁻⁶ The fact that carbon dioxide, which serves as the source of both carbon atoms in acetate, is not incorporated into acetate by direct insertion into the metal-methyl is perhaps even more remarkable. Instead, CO₂ is reduced both to the methyl and to CO by CO dehydrogenase.^{4,5} Similarly in synthetic chemistry, the synthesis of acetate or acetic acid via the Monsanto process involves CO and oxidation rather than direct insertion of CO₂. These oxidative

carbonylations result in oxygenation of an acyl to carboxylate, but the pathway invokes hydrolysis followed by oxidation at the metal center rather than by direct oxygenation of the metal acyl species. The distinction between oxidation catalysis (including reactions mediated by oxidases) and oxygenation catalysis (catalyzed by oxygenases) affects the choice of reagent as the oxygen source and oxidant, as well as the conditions and occasions for their use. Nonetheless, acyl species are proposed as likely intermediates in multiple pathways, and identifying the conditions by which acyl metal compounds form and their subsequent reaction pathways are key to developing new transformations.

Routes to acyl compounds involve an insertive combination of CO and organometallic compounds. For tetrahedral organometallic compounds, however, a number of species and pathways can result from interactions with CO. The coordination of CO to the metal center gives a metal hydrocarbyl carbonyl adduct, which can undergo insertion to form an isomeric acyl species. Further coordination of one or two CO ligands is likely influenced by the steric properties of the ancillary ligand or acyl group and by the electronic configuration of the metal center. Alternatively, reactions of organometallics with CO can result in $1 e^-$ reduction to form carbonyl adducts.^{7,8} Reduction is typically observed with bulky ancillary ligands, such as in the reactions of CO and $\text{Tp}^{\text{tBuMe}}\text{CoMe}$ or $\text{PhTp}^{\text{tBu}}\text{FeMe}$ that form cobalt(I) or iron(I) carbonyls respectively. Homolysis of tetrahedral cobalt alkyls is also proposed as the first step in the rearrangement of $\text{Tp}^{\text{PhMe}}\text{Co}^{\text{tBu}}$ to $\text{Tp}^{\text{PhMe}}\text{CoCH}_2\text{CHMe}_2$.⁹ Interestingly, $\text{Tp}^{\text{R}'}\text{CoEt}$ ($\text{Tp}^{\text{R}'} = \text{HB}(3,5\text{-}i\text{Pr}_2\text{-N}_2\text{C}_3\text{H})_3, \text{HB}(3,4,5\text{-Me}_3\text{N}_2\text{C}_3)_3$) and CO provides first the acylcobalt carbonyl species, which forms $\text{Tp}^{\text{R}'}\text{CoCO}$ upon removal of volatiles and this is suggested to occur by homolysis of $\text{Tp}^{\text{R}'}\text{CoEt}(\text{CO})$.¹⁰ In contrast, allyl and benzyl derivatives

$\text{Tp}^{\text{R}}\text{Co}\{\text{C}(\text{O})\text{R}\}\text{CO}$ ($\text{R} = \text{CH}_2\text{C}_6\text{H}_4\text{OMe}, \text{C}_3\text{H}_5$) are isolable. The fate of the organometallic ligand in these reductive pathways has not been identified.

Conceivably, a metal acyl species in equilibrium with the metal alkyl could undergo ligand rearrangement to form a ketone that then inserts into a cobalt acyl species to form an OC–CO moiety. It is worth noting that such C–C bond formation to form OC–CO is extremely unusual, and to the best of our knowledge, is not known to occur under carbonylation conditions. Instead, complexes that contain coordination of an OC–CO moiety to the metal center are typically synthesized by ligand substitution reactions with an organic compound that already contains this structural feature.¹¹⁻¹³

Previously, we reported the synthesis of $\text{To}^{\text{M}}\text{CoMe}$ by reaction of $\text{To}^{\text{M}}\text{CoCl}$ with MeLi confirming that salt metathesis is a viable route to cobalt(II) organometallic complexes despite the hard basic nature of the To^{M} ancillary ligand that can at times instead result in transmetalation to Mg or Li rather than the desired alkylation.^{14,15} $\text{To}^{\text{M}}\text{CoMe}$ reacts readily with CO to form $\text{To}^{\text{M}}\text{Co}\{\text{C}(\text{O})\text{Me}\}\text{CO}$ followed by rapid reaction with O_2 to produce $\text{To}^{\text{M}}\text{CoOAc}$. Direct insertion of CO_2 into $\text{To}^{\text{M}}\text{CoMe}$ also affords $\text{To}^{\text{M}}\text{CoOAc}$, but the reaction requires several weeks. The observation that the multistep pathway is, at least in this case, significantly faster than direct insertion, motivated us to expand our study to other R groups to determine if this reactivity is general to other alkyl and aryl groups.

Herein, we prepare a series of alkyl, aryl, and benzyl cobalt(II) compounds supported by a tris(oxazolinyl)borate ligand. The spectroscopic, electronic, and structural features are compared within the series of organocobalt(II) compounds and to halide and pseudo-halide analogues, to identify signatures of classes of these paramagnetic

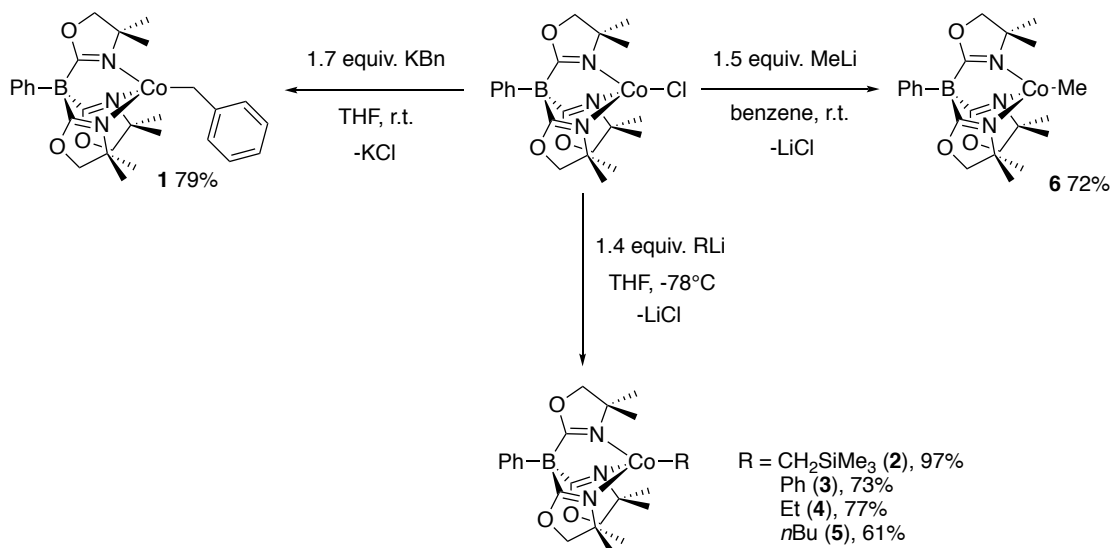
compounds and discover distinguishing features that might parallel reactivity differences within the series of compounds and to related four-coordinate cobalt alkyls. The products of carbonylation are characteristic of the hydrocarbyl ligand, as identified by signals observed in the infrared spectra in carbonyl and acyl C=O stretching regions. These carbonylation products are oxygenated by reaction with O₂, which occurs rapidly, in contrast to sluggish reactions of the organocobalt compounds and carbon dioxide.

Results and Discussion

Synthesis and characterization of To^MCoR. The organometallic cobalt(II) complexes To^MCoR (R = Bn (**1**), CH₂SiMe₃ (**2**), Ph (**3**), Et (**4**), *n*Bu (**5**), Me (**6**); To^M = tris(4,4-dimethyl-2-oxazoliny)phenylborate) are prepared by salt metathesis reactions involving excess (1.4 – 1.7 equiv.) organopotassium (PhCH₂K) or organolithium (Me₃SiCH₂Li, PhLi, EtLi, *n*BuLi, MeLi) reagents and To^MCoCl (Scheme 1).¹⁶ To^MCoMe and To^MCoBn are the most straightforward to prepare and form in good yields at room temperature under dilute conditions. For example, To^MCoBn (**1**, 0.129 g, 0.242 mmol, 78.7%) is synthesized from To^MCoCl (0.308 mmol, 0.031 M) and 1.7 equiv. of KBn in THF at room temperature.

Dilute conditions (~0.02 M) are also effective on a ~0.03 mmol scale for synthesizing organocobalt(II) complexes **2** – **5** in good yield (>50%). In contrast, preparative scale reactions for **2** – **5** (>0.06 mmol) under these dilute conditions consistently give less than 30% yield. Instead, **2** – **5** require more concentrated conditions (~0.1 M) and low temperature. Using 0.1 M To^MCoCl, 1.4 equiv. of alkyllithium, and mixtures cooled to –78 °C, To^MCoCH₂SiMe₃ (**2**), To^MCoPh (**3**), To^MCoEt (**4**) and To^MCo^{*n*}Bu (**5**) are reproducibly synthesized in greater than 0.20 mmol quantities and

>60% yields. These conditions provide spectroscopically pure and analytically pure $\text{To}^{\text{M}}\text{CoR}$. Signals for $\text{To}^{\text{M}}\text{CoCl}$ in NMR and UV-vis spectra, even as a trace impurity, were not detected for these samples.



Scheme 1. Synthesis of $\text{To}^{\text{M}}\text{CoBn}$ (1), $\text{To}^{\text{M}}\text{CoCH}_2\text{SiMe}_3$ (2), $\text{To}^{\text{M}}\text{CoPh}$ (3), $\text{To}^{\text{M}}\text{CoEt}$ (4), $\text{To}^{\text{M}}\text{Co}^n\text{Bu}$ (5), and $\text{To}^{\text{M}}\text{CoMe}$ (6).

NMR spectroscopy provided an initial assay for alkyl- or arylation of $\text{To}^{\text{M}}\text{CoCl}$. Despite the paramagnetic nature of these cobalt(II) complexes, both ^1H and ^{11}B NMR spectroscopy clearly distinguished $\text{To}^{\text{M}}\text{CoCl}$ from the organocobalt(II) complexes by their chemical shifts (Table 1). The To^{M} -based chemical shifts were consistent with C_{3v} -symmetric species and appeared in similar regions for compounds 1 – 6. For example, the signals attributed to the oxazoline methyl groups ranged from -9.6 to -14.5 ppm, which was more than 15 ppm upfield compared to corresponding signals in $\text{To}^{\text{M}}\text{CoCl}$ at 8.38 ppm. The oxazoline methylene peaks' range was even smaller, from 14.8 – 16.7 ppm, whereas the corresponding signal in $\text{To}^{\text{M}}\text{CoCl}$ was observed at 24.88 ppm.

While the chemical shifts for the To^{M} ligand were consistent across the organometallic complexes, the detectable signals for the alkyl and aryl ligands were wide ranging. For example, the benzyl ligand resonances were observed at 34, -77, and -89 ppm. ^1H NMR peaks that might be attributed to hydrogen on the α -carbon were not detected in any of the alkyl compounds, which is typical for organic groups in close proximity to paramagnetic centers.

The ^{11}B NMR spectra of these complexes each contained one peak, the chemical shift of which ranged from 86.6 to 116.7 ppm. These signals were far downfield compared to the resonances observed for the chloride (-29 ppm) as well as diamagnetic species resulting from transmetalation of To^{M} (ca. -17 ppm). Overall, the ^1H and ^{11}B NMR spectra associated with the To^{M} ligand in the series of organometallic species are comparable, whereas the chemical shifts for the oxazolinylborate ligand in $\text{To}^{\text{M}}\text{CoX}$ (e.g. $\text{X} = \text{Cl}, \text{O}^i\text{Bu}, \text{OAc}$) complexes vary considerably. These data suggest that the organometallic compounds' electronic structures, which are responsible for the paramagnetic chemical shifts, are similar between simple alkyl, β -H containing alkyl, trimethylsilyl-substituted alkyl, aryl, and benzyl ligands.

Table 1. NMR Data for $\text{To}^{\text{M}}\text{CoR}$ ($\text{R} = \text{Me}, \text{Bn}, \text{CH}_2\text{SiMe}_3, \text{Ph}, \text{Et}, \text{and } ^n\text{Bu}$). N.D. indicates not detected. ^aSee reference.¹⁵ ^bSee reference.¹⁶

Compound	^1H NMR (ppm)				^{11}B NMR (ppm)
	To^{M} (CH_2)	To^{M} (CH_3)	To^{M} (C_6H_5)	R	
$\text{To}^{\text{M}}\text{CoBn}$ (1)	16.33	-12.46	14.90, 10.96, 9.14	34.47, -89.01, -77.45	100.4
$\text{To}^{\text{M}}\text{CH}_2\text{SiMe}_3$ (2)	15.73	-9.58	12.72, 10.08, 8.54	8.54	86.6
$\text{To}^{\text{M}}\text{CoPh}$ (3)	16.73	-13.68	15.74, 11.30, 9.42	73.95, 10.61	107.7
$\text{To}^{\text{M}}\text{CoEt}$ (4)	14.85	-14.45	15.95, 11.33, 9.42	-31.31	116.7
$\text{To}^{\text{M}}\text{Co}^n\text{Bu}$ (5)	14.88	-14.31	15.91, 11.38, 9.47	14.21, -2.7	115.0
$\text{To}^{\text{M}}\text{CoMe}$ (6) ^a	15.44	-12.05	14.18, 10.61, 8.88	n.d.	100.3
$\text{To}^{\text{M}}\text{CoCl}$ ^b	24.88	8.38	4.77, 4.25, -0.41	n.a.	-29

A single ν_{CN} band at $\sim 1590 \text{ cm}^{-1}$ in the IR spectra of **1** – **6** provided additional support for tridentate coordination of the To^{M} ligand to cobalt. Signals associated with C=N stretching modes of non-coordinated oxazolinyl groups ($\sim 1630 \text{ cm}^{-1}$) were not detected. In the series, $\text{To}^{\text{M}}\text{CoPh}$ displayed the lowest energy ν_{CN} band at 1582 cm^{-1} , $\text{To}^{\text{M}}\text{CoEt}$ the highest at 1592 cm^{-1} , while $\text{To}^{\text{M}}\text{CoBn}$ was equivalent to that observed for $\text{To}^{\text{M}}\text{CoCl}$ (1588 cm^{-1}). The IR spectrum of **1** provided additional evidence of benzylation, revealing a new aromatic $\nu_{\text{C-H}}$ mode at 3012 cm^{-1} in addition to the aromatic To^{M} bands at ca. 3070 and 3050 cm^{-1} . The aromatic $\nu_{\text{C-H}}$ bands of $\text{To}^{\text{M}}\text{CoPh}$ were more intense than in the spectra of **3**, **4**, or **5**, but lacked additional bands. We attributed these observations to overlapping modes for CoPh and BPh.

The UV-vis spectra (Figure 1, Table 2) of compounds **1** – **6** contained intense absorptions at ca. 350 nm (ϵ : $1400\text{-}2200 \text{ M}^{-1}\text{cm}^{-1}$) and 700 nm (ϵ : $1200\text{-}1500 \text{ M}^{-1}\text{cm}^{-1}$) and two weaker bands at ca. 570 nm (ϵ : $300\text{-}400 \text{ M}^{-1}\text{cm}^{-1}$) and 620 nm (ϵ : $200\text{-}450 \text{ M}^{-1}\text{cm}^{-1}$). The former features are characteristic of these organometallic complexes and are attributed to transitions associated with the alkyl or aryl ligand on the basis of the lack of equivalent bands in $\text{To}^{\text{M}}\text{CoCl}$. The latter bands in the region of $500\text{-}650 \text{ nm}$ were attributed to $d \leftarrow d$ transitions and were similar to the bands observed for $\text{To}^{\text{M}}\text{CoCl}$ at 568 nm ($\epsilon = 362 \text{ M}^{-1} \text{ cm}^{-1}$) and 635 nm ($\epsilon = 641 \text{ M}^{-1} \text{ cm}^{-1}$). The observed $d \leftarrow d$ transitions are related to the ${}^4\text{T}_1(\text{P}) \leftarrow {}^4\text{A}_2(\text{F})$ transition in $[\text{CoCl}_4]^{2-}$ that split in lower symmetry. Across the organometallic compounds, the wavelengths of these $d \leftarrow d$ bands do not vary very much, further supporting the idea, from the NMR chemical shift analysis discussed above, that their electronic structures are similar. It is worth noting that the benzyl compound **1**, which also showed unique reactivity (see below), contained an additional

strong absorption at 439 nm (ϵ : 1964 M⁻¹cm⁻¹; see Figure 1) as well as the absorptions at 339 (ϵ : 3205 M⁻¹cm⁻¹), 589 nm (ϵ : 332 M⁻¹cm⁻¹), 628 (ϵ : 365 M⁻¹cm⁻¹), and 704 nm (ϵ : 1444 M⁻¹cm⁻¹).

The spectroscopic features assigned to transitions associated with the organometallic moiety on the basis of their absence in halide, alkoxide, and carboxylate analogues, are similar for compounds **1** – **6**, irrespective of methyl, ethyl, butyl, phenyl, trimethylsilylmethyl, or benzyl groups that might be expected to have variable bonding and orbital energies. A possible interpretation of these observations is that the transfers are delocalized to include wavefunctions from the To^M ligand (which is common to the series of compounds), and the allowedness of the transfer is enhanced by the organometallic ligand. This idea, at least in part, is supported by comparison with the spectra of reported for Tp^{iPr₂}CoR complexes (Tp^{iPr₂} = tris(3,5-diisopropylpyrazolyl)borate). For example, the spectrum of Tp^{iPr₂}CoEt, which had maxima at λ = 388 (1030 M⁻¹cm⁻¹), 580, 610, and 690 nm (810 M⁻¹cm⁻¹), contained similar features as To^MCoEt.¹⁰ The absorption at 705 nm for To^MCoEt was 15 nm lower energy than the corresponding band in Tp^{iPr₂}CoEt at 690 nm, whereas the d←d bands appeared at similar energies. From these observations, we suggest that the wavefunctions contributed by the To^M and Tp^{iPr₂} affect the energy of the transition. Tp^{iPr₂}Co-*p*-tol also contains an intense absorption at 697 nm (1304 M⁻¹cm⁻¹).¹⁷ However, the intense absorption at ca. 700 nm is not a universal features of cobalt(II) alky complexes. For example, [PhTt^{*t*-Bu}]CoCl contains absorptions at 664 (880 M⁻¹cm⁻¹) and 695 nm (740 M⁻¹cm⁻¹), which are more intense than any of the absorptions present in the corresponding methyl phenyl, or benzyl complex (e.g. [PhTt^{*t*-Bu}]CoMe 632 (570 M⁻¹cm⁻¹) and 725 nm

(574 $M^{-1}cm^{-1}$); [PhTt^{t-Bu}]CoPh (643 (249 $M^{-1}cm^{-1}$), 719 (359 $M^{-1}cm^{-1}$), and 743 nm (578 $M^{-1}cm^{-1}$); [PhTt^{t-Bu}]CoBn (511 (682 $M^{-1}cm^{-1}$), 655 (346 $M^{-1}cm^{-1}$), 711 (258 $M^{-1}cm^{-1}$), and 761 nm (430 $M^{-1}cm^{-1}$)).^{18,19} In addition, even when a strong absorption is observed at ca. 700 nm, the molar absorptivity value is typically less than 1,000 making it much weaker than the absorption at ca. 700 nm observed for this series of To^MCoR complexes (Tp^{t-Bu,Me}CoMe 580 (235 $M^{-1}cm^{-1}$), 614 (293 $M^{-1}cm^{-1}$), and 685 nm (499 $M^{-1}cm^{-1}$); Tp^{t-Bu}CoMe 577 (277 $M^{-1}cm^{-1}$), 611 (374 $M^{-1}cm^{-1}$), and 688 nm (839 $M^{-1}cm^{-1}$); Tp^{t-Bu,Me}CoEt 581 (220 $M^{-1}cm^{-1}$), 617 (275 $M^{-1}cm^{-1}$), and 688 nm (510 $M^{-1}cm^{-1}$)).⁷

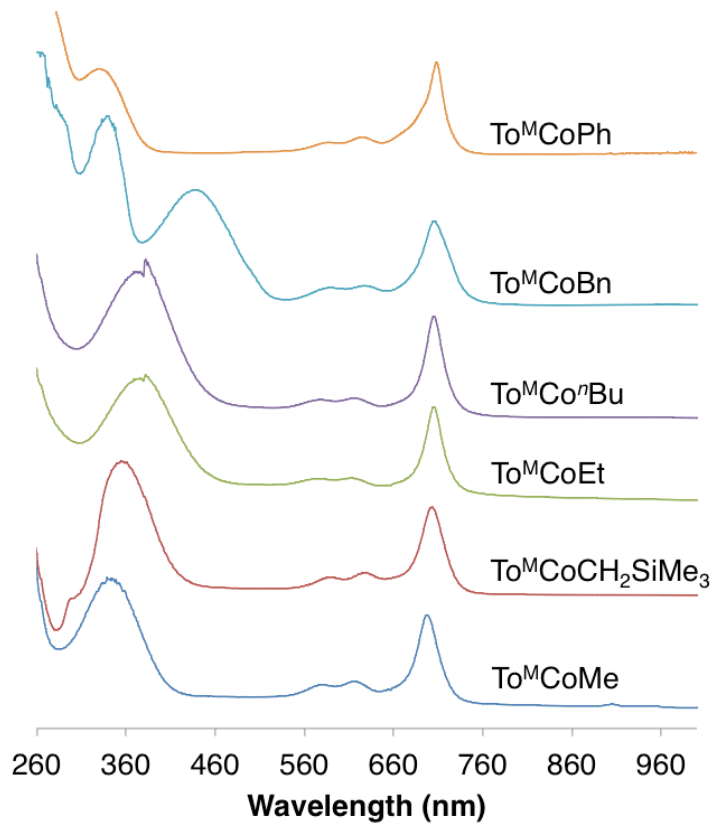


Figure 1. UV-vis spectra of To^MCoBn (1), To^MCoCH₂SiMe₃ (2), To^MCoPh (3), To^MCoEt (4), To^MCoⁿBu (5), and To^MCoMe (6) measured in diethyl ether. The d←d transitions are ~1 order of magnitude weaker intensity than those observed at ca. 300 and 700 nm.

Table 2. UV-vis spectroscopic data for compounds **1 – 6**.

Compound	Intense absorptions ($\epsilon > 1000$), nm ($\epsilon, M^{-1}cm^{-1}$)			d←d bands, nm ($\epsilon, M^{-1}cm^{-1}$)		μ_{eff} (μ_B)
To ^M CoBn (1)	339 (3205)	439 (1964)	704 (1444)	589 (332)	628 (365)	4.2(7)
To ^M CoCH ₂ SiMe ₃ (2)	355 (2228)		703 (1495)	591 (374)	628 (448)	4.9(3)
To ^M CoPh (3)	330 (1245)		708 (1333)	587 (176)	625 (252)	4.0(1)
To ^M CoEt (4)	382 (1935)		705 (1255)	579 (268)	615 (286)	4.1(6)
To ^M Co ⁿ Bu (5)	382 (1679)		705 (1291)	576 (406)	613 (422)	4.5(2)
To ^M CoMe (6)	346 (1412)		697 (1078)	581 (388)	617 (424)	4.2(2)
To ^M CoCl	n.a.			568 (362)	635 (641)	4.5(2)

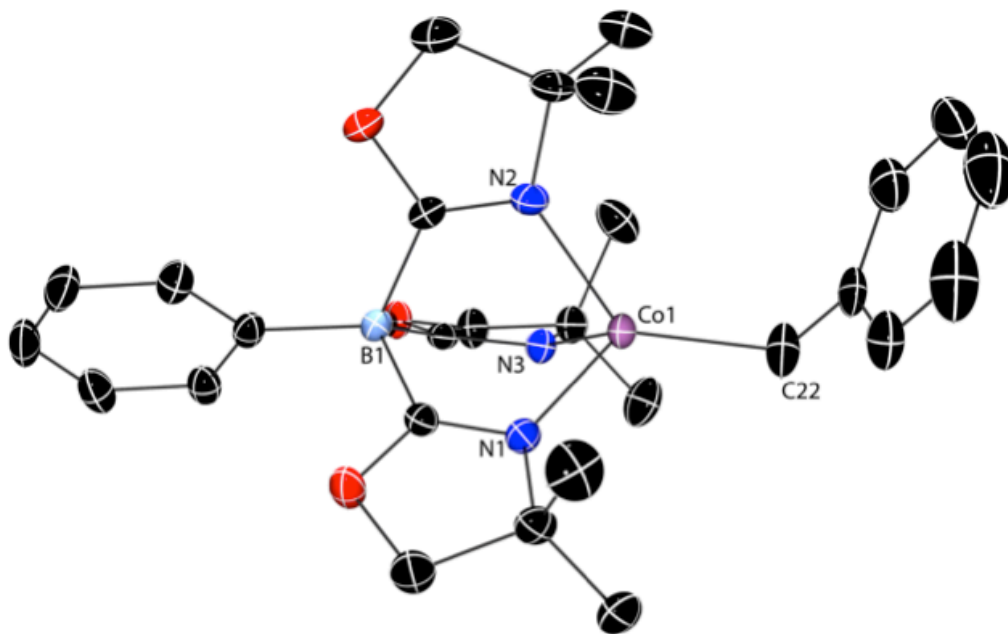
Solution-phase magnetic moments of compounds **1 – 6** (Table 2) at room temperature, measured using Evans method, were consistent with high-spin cobalt(II) ($S = 3/2$, spin-only $\mu_{eff} = 3.87 \mu_B$). With the exception of To^MCoPh, the effective magnetic moments are within the range reported for other tetrahedral organocobalt(II) complexes.^{7,20} In high spin, tetrahedral cobalt(II) with an $e^4t_2^3$ configuration, orbital contributions to the magnetic moment are expected to be quenched in the ground state, but low-lying excited state mixing results in μ_{eff} ranging from 4 – 5 μ_B .²¹ EPR spectra for **1 – 6** all contain striking eight-line patterns resulting from hyperfine coupling (54 G) to the ⁵⁹Co center ($I = 7/2$). Other four-coordinate $\{\kappa^3\text{-To}^M\}\text{Co}^{II}$ species, namely To^MCoCl and To^MCoOⁿBu, produced rhombic signals that were devoid of hyperfine coupling.

Ultimately, the spectroscopic assigned structures of compounds **1 – 6** were validated by X-ray diffraction studies of single crystals obtained from saturated pentane solutions cooled at $-40 \text{ }^\circ\text{C}$ (Figures 2-6, Table 3). The molecular structures are similar to previously reported tris(oxazolinyl)borate magnesium (d^0) and zinc (d^{10}) organometallic

compounds.^{22,23} In each cobalt complex, the tris(oxazoliny)borate ligand is coordinated in a tridentate motif, and the To^M and alkyl or aryl ligands provide a distorted tetrahedral geometry (the τ_4 scale for accessing distortions of four-coordinate compounds, is defined as $\tau_4 = 1$ for a T_d geometry, 0.85 for a trigonal pyramid (C_{3v}), and 0 for a square planar geometry) for the cobalt centers ($\tau_4 = 0.75 - 0.82$), which is similar to $To^M MgMe$ ($\tau_4 = 0.75$) and $To^M ZnMe$ ($\tau_4 = 0.76$).²⁴ In this series of cobalt compounds, the $\angle N-Co-N$ angles range over $91 - 93^\circ$, whereas $\angle N-Co-C$ angles vary from 116 to 131° . For comparison, the ranges of angles for $To^M MgMe$ and $To^M ZnMe$ are $122 - 130^\circ$ and $120 - 131^\circ$, respectively. The τ_4 scale, the $\angle N-Co-C$ angles, and the $B-M-Me$ angles describe the distortion of the alkyl ligand away from the C_3 axis in the $\{\kappa^3-To^M\}M$ motif. The $\angle B-M-Me$ in $To^M MgMe$ (172.89°), $To^M ZnMe$ (174.74) and $To^M CoMe$ (172.83°) are similar. That is, the three unpaired d electrons in the high spin cobalt(II) compounds appear to have little consequence on the coordination geometry. The $Co-C$ interatomic distances in compounds **1 - 6** are similar and vary only from $1.994(2)$ ($To^M CoMe$) to $2.023(2)$ Å for $To^M CoBn$ (see Table 3). The $Co-N$ interatomic distances are also similar across the series, varying from $2.019(2)$ to $2.062(3)$ Å. Thus, the similar electronic features identified by UV-vis, EPR, and NMR spectroscopies are also reflected in similar structural parameters. The $M-Me$ distances follow the expected periodic trend based on ionic radii (Mg ($2.108(1)$ Å) > Co ($1.994(2)$ Å) > Zn ($1.972(1)$ Å)). A comparison of $To^M CoBn$ with $To^M MgBn$ reveals that the $Co-C$ interatomic distance in $To^M CoBn$ ($2.023(2)$ Å) is significantly shorter (by 0.12 Å) than in $To^M MgBn$ ($2.143(2)$ Å). The $Co-C$ distance of $To^M CoCH_2SiMe_3$ ($1.999(4)$ Å) was similar to that reported for $Tp^{Ph,Me}CoCH_2SiMe_3$ ($2.017(2)$ Å).⁹

Table 3. Selected interatomic distances (Å) and angles (°) for compounds **1-6**.

	1 (Bn)	2 (CH₂SiMe₃)	3 (Ph)	4 (Et)	5 (ⁿBu)	6 (Me)
Co1-C22	2.023(2)	1.999(4)	1.996(2)	1.980(3)	2.010(3)	1.994(2)
Co1-N1	2.040(1)	2.044(3)	2.041(2)	2.046(2)	2.046(3)	2.0608(2)
Co1-N2	2.055(1)	2.062(3)	2.019(2)	2.045(2)	2.047(3)	2.0354(2)
Co1-N3	2.041(1)	2.059(3)	2.048(2)	2.046(2)	2.054(3)	2.0559(2)
N1-Co1-C22	122.94(6)	126.26(2)	121.41(9)	119.66(13)	121.34(2)	130.77(8)
N2-Co1-C22	131.33(6)	117.95(2)	121.50(9)	126.90(13)	124.37(2)	118.39(8)
N3-Co1-C22	116.37(6)	125.72(2)	128.00(1)	125.23(13)	126.29(2)	122.52(8)
N1-Co1-N2	91.68(5)	91.45(2)	92.29(9)	91.07(9)	91.23(1)	92.49(5)
N1-Co1-N3	94.00(4)	94.25(1)	91.37(9)	92.51(9)	91.52(1)	90.16(6)
N2-Co1-N3	91.00(5)	91.71(1)	92.95(9)	91.76(10)	92.39(1)	92.82(6)
B1-Co1-C22	169.8	173.8	175.6	175.4	176.9	172.8

**Figure 2.** Thermal ellipsoid diagram of To^MCoBn (**1**) with ellipsoids plotted at 50% probability. H atoms are omitted for clarity. Selected interatomic distances (Å) and angles (°): Co1-C22 2.023(2), Co1-N1 2.040(1), Co1-N2 2.055(1), Co1-N3 2.041(1); N1-Co1-C22 122.94(6), N2-Co1-C22 131.33(6), N3-Co1-C22 116.37(6), N1-Co1-N2 91.68(5), N1-Co1-N3 94.00(4), N2-Co1-N3 91.00(5).

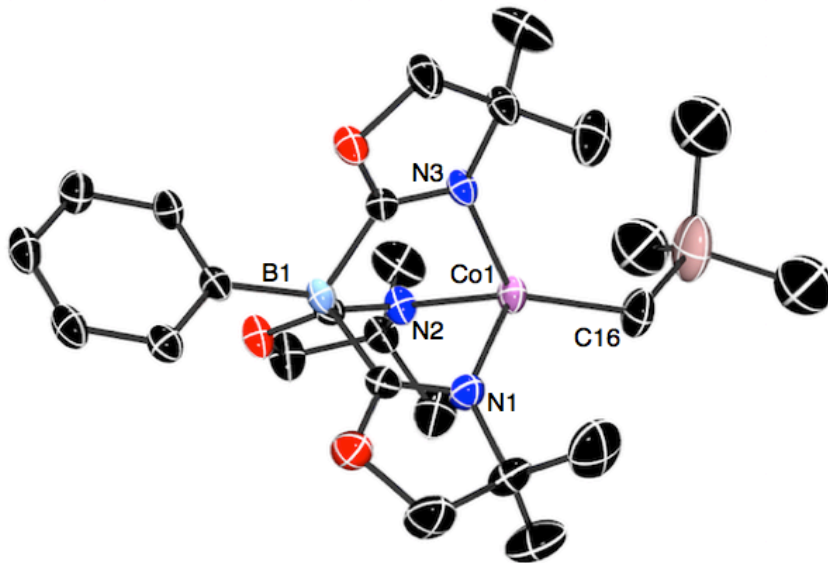


Figure 3. Thermal ellipsoid plot of $To^M CoCH_2SiMe_3$ (**2**) with ellipsoids at 50 % probability. Hydrogen atoms are omitted for clarity. Selected interatomic distances (Å) and angles (°): Co1-C41 1.999(4), Co1-N1 2.044(3), Co1-N2 2.062(3), Co1-N3 2.059(3); N1-Co1-C22 126.3(2), N2-Co1-C22 118.0(1), N3-Co1-C22 125.7(2), N1-Co1-N2 91.5(1), N1-Co1-N3 94.3(1), N2-Co1-N3 91.7(1).

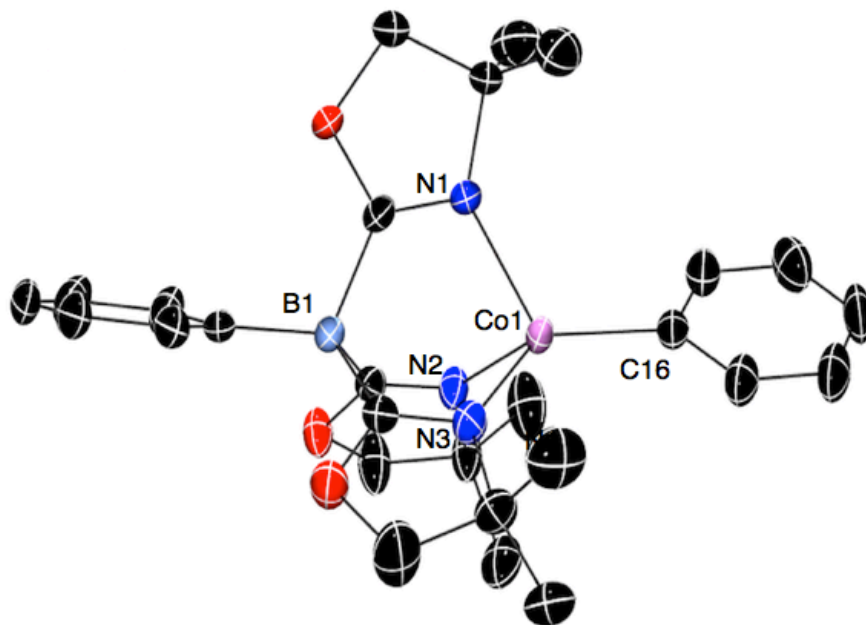


Figure 4. Thermal ellipsoid plot of $To^M CoPh$ (**3**) with ellipsoids at 50 % probability. Hydrogen atoms are omitted for clarity. Selected interatomic distances (Å) and angles (°): Co1-C16 1.996(2), Co1-N1 2.041(2), Co1-N2 2.019(2), Co1-N3 2.048(2); N1-Co1-C16 121.41(9), N2-Co1-C16 121.50(9), N3-Co1-C16 128.00(1), N1-Co1-N2 92.29(9), N1-Co1-N3 91.37(9), N2-Co1-N3 92.95(9).

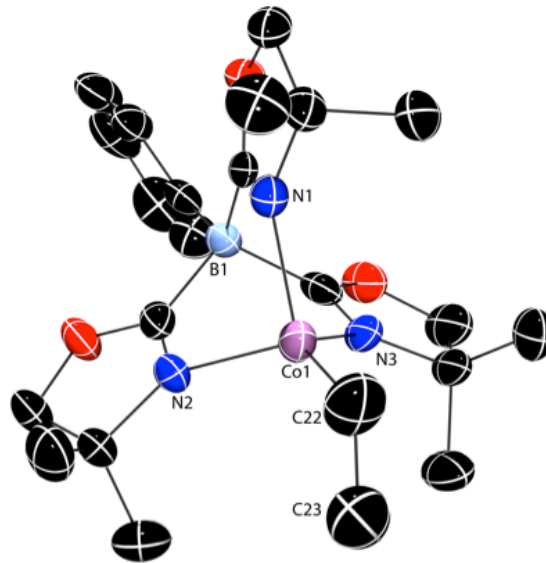


Figure 5. Thermal ellipsoid plot of $To^M CoEt$ (**4**) with ellipsoids at 50 % probability. Hydrogen atoms are omitted for clarity. Selected interatomic distances (Å) and angles (°): Co1-C22 1.980(3), Co1-N1 2.046(2), Co1-N2 2.045(2), Co1-N3 2.046(2); N1-Co1-C22 119.7(1), N2-Co1-C22 126.9(1), N3-Co1-C22 125.2(1), N1-Co1-N2 91.07(9), N1-Co1-N3 92.51(9), N2-Co1-N3 91.8(1).

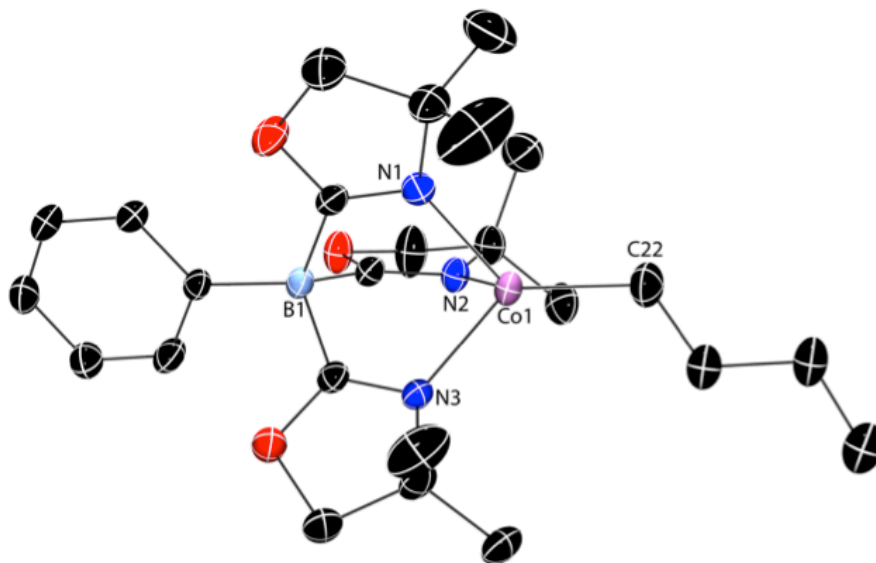


Figure 6. Thermal ellipsoid plot of $To^M Co^i Bu$ (**5**) with ellipsoids at 50% probability. H atoms are omitted for clarity. Selected interatomic distances (Å) and angles (°): Co1-C22 2.010(3), Co1-N1 2.046(3), Co1-N2 2.047(3), Co1-N3 2.054(3); N1-Co1-C22 121.34(2), N2-Co1-C22 124.37(2), N3-Co1-C22 126.29(2), N1-Co1-N2 91.23(1), N1-Co1-N3 91.52(1), N2-Co1-N3 92.39(1).

The absorption spectra for the series of organocobalt $\text{To}^{\text{M}}\text{CoR}$ (**1** – **6**) and heteroatom-bonded species $\text{To}^{\text{M}}\text{CoX}$ ($X = \text{Cl}, \text{OtBu}, \text{OAc}$) were further studied with representative electronic structure calculations. Gas-phase models for $\text{To}^{\text{M}}\text{CoBn}$ (**1-calc**), $\text{To}^{\text{M}}\text{CoMe}$ (**6-calc**) and $\text{To}^{\text{M}}\text{CoCl}$ (**To^MCoCl-calc**) were optimized using the coordinates from X-ray diffraction as initial geometries, to confirm tetrahedral geometries.²⁵⁻²⁷ The vibrational calculations for **6-calc** and **To^MCoCl-calc** contained ν_{CN} at 1667 and 1677 cm^{-1} , respectively. The high spin state for **1-calc** and **6-calc** are calculated to be 46 and 48 kcal/mol lower in energy than the low spin, respectively.

TDDFT calculations on $\text{To}^{\text{M}}\text{CoCl}$ and $\text{To}^{\text{M}}\text{CoMe}$ revealed transitions at 602, 740 and 743 nm for both species. However, the characteristic and intense low-energy experimental band at 697 nm is not calculated by this TDDFT model. We previously postulated that the single configuration TDDFT approach is insufficient to correctly model the electronic features of these compounds. In contrast, configuration interaction (CI) singles calculations show that the ground state wave functions of $\text{To}^{\text{M}}\text{CoBn}$, $\text{To}^{\text{M}}\text{CoMe}$ and $\text{To}^{\text{M}}\text{CoCl}$ are inequivalent. The ground state electronic structure of $\text{To}^{\text{M}}\text{CoCl}$ is best described by a single-reference wavefunction. In contrast, the $\text{To}^{\text{M}}\text{CoBn}$ and $\text{To}^{\text{M}}\text{CoMe}$ ground state wave functions contain multireference character (i.e., the ground state has more than one contributing electronic configuration). The additional contributing electronic configuration contains an excitation from a doubly occupied anti-bonding orbital to a singly occupied anti-bonding orbital both centered around the phenyl ring on the To^{M} ligand. Multireference character in the ground state wave function of the $\text{To}^{\text{M}}\text{CoMe}$ helps to explain why the excitation at 697 nm from the experimental UV-Vis was not found in earlier TDDFT calculations. The CI singles calculation of $\text{To}^{\text{M}}\text{CoMe}$

contained an excited state (3^{rd} excited state) with an energy difference from the ground state corresponding to an excitation at 661 nm. The excitation is from a doubly occupied bonding orbital to a singly occupied anti-bonding orbital centered on the cobalt. The orbitals involved in this excitation are mostly, but not purely d orbitals and included contributions from the oxazolines and the methyl group; however, the d orbitals had the largest changes in electron density. The conclusions from CI calculations on $\text{To}^{\text{M}}\text{CoBn}$ are consistent with those from the $\text{To}^{\text{M}}\text{CoMe}$ study.

The complexes **1** – **6** persist in solution at elevated temperatures (in the absence of air and moisture). For example, ethyl and butyl compounds **4** and **5** do not eliminate detectable quantities of ethylene or butene, respectively, after thermal treatment at 120 °C, despite the possibility for β -hydrogen elimination. Similar resistance toward β -hydrogen elimination in a bulkier tris(pyrazolyl)borato cobalt ethyl $\text{Tp}^{\text{iPr}}\text{CoEt}$ was attributed to its high spin electronic configuration.²⁰ Products of Co–C bond homolysis, such as ethane or butane, are also not formed.

Unexpectedly, reactions of **2** – **5** and CO or CO_2 to form $\text{To}^{\text{M}}\text{Co}\{\text{C}(\text{R})\text{O}\}\text{CO}$ or $\text{To}^{\text{M}}\text{CoO}_2\text{CR}$, respectively (see below), gave product mixtures that contained small signals associated with $\text{To}^{\text{M}}\text{CoCl}$ (<10%). Although the ^1H and ^{11}B NMR signals for **1** – **6** were paramagnetically shifted (see below), the peaks were characteristic and distinct from $\text{To}^{\text{M}}\text{CoCl}$. Moreover, samples of $\text{To}^{\text{M}}\text{CoR}$, apparently pure and $\text{To}^{\text{M}}\text{CoCl}$ -free as determined by ^1H NMR, ^{11}B NMR and UV-vis spectroscopy, revealed $\text{To}^{\text{M}}\text{CoCl}$ after addition of CO. Strangely, reactions of either **1** or **6** and CO or CO_2 provide acyl or carboxylate products that are free of $\text{To}^{\text{M}}\text{CoCl}$, implying that the source of $\text{To}^{\text{M}}\text{CoCl}$ is not present in either the cobalt benzyl or methyl samples. The syntheses of **1** – **6** were

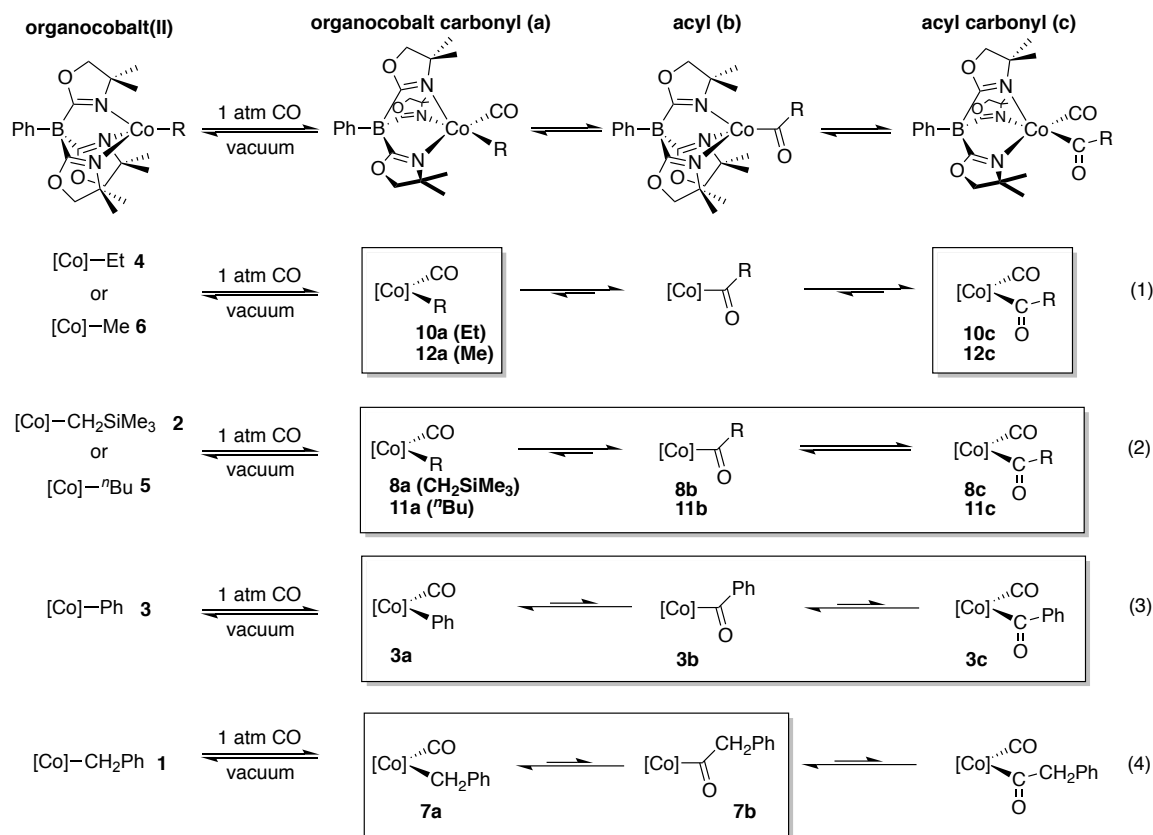
also attempted by reaction of $\text{To}^{\text{M}}\text{CoCl}$ with Grignard reagents, but transmetalation occurred to form $\text{To}^{\text{M}}\text{MgBr}$ as the dominant product rather than the desired alkylation of cobalt. Ultimately, recrystallization of organocobalt(II) species **2** – **5** afforded isolable organometallic species that did not generate detectable $\text{To}^{\text{M}}\text{CoCl}$ in subsequent reactions.

Carbonylation of $\text{To}^{\text{M}}\text{CoR}$.

Complexes **1** – **6** rapidly react with CO (1 atm) in benzene- d_6 at room temperature (Scheme 2), as evidenced by an immediate color change from blue/green to orange to give compounds labeled as **7** – **12** (**7**, Bn; **8**, CH_2SiMe_3 ; **9**, Ph; **10**, Et; **11**, *n*Bu; **12**, Me). Reactions of organometallics with CO are among the most studied, and the interaction of CO with four-coordinate iron, cobalt, and nickel alkyls can be complicated by the many pathways that lead to a wide range of products including coordination to Co(II) to give carbonyl adducts of cobalt alkyls, insertion to form the acyl isomer, and coordination of one or two carbon monoxide ligands to the cobalt acyl. In addition, CO could substitute one or more of the oxazoline groups to give bidentate coordinated To^{M} . Finally, 1 e^- reduction to form Co(I) monocarbonyl or dicarbonyl adducts is presumed to involve M–C bond homolysis and occurs with bulky tris(pyrazolyl)borate iron or cobalt alkyls upon heating under CO.^{7,28} Alkyl group-derived byproducts, presumably resulting from further reactions of alkyl radical species, are not described in those reactions.

The results may be summarized as follows: the reactions of $\text{To}^{\text{M}}\text{CoR}$ and CO give mixtures containing organocobalt carbonyl $\text{To}^{\text{M}}\text{CoR}(\text{CO})$ (**7a** – **12a**), acyl $\text{To}^{\text{M}}\text{Co}(\text{C}=\text{O})\text{R}$ (**7b** – **12b**), and acyl carbonyl $\text{To}^{\text{M}}\text{Co}\{\text{C}(\text{O})\text{R}\}\text{CO}$ (**7c** – **12c**), and these species interconvert by insertion and CO coordination, or CO dissociation and decarbonylation (Scheme 2). ^1H and ^{11}B NMR spectroscopy suggest only a single species

is formed, whereas multiple ν_{CO} and $\nu_{(\text{C}=\text{O})\text{R}}$ in the IR spectra indicate that several species are present in each reaction mixture. Together, NMR and IR spectroscopy suggest that organocobalt carbonyl **a**, acyl **b**, and acyl carbonyl **c** species are interconverted through a process that is faster than the NMR timescale and slower than the IR timescale. An additional interesting feature is that the apparent distribution of products depends on the R group (Scheme 2, eqn (1) – (4)).



Scheme 2. Carbonylation of **1 – 6** to form interconverting mixtures of organocobalt(II) carbonyl (**a**), acyl (**b**), and acyl carbonyl (**c**) complexes. Species observed by IR spectroscopy are enclosed in boxes, and equilibrium arrows indicate favored and disfavored compounds. $[\text{Co}] = \kappa^3\text{-To}^{\text{M}}\text{Co}$.

Benzene-*d*₆ solutions of **7 – 12** were first assayed by ¹¹B NMR spectroscopy in the presence of excess CO (1 atm). The ¹¹B NMR resonance for **8 – 12** appeared at ca. –4 ppm, which was distinct from the downfield chemical shift range for the organocobalt(II)

1 – 6 from 87 to 116 ppm. Unexpectedly, the ^{11}B NMR chemical shift for the carbonylated benzyl derivative **7** at 88 ppm was located in the region associated with four-coordinate cobalt alkyl/aryl or five-coordinate cobalt carboxylate compounds (e.g., $\text{To}^{\text{M}}\text{CoO}_2\text{CCH}_2\text{Ph}$: 84 ppm). Still, the ^{11}B NMR spectrum provided evidence of carbonylation, giving a distinct signal from its precursor **1** (100 ppm). The benzyl compound **7** is also distinguished from the other tris(oxazoliny)borate organocobalt compounds by its ^1H NMR spectrum, its IR spectrum and its reactivity (see below).

Compounds **8 – 12** gave similar ^1H NMR spectra that contained five, broad signals from 10 to -7 ppm, which were distinct from the spectra for the organocobalt(II) starting materials. Four of the ^1H NMR signals were attributed to the To^{M} ligand on the basis of their consistent chemical shifts across complexes **8 – 12** (9.6, 8.1, 7.7, and -1.2 ppm); however, additional assignments based on integration were impeded by their broad appearance. The fifth was assigned to the R group on the basis of its varying chemical shift among the complexes (e.g., -0.09 ppm for the CH_2SiMe_3 group in **8**, and -7.7 ppm for the ethyl group in **10**). The ^1H NMR spectrum of cobalt benzyl-derived **7** contained many (>15) signals from 82 to -28 ppm that were not readily assigned to specific moieties in the complex.

The infrared spectra of **7 – 12** contained signals that were assigned to terminal carbonyl ($\nu_{\text{C}=\text{O}}$, 1886 and 1973 to 1986 cm^{-1}), acyl ($\nu_{\text{C}(\text{=O})\text{R}}$, 1650 to 1718 cm^{-1}), and the oxazoline regions (ν_{CN} : 1582 to 1594 cm^{-1} ; see Table 4). Due to reactivity of the compounds, these infrared spectra were recorded in THF solutions saturated with CO in an air-free ATR configuration. The spectra of all of the compounds **7 – 12** contained a $\nu_{\text{C}=\text{O}}$ band at ca. 1886 cm^{-1} (see Figure S36 – S40). This signal was the only $\nu_{\text{C}=\text{O}}$ in

benzyl **7**, the dominant $\nu_{\text{C}=\text{O}}$ in phenyl-derived **9**, a significant signal in **8** and **11** from trimethylsilyl- and n-butylcobalt species, and the minor signal in ethyl **10** and methyl **12**. A higher energy $\nu_{\text{C}=\text{O}}$ band at approximately 1980 cm^{-1} was observed for complexes **8** – **12** and appeared at the expense of the 1886 cm^{-1} signal. These peaks were assigned to organocobalt carbonyl $\text{To}^{\text{M}}\text{Co}(\text{R})\text{CO}$ **a** and acylcobalt $\text{To}^{\text{M}}\text{Co}\{\text{C}(\text{O})\text{R}\}\text{CO}$ **c**, on the basis of the expected increased π -backdonation from organocobalt compared to acylcobalt species. This idea was supported by DFT calculations of $\text{To}^{\text{M}}\text{Co}(\text{Me})\text{CO}$ (**12a**) and $\text{To}^{\text{M}}\text{Co}\{\text{C}(\text{O})\text{Me}\}\text{CO}$ (**12c**), which reproduced the trend in $\nu_{\text{C}=\text{O}}$ with **12a** (2030 cm^{-1}) < **12c** (2117 cm^{-1}). The acyl ($\nu_{\text{C}(\text{=O})\text{R}}$) signals were less intense than $\nu_{\text{C}=\text{O}}$ and appeared as one (R = CH_2SiMe_3 or Ph) or two signals (R = Et, ^nBu , or Me) in the region from 1650 to 1690 cm^{-1} , but were absent for R = Bn (**7**). A $\nu_{\text{C}(\text{=O})\text{R}}$ at 1717 cm^{-1} was also observed for R = Bn, CH_2SiMe_3 , Ph, or ^nBu and was assigned to an intermediate acyl species (see Table 4).

Table 4. Infrared spectroscopic data of **7** – **12** collected in CO-saturated THF using a ZnSe crystal in ATR mode. Not detected (N.D.) in the IR spectrum.

R	$\nu_{\text{C}=\text{O}}$ (cm^{-1}) (7a – 12a)	$\nu_{\text{C}(\text{=O})\text{R}}$ (cm^{-1}) (7b – 12b)	$\nu_{\text{C}=\text{O}}$ and $\nu_{\text{C}(\text{=O})\text{R}}$ (cm^{-1}) (7c – 12c)
Bn (7)	1887	1716	N. D.
CH_2SiMe_3 (8)	1887	1718	1973 1673
Ph (9)	1886	1715	1986 1686
Et (10)	1887	N.D.	1980 1677 1650
^nBu (11)	1887	1717	1979 1687 1662
Me (12)	1887	N.D.	1984 1687 1655

In the ν_{CN} region, complexes **7** – **12** contain a single ν_{CN} band in the region from 1590 to 1600 cm^{-1} that is associated with coordinated oxazolines. In compound **12**, a shoulder at 1630 cm^{-1} was assigned to a non-coordinated oxazoline. This experimental result is consistent with the results of DFT calculations on **12**. The optimized geometry of **12** (PBE0) contained a long apical Co–N interatomic distance in a square pyramidal structure (see X-ray discussion below). Computed ν_{CN} for **12c** were found at 1611 cm^{-1} , 1641 cm^{-1} , and 1679 cm^{-1} , with the highest energy stretch corresponding to the weakly-coordinated oxazoline. In contrast the IR spectra of compounds **7** – **11** did not contain peaks that might be associated with non-coordinated oxazoline groups.

The orange carbonylated compounds **7** – **12** have distinct UV-vis spectra from their blue or green starting materials. The dominating bands at 350 nm and 700 nm in the starting materials are absent in the carbonylated product. Instead **7** – **12** are characterized by weak signals from 700 to 500 nm (ϵ : 100–170 $\text{M}^{-1}\text{cm}^{-1}$) and a strong, tailing absorption from 200 to 500 nm. In addition, compounds **7** – **12** are low spin ($\mu_{\text{eff}} = 2.4 - 3.4(2) \mu_{\text{B}}$) as determined by the Evans method. The optimized geometries of both $\text{To}^{\text{M}}\text{CoMe}(\text{CO})$ (**12a**) and $\text{To}^{\text{M}}\text{Co}\{\text{CO}\text{Me}\}(\text{CO})$ (**12c**) were found to be square-based pyramidal, with the low spin states being 30 and 33 kcal/mol lower than the high spin for **12a** and **12c** respectively. The magnetic moments are higher than the spin-only μ_{eff} value (1.73 μ_{B}) for low spin Co(II) ($S = 1/2$). A square pyramidal geometry with long axial Co–N interactions could be used to explain the higher than expected magnetic moments as square planar Co(II) complexes typically have magnetic moments in this range (2.1 – 2.9 μ_{B}).²⁹ Alternatively, contributions from the acyl species **7b** – **12b** (which are expected to be high spin) could also result in higher-than-expected magnetic moments. This idea

suggests that methyl (**12**) and ethyl (**10**) derivatives would have the lowest μ_{eff} values, because their IR spectra are dominated by the CO-coordinated species. Instead, experimental μ_{eff} values for **10** and **12** are in the middle of the series ($2.7 \mu_{\text{B}}$).

A pentane solution of **10**, cooled to $-30\text{ }^{\circ}\text{C}$ provides X-ray quality crystals, and a single crystal diffraction study reveals the five-coordinate, acyl carbonyl form $\text{To}^{\text{M}}\text{Co}\{\text{C}(\text{O})\text{Et}\}\text{CO}$ (**10c**) as a square pyramidal complex (Figure 7). Although the oxazolines are disposed trans to either CO, an acyl, or an open coordinate site, the Co1–N1 (2.037(3) Å), Co1–N2 (2.067(2) Å) and Co1–N3 (2.050(2) Å) distances are similar to each other and to the four-coordinate tris(oxazolinyl)borato organocobalt(II) compounds described above. Related $[\text{PhTt}^{\text{tBu}}]\text{Co}(\text{CO})(\text{C}(\text{O})\text{R})$ (R = Me, Et, or Ph) are also square pyramidal, with similar Co–S distances for basal and apical groups.¹⁹

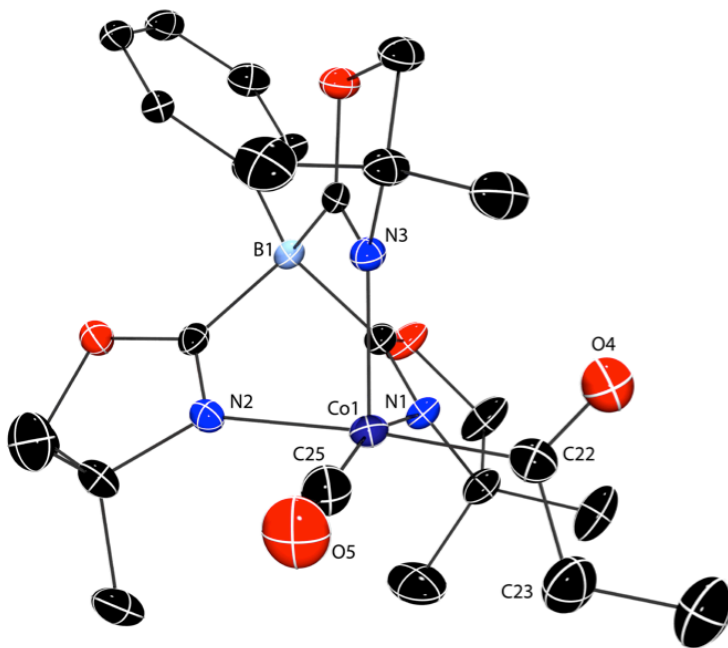


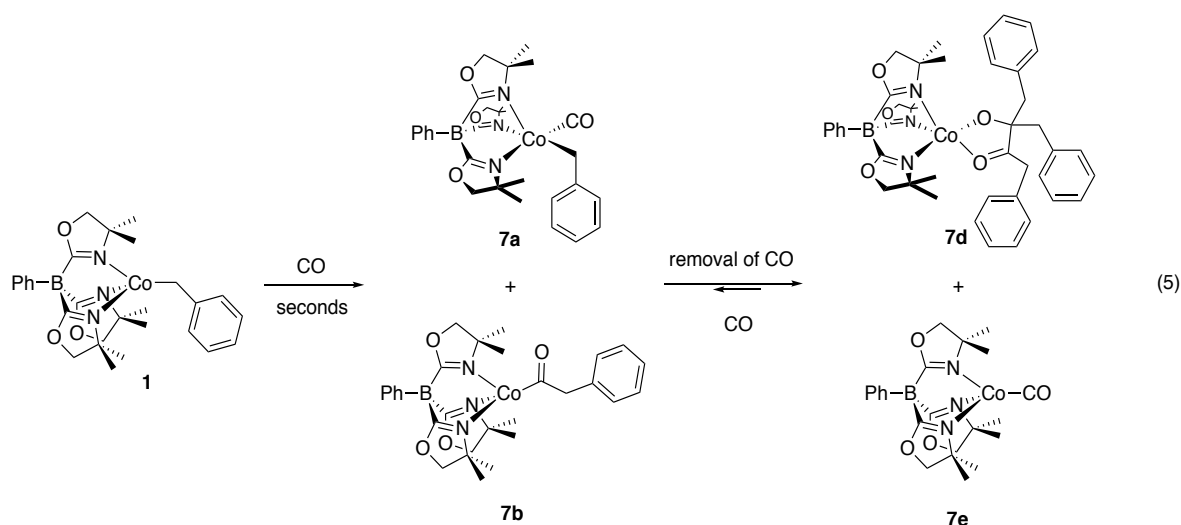
Figure 7. Thermal ellipsoid plot of $\text{To}^{\text{M}}\text{Co}\{\text{C}(\text{O})\text{Et}\}\text{CO}$ (**10**) plotted at 35% probability. H atoms are omitted for clarity. Selected interatomic distances (Å) and angles ($^{\circ}$): Co1–C22 1.973(4), Co1–C25 1.751(4), Co1–N1 2.037(3), Co1–N2 2.066(3), Co1–N3 2.050(2), C22–O4, 1.207(5), C25–O5 1.156(5), N1–Co1–C22 89.7(1), N2–Co1–C22 174.0(1), N3–Co1–C22 97.1(1), N1–Co1–N2 87.0(1), N1–Co1–N3 92.6(1), N2–Co1–N3 88.1(1), C22–Co1–C25 85.5(2).

Comparison of the structure of ethyl **10**, determined by X-ray diffraction, with minimum energy structures for $\text{To}^{\text{M}}\text{Co}\{\text{C}(=\text{O})\text{Et}\}\text{CO}$ and $\text{To}^{\text{M}}\text{Co}\{\text{C}(=\text{O})\text{Me}\}\text{CO}$ calculated using density functional theory (DFT) reveals that although all three species are square pyramidal, the geometry of the calculated energy minimized structure of $\text{To}^{\text{M}}\text{Co}\{\text{C}(\text{O})\text{Me}\}\text{CO}$ contains a long apical Co–N bond (2.19 Å). The calculated Co–N distances of **13** in the basal plane (2.04 and 2.06 Å) are significantly shorter than the apical Co–N interatomic distance. In comparison, the apical Co–N bond in the DFT optimized geometry of **10** is only 2.12 Å, while calculated Co–N distances in the basal plane are 2.03 and 2.07 Å.

We have not been able to obtain X-ray quality crystals of any of the other species in the mixture of **10**, nor have acyl or carbonyl containing compounds of **7** – **9**, **11**, or **12** been isolated. Attempts to crystallize **12**, for example, provide either $\text{To}^{\text{M}}\text{CoMe}$ (**6**) or $\text{To}^{\text{M}}\text{CoOAc}$ (**18**, see below). It is likely that X-ray quality crystals of **10c** are obtained because that is the most crystalline species in the reaction mixture. Additionally, the reversibility of the carbonylation of the organocobalt(II) alkyls posed challenges to the compounds' isolation. Thus, evaporation and exhaustive drying of $\text{To}^{\text{M}}\text{Co}\{\text{C}(\text{O})\text{Me}\}\text{CO}$ provides **6** after 24 h under dynamic vacuum, whereas complexes **9** – **11** show only partial conversion to **3** - **5** under these condition as assessed by ^{11}B NMR spectroscopy. Complex **8** is fully consumed upon evaporation, with $\text{To}^{\text{M}}\text{CoCH}_2\text{SiMe}_3$ as one of several other products that remain unidentified, as determined by ^1H and ^{11}B NMR spectroscopy.

An entirely unique outcome occurs when **7** is exposed to vacuum (Scheme 3). Unlike the evaporation of **8** – **12**, which produces the corresponding organocobalt compounds **2** – **6**, evaporation of solutions containing **7** does not produce $\text{To}^{\text{M}}\text{CoBn}$.

Instead, a mixture was obtained that gives two signals in the ^{11}B NMR spectrum at 86 and 87 ppm. The former is assigned to **7**, while the second signal and a corresponding dominant peak in the ^1H NMR spectrum at -18 ppm were attributed to an alkoxy ketone cobalt(II) species (**7d**). The evidence for that structure is provided by X-ray diffraction studies of crystals grown from degassed solutions of $\text{To}^{\text{M}}\text{CoBn}$ and CO (Figure 8). In that compound, one $\text{To}^{\text{M}}\text{Co}$, two CO, and three benzyl groups are combined to form $\text{To}^{\text{M}}\text{Co}\{O, O-\kappa^2-O-C(\text{Bn})_2-C(=\text{O})\text{Bn}\}$.



Scheme 3. Carbonylation of $\text{To}^{\text{M}}\text{CoBn}$ (**1**) followed by removal of volatile materials provides **7d** as confirmed by X-ray crystallography and a species tentatively assigned as $\text{To}^{\text{M}}\text{CoCO}$ (**7e**) as determined by IR spectroscopy.

The structure of **7d** displays a distorted trigonal bipyramidal geometry ($\tau_5 = 0.5$) composed of N1-Co1-N2 88.8(1), N2-Co1-O4 129.4(1), and N1-Co1-O4 141.4(1) angles that sum to 359.6° and a nearly linear N3-Co1-O5 angle of $172.8(1)^\circ$. The interatomic distance between cobalt and the coordinated ketone oxygen (Co1-O5, 2.212(2) Å) is longer than the interatomic distance between cobalt and the alkoxy

oxygen (Co1–O4, 1.972(2) Å) while the ketone carbon-oxygen distance is shorter (O5–C37, 1.231(4) Å) than in the alkoxide (O4–C22, 1.386(4) Å). The Co–N interatomic distances (Co1–N1 2.098(3), Co1–N2 2.086(3), Co1–N3 2.136(3) Å; $\text{Co–N}_{\text{average}} = 2.11$ Å) are all longer than other structurally characterized Co(II) complexes supported by To^{M} (e.g. $\text{To}^{\text{M}}\text{CoBn}$ $\text{Co–N}_{\text{average}} = 2.055$ Å).

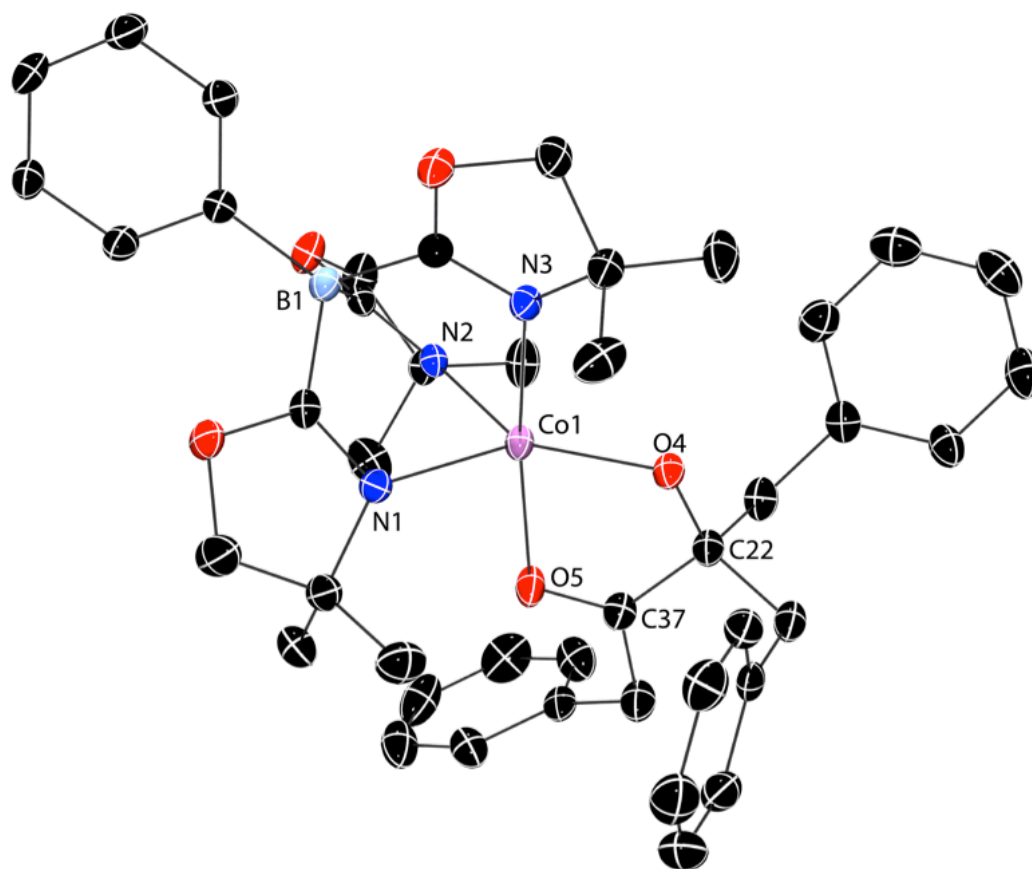
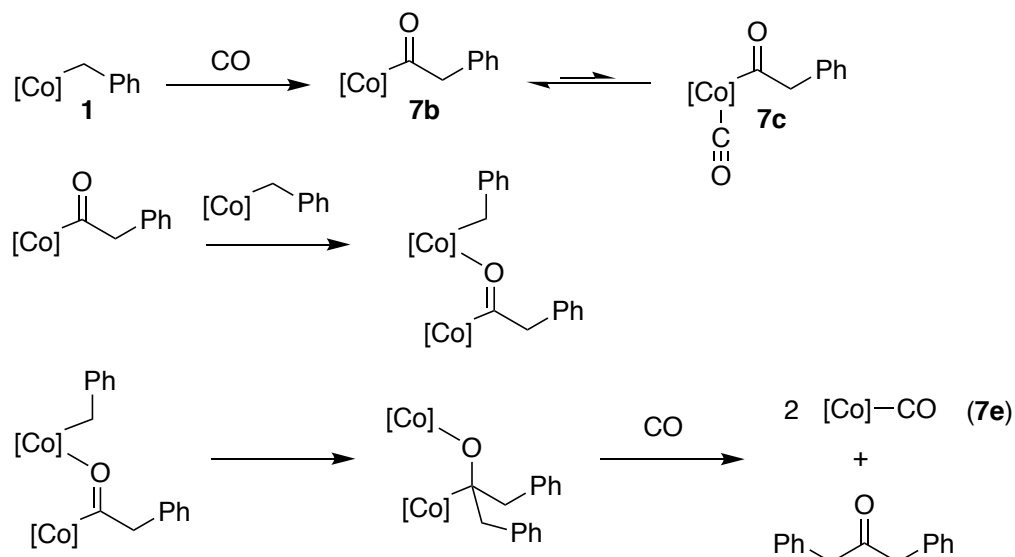


Figure 8. Thermal ellipsoid plot of **7d** with ellipsoids at 35% probability. H atoms and a pentane molecule in the unit cell are omitted for clarity. Selected interatomic distances (Å) and angles (°): Co1–O4 1.927(2), Co1–O5 2.212(2), Co1–N1 2.098(3), Co1–N2 2.086(3), Co1–N3 2.136(3); N1–Co1–N2 88.8(1), N2–Co1–O4 129.4(1), N1–Co1–O4 141.4(1), N3–Co1–O5 172.8(1), O4–Co1–O5 77.52(9).

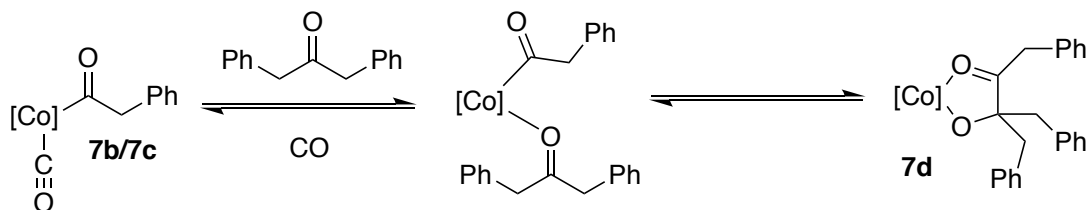
The latter alkoxy ketone species **7d** is attributed to the ^{11}B NMR signal at 87 ppm that appears upon evaporation of **7** under vacuum overnight. IR spectroscopy (KBr) of the crystals contained a $\nu_{\text{C}=\text{O}}$ band (1943 cm^{-1}) and $\nu_{\text{C(=O)R}}$ band (1671 cm^{-1}). The $\nu_{\text{C(=O)R}}$ band is assigned to the alkoxy ketone species **7d** while the $\nu_{\text{C}=\text{O}}$ band is tentatively assigned to a reduced $\text{To}^{\text{M}}\text{CoCO}$ (**7e**) species based upon its similar frequency to signals in $\text{Tp}'\text{CoCO}$ complexes (e.g., $\text{Tp}^{\text{iPr}_2}\text{CoCO}$, $\nu_{\text{C}=\text{O}} \sim 1950\text{ cm}^{-1}$; $\text{Tp}^{\text{iPr,Me}}\text{CoCO}$, $\nu_{\text{C}=\text{O}} = 1946\text{ cm}^{-1}$ and; $\text{Tp}^{\text{Np}}\text{CoCO}$, $\nu_{\text{C}=\text{O}} = 1950\text{ cm}^{-1}$, $\text{Tp}^{\text{Np}} = \text{tris}(3\text{-neopentylpyrazolyl})\text{borate}$; $\text{Tp}^{\text{iPr,Me}} = \text{tris}(3\text{-isopropyl-5-methylpyrazolyl})\text{borate}$).^{10,28,30} In these Co(I) compounds, the $\nu_{\text{C}=\text{O}}$ appears at lower energy than in the cobalt(II) acyl carbonyls (e.g., $\text{Tp}^{\text{iPr}_2}\text{Co}\{\text{C}(\text{O})\text{Et}\}\text{CO}$, $\nu_{\text{C}=\text{O}} = 1999\text{ cm}^{-1}$). Unfortunately, X-ray quality crystals of $\text{To}^{\text{M}}\text{CoCO}$ were not obtained to support this assignment. When the crystals were dissolved in C_6D_6 and CO was re-introduced, the diagnostic ^1H NMR signal at -18 ppm assigned to the alkoxy ketone species disappeared and the remaining signals match those that have been assigned to $\text{To}^{\text{M}}\text{Co}\{\text{C}(\text{O})\text{Bn}\}\text{CO}$ suggesting that its formation is reversible.

A possible mechanism is suggested (Scheme 4). The first step is formation of a ketone species that is proposed to occur by combination of the cobalt(II) acyl with cobalt(II) benzyl forming dibenzylketone and a reduced Co–CO species. The combination of an acyl and alkyl species to form a ketone has been proposed in the Fischer Tropsch reaction.³¹ Then, species **7d** could form by insertion of dibenzylketone into the cobalt-carbon bond of the cobalt acyl species (**7b**). Nucleophilic acylation of ketones to form alpha hydroxy ketones has been proposed using acyllithium reagents.³²

A) Ketone formation



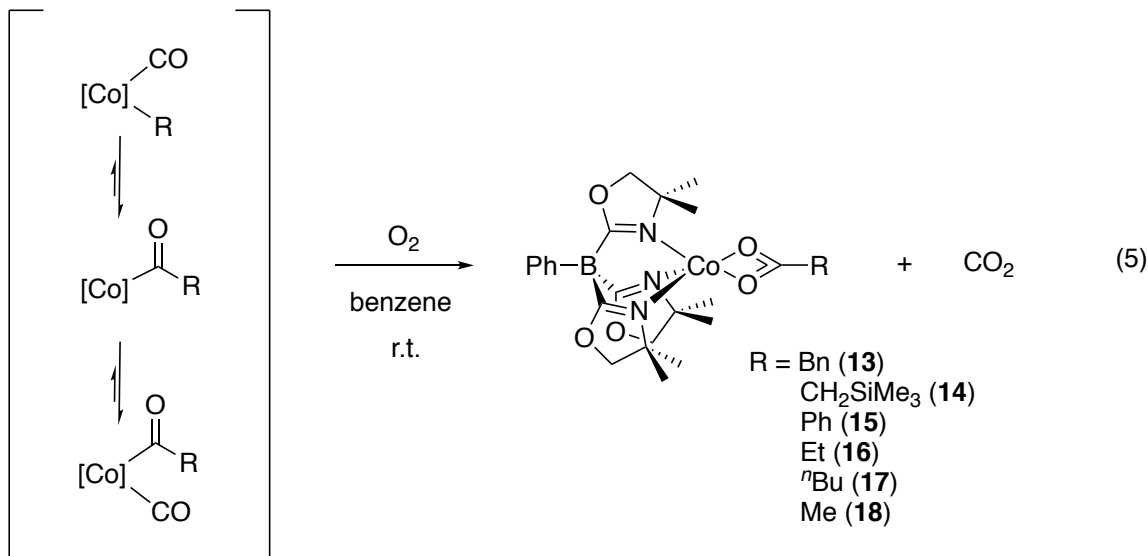
B) C-C bond formation



Scheme 4. Proposed formation of **7d** and **7e** by reaction of $\text{To}^{\text{M}}\text{CoBn}$ (**1**) and CO.

Oxidation of $\text{To}^{\text{M}}\text{Co}\{\text{C}(\text{O})\text{R}\}\text{CO}$ and Carboxylation of $\text{To}^{\text{M}}\text{CoR}$.

Complexes **7** – **12** rapidly react with O_2 to form the corresponding carboxylate complexes ($\text{To}^{\text{M}}\text{CoO}_2\text{CBn}$ (**13**), $\text{To}^{\text{M}}\text{CoO}_2\text{CCH}_2\text{SiMe}_3$ (**14**), $\text{To}^{\text{M}}\text{CoO}_2\text{CPh}$ (**15**), $\text{To}^{\text{M}}\text{CoO}_2\text{CEt}$ (**16**), $\text{To}^{\text{M}}\text{CoO}_2\text{C}^n\text{Bu}$ (**17**), and $\text{To}^{\text{M}}\text{CoO}_2\text{CMe}$ (**18**)) (eqn (5)).



The orange mixtures of carbonyl and acyl immediately change to purple solutions upon addition of O₂ at room temperature. The ¹H NMR spectra of the products were characteristic, with assignable signals for methyl (18 H) at an unusually upfield chemical shift of ca. -45 ppm and methylene (6 H) groups from the oxazoline. For comparison, the oxazoline methyl signals in the organocobalt starting materials appear at -12 ppm. The ¹¹B NMR spectra of **13** – **18** displayed a single signal in the region from 86 to 112 ppm, which is also distinct from that observed for the carbonylated species (c.a. -4 ppm) but similar to the region observed for To^MCoR.

A second route, involving reaction of To^MCoCl and MO₂CR (M = Na or K; R = Bn, Ph, Et, Me) provides **13**, **15**, **16**, and **18**. Unfortunately, we were unable to isolate the carboxylate products from this route; however, the ¹H and ¹¹B NMR spectra, UV-Vis spectra (as THF solutions), and IR spectra (as KBr pellets) of these samples matched the spectra obtained from sequential carbonylation and oxygenation.

Additionally, the reaction of $\text{To}^{\text{M}}\text{CoCH}_2\text{SiMe}_3$ (**2**) and CO_2 provides $\text{To}^{\text{M}}\text{CoO}_2\text{CCH}_2\text{SiMe}_3$ (**14**), and $\text{To}^{\text{M}}\text{Co}^n\text{Bu}$ (**5**) and CO_2 provides $\text{To}^{\text{M}}\text{CoO}_2\text{C}^n\text{Bu}$ (**17**). These species were not accessible through salt metathesis. Likewise, compounds **3**, **4**, and **6** react with CO_2 to provide the corresponding carboxylates. Again, the ^1H and ^{11}B NMR spectra, UV-vis spectra, and IR spectra matched the material obtained from oxygenation. Notably, direct insertion of CO_2 into the Co-C bond required longer reaction times of three days for $\text{R} = \text{Ph}$ and over two weeks for $\text{R} = \text{Me}$, Et , ^nBu , or CH_2SiMe_3 . Strangely, the reaction of $\text{To}^{\text{M}}\text{CoBn}$ (**1**) and CO_2 provides a compound with an ^{11}B NMR signal at 108 ppm that does not match the ^{11}B NMR signal of $\text{To}^{\text{M}}\text{CoO}_2\text{CBn}$ (**13**) (86 ppm).

Finally, the structural assignments of **13** and **15** – **18** were confirmed by X-ray diffraction studies of X-ray quality crystals grown from saturated pentane solutions at $-40\text{ }^\circ\text{C}$ (Figures 9-11). The crystals of **13** were obtained from reaction of $\text{To}^{\text{M}}\text{CoCl}$ with KO_2Bn , **16** – **18** by reaction of $\text{To}^{\text{M}}\text{CoR}$ ($\text{R} = \text{Et}$, ^nBu , and Me) with CO followed by O_2 , and **15** by reaction of $\text{To}^{\text{M}}\text{CoPh}$ with CO_2 . The cobalt-oxygen interatomic distances associated with the carboxylate moiety are inequivalent in each of these structures. For example, in **13** the Co–O4 and Co–O5 interatomic distances are 2.040(2) and Co1–O5 2.14(2) Å, respectively. The Co–O4 and Co–O5 interatomic distance in each of the carboxylate complexes characterized by X-ray diffraction are less than or similar to the covalent radii of Co–O (2.2 Å). As comparison, the Co–O interatomic distance in $\text{To}^{\text{M}}\text{CoO}^n\text{Bu}$ is 1.821(2) Å.

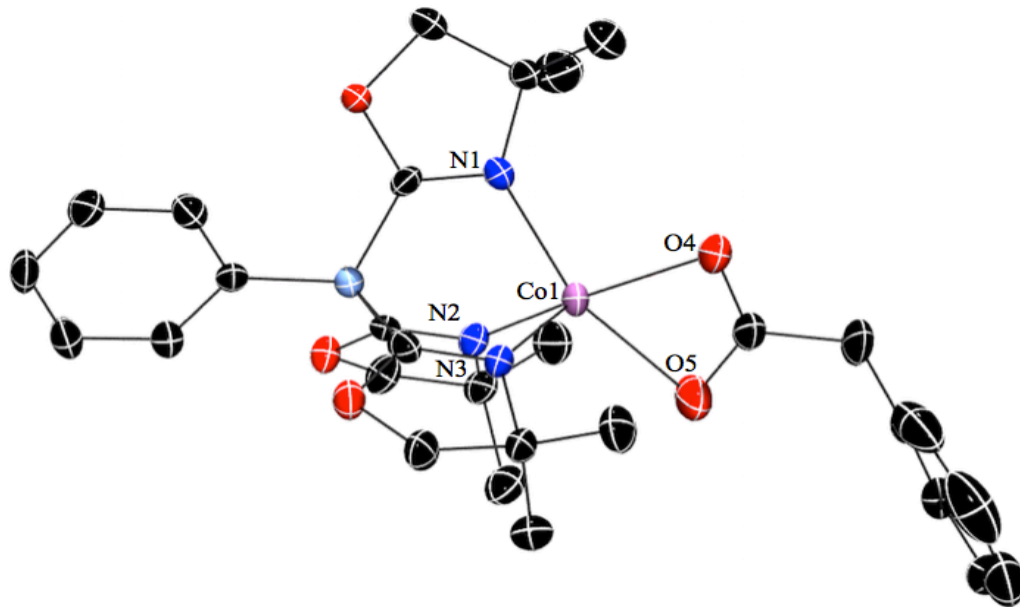


Figure 9. Thermal ellipsoid plot of $To^M CoO_2CBn$ (**13**) with ellipsoids at 50% probability. Hydrogen atoms are omitted for clarity. Selected interatomic distances (\AA) and angles ($^\circ$): Co1-O4 2.040(2), Co1-O5 2.214(2), Co1-N1 2.066(3), Co1-N2 2.023(3), Co1-N3 2.059(3); N1-Co1-N2 92.2(1), N1-Co1-N3 88.6(1), N2-Co1-N3 89.9(1), N1-Co1-O4 98.4(1), N2-Co1-O4 118.2(1), N3-Co1-O4 150.6(1), O4-Co1-O5 61.3(1).

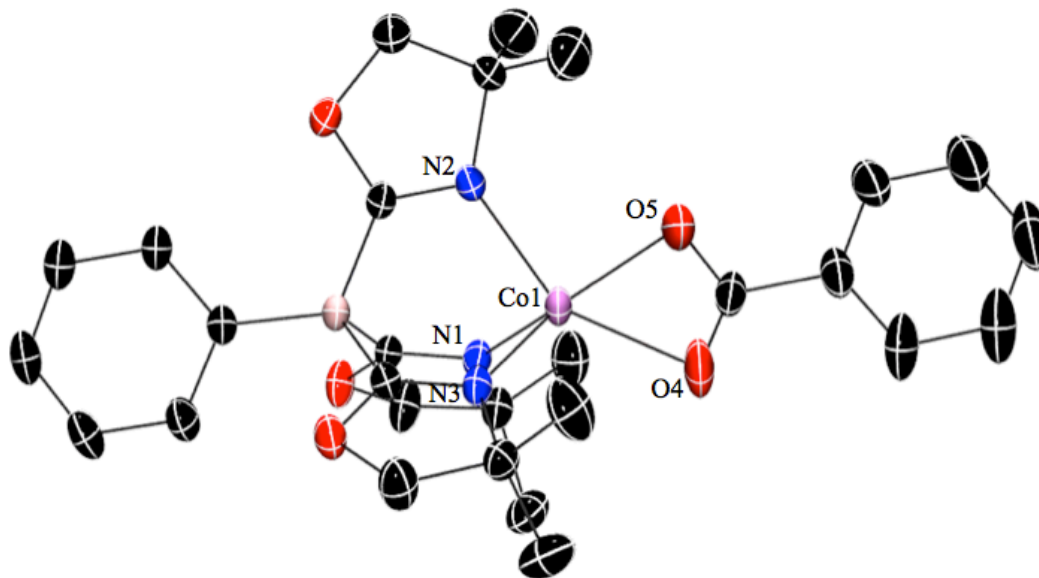


Figure 10. Thermal ellipsoid plot of $To^M CoO_2CPh$ (**15**) with ellipsoids at 20 % probability. Hydrogen atoms are omitted for clarity. Selected interatomic distances (\AA) and angles ($^\circ$): Co1-O4 2.150(3), Co1-O5 2.085(3), Co1-N1 2.024(3), Co1-N2 2.057(3), Co1-N3 2.062(3); N1-Co1-N2 91.3(1), N1-Co1-N3 90.5(1), N2-Co1-N3 89.4(1), N1-Co1-O4 119.3(1), N2-Co1-O4 146.5(2), N3-Co1-O4 102.7(1), O4-Co1-O5 58.7(1).

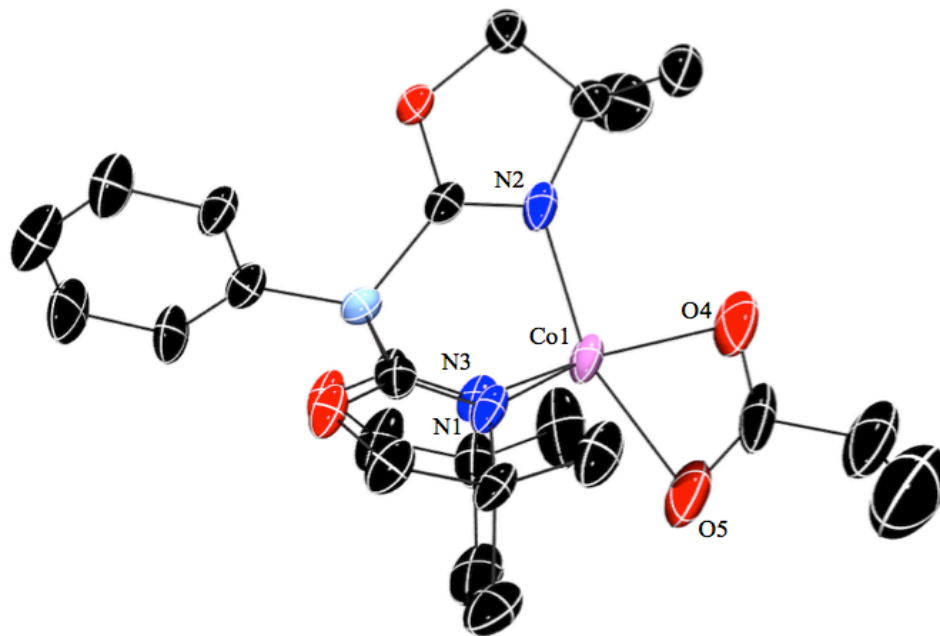


Figure 11. Thermal ellipsoid plot of $To^M CoO_2CEt$ (**16**) with ellipsoids at 50 % probability. Hydrogen atoms are omitted for clarity. Selected interatomic distances (Å) and angles (°): Co1-O4 2.006(4), Co1-O5 2.185(5), Co1-N1 2.102(4), Co1-N2 2.080(4), Co1-N3 2.030(4); N1-Co1-N2 102.4(2), N1-Co1-N3 89.9(2), N2-Co1-N3 87.7(2), N1-Co1-O4 90.6(2), N2-Co1-O4 160.0(2), N3-Co1-O4 107.7(2), O4-Co1-O5 67.0(2).

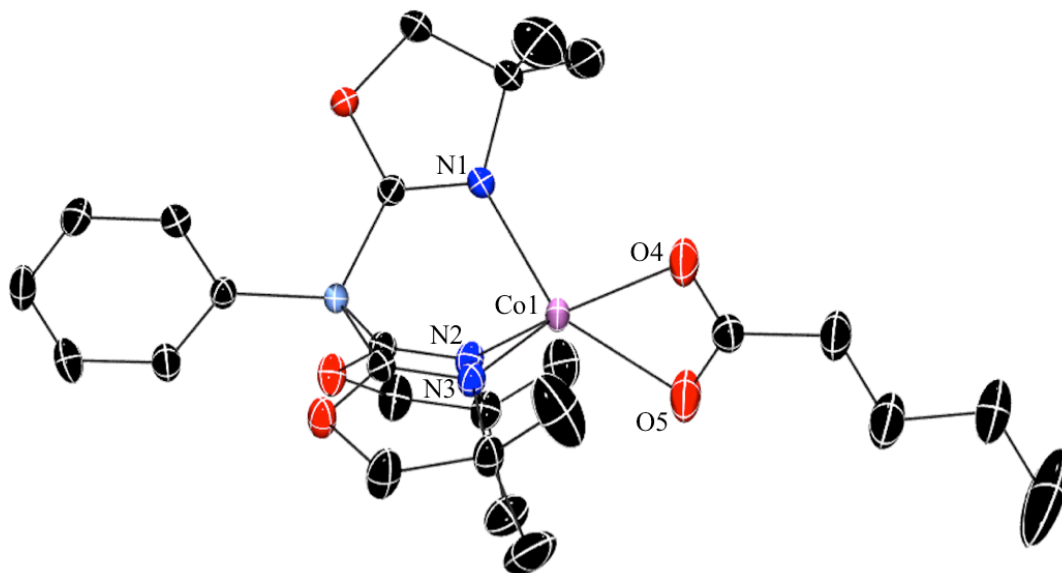
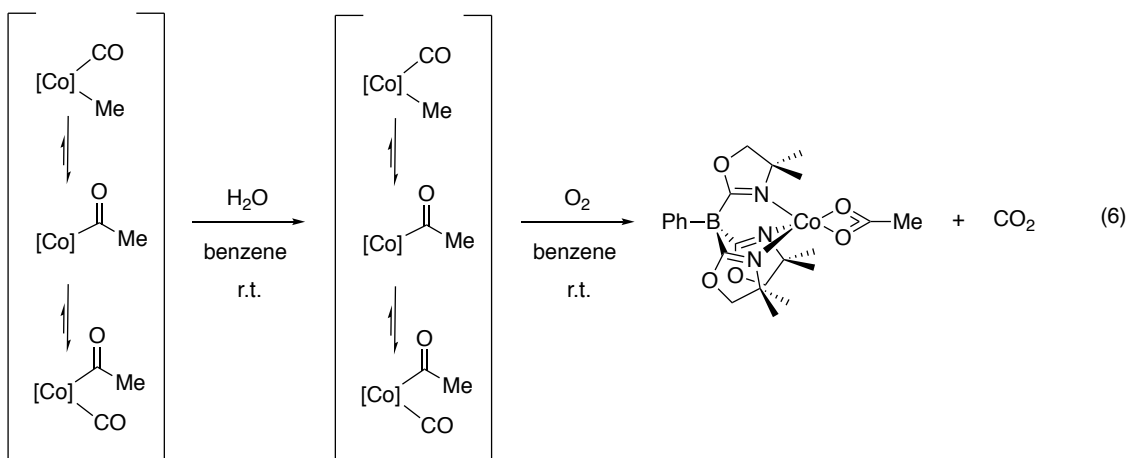


Figure 12. Thermal ellipsoid plot of $To^M CoO_2C^rBu$ (**17**) with ellipsoids at 50 % probability. Hydrogen atoms are omitted for clarity. Selected interatomic distances (Å) and angles (°): Co1-O4 2.054(2), Co1-O5 2.173(2), Co1-N1 2.073(2), Co1-N2 2.068(2), Co1-N3 2.023(2); N1-Co1-N2 87.79(6), N1-Co1-N3 90.70(6), N2-Co1-N3 90.76(6), N1-Co1-O4 98.47(6), N2-Co1-O4 154.95(8), N3-Co1-O4 113.25(8), O4-Co1-O5 60.94(6).

The possibility of adventitious H₂O serving as the source of oxygen was ruled out by the independent reaction of **12** with over 10 equivalents of H₂O (eqn (6)). ¹H NMR spectrum analysis revealed only **12** remained after 30 minutes. Upon introduction of O₂ to this same sample, within seconds complete conversion to **18** was observed.



When complex **12** was generated using isotopically labeled ¹³CO and then reacted with O₂, a new signal at 124 ppm assigned to ¹³CO₂ was detected in the ¹³C{¹H} NMR spectrum of complex **18**.³³ The ¹³C{¹H} NMR spectrum of **18** also contained an isotopically enriched signal at 82 ppm that was assigned to the O₂¹³CMe moiety. The latter observation supports the formation of the carboxylic group as occurring by O₂ oxygenation of the acetyl moiety. Together, these studies suggest that the oxidation of the acyl carbonyl complex **12** involves oxidation of both the acyl moiety to form the carboxylate derivative as well as oxidation of the terminal carbonyl to form CO₂ as a byproduct. A potential intermediate is an acylperoxo species formed from O₂ insertion into the cobalt acyl bond. Such a species is proposed by Akita and coworkers in an analogous reaction involving a cobalt(II) *p*-tolyl complex, CO, and O₂ to form a carboxylate species.¹⁷ Similarly, oxidations of hydrocarbons to form alcohols involving

*m*CPBA as the oxidant are proposed to involve binding of *m*CPBA to the metal center to form an acylperoxy species that undergoes O atom transfer to the hydrocarbon and release of a benzoic derivative. To^MCoOAc has been reported to be reactive in oxidations of hydrocarbons using *m*CPBA. Conceptually, under the conditions presented here, a similar reaction could occur with oxidation of a acyl ligand rather than a hydrocarbon substrate.³⁴

Conclusion

The series of organocobalt(II) complexes **1–6** share similar spectroscopic features by 1H and ^{11}B NMR, IR, and UV-Vis spectroscopy. Particularly, characteristic intense absorptions at ca. 350 and 700 nm in the UV-Vis spectra are a general feature of tetrahedral alkyl or aryl $To^MCo(II)$ complexes and distinguishes them from other four-coordinate compounds lacking a Co–C bond such as To^MCoOAc , $To^MCoOtBu$ or To^MCoCl . Reactions of **1–6** with CO afford mixtures containing organocobalt carbonyl, cobalt acyl, and/or cobalt acyl carbonyl species that interconvert. The speciation of the mixture varies, depending upon the R group, with only the benzyl (**7**) favoring organocobalt carbonyl and cobalt acyl, whereas ethyl (**10**) and methyl (**12**) favor cobalt acyl and its carbonyl adduct. The reactivity of the mixtures appears to correlate with this speciation. Evaporation of solutions of **8–12** provides the starting alkyl or aryl compounds via decarbonylation; however, evaporation of solutions of **7** (R = Bn) results in combination of three benzyl groups, two CO and one To^MCo -moiety to form an alkoxy ketone species. The CO is formally oxidized in this process, and we propose that two of the three benzyl groups are derived from To^MCoBn species in which Co is reduced to Co(I). Reaction of O_2 and in situ-generated carbonylated species provides the

carboxylate complexes. The rapid multi-step oxidative carbonylation route to form the carboxylate derivatives sharply contrasts the timescale of the alternative direct insertion of CO₂ into the cobalt carbon bond, which requires several days to weeks. In addition, oxidative carbonylation selectively yields the carboxylates making it superior to the independent salt metathesis reaction of To^MCoCl with the KOO₂CR salts, which yields unidentified byproducts. Importantly, if C–H activation of a hydrocarbon could complete the cycle to form the starting cobalt alkyl and the carboxylate, this reactivity could be incorporated into new catalytic cycles for making carboxylate acids. The general oxidative carbonylation reactivity observed for R = Bn, CH₂SiMe₃, Ph, Et, ^tBu, and Me demonstrates the versatility of this reaction that could prove useful in synthesizing an array of carboxylates. Further studies will explore such catalytic application of this oxidative carbonylation reactivity as well comparison with other late transition metals such as iron and nickel in place of cobalt.

Experimental Section

General Procedures. All reactions were performed using standard Schlenk techniques under an atmosphere of dry argon. Benzene and diethyl ether were dried and deoxygenated using an IT PureSolv system. Benzene-*d*₆ was degassed with freeze-pump-thaw cycles, heated to reflux over a Na/K alloy, and then vacuum transferred. To^MCoCl, To^MCoMe, and To^MCoOAc were synthesized following the reported procedures.^{1,3} ¹H and ¹¹B NMR spectra were collected on a Bruker Avance III 600 spectrometer. ¹¹B NMR spectra were referenced to an external sample of BF₃·Et₂O. Infrared spectra were measured on a Bruker Vertex 80 FTIR spectrometer. EPR were obtained on an X-band Elexsys 580 FT- EPR spectrometer in continuous wave mode. UV-Vis spectra were

recorded on an Agilent 8453 UV-vis spectrophotometer. Elemental analyses were performed using a Perkin-Elmer 2400 Series II CHN/S. Single crystal X-ray diffraction data was collected on an APEX II.

Computational methods. Density Functional Theory (DFT) optimizations were performed using NWChem³⁵ on **6**, **10c**, **12a**, **12c**, and $\text{To}^{\text{M}}\text{CoCl}$ using the PBE0 hybrid functional,²⁵ the 6-311+G* basis²⁶ for first and second row elements, and the Stuttgart RSC 1997²⁷ effective core potential for the cobalt. Single-point energy calculations were also performed on both the high-spin and low-spin configurations to determine the lowest energy spin state for each structure. DFT Hessians were performed on **6**, **12a**, and **12c** to compute vibrational frequencies. A Time-Dependent DFT (TDDFT) calculation using implicit solvation³⁶ was initially performed to calculate excited states for **6**, but it was determined that a more robust method allowing for multiple electronic configurations was needed due to missing excitations in the results. Gas-phase configuration interaction (CI) singles calculations were performed using the GAMESS quantum chemistry package³⁷ on **6** and $\text{To}^{\text{M}}\text{CoCl}$ to compute the first 25 excited states for each structure.

$\text{To}^{\text{M}}\text{CoBn}$ (1**).** $\text{To}^{\text{M}}\text{CoCl}$ (0.147 g, 0.308 mmol) and KBn (0.067g, 0.515 mmol) were stirred in tetrahydrofuran (10 mL) for 2 h. The green solution was dried under vacuum, the residue was extracted with benzene (10 mL), and the extracts were dried *in vacuo* to afford $\text{To}^{\text{M}}\text{CoBn}$ as a green solid (0.129 g, 0.242 mmol, 78.7%). X-ray quality crystals were obtained from a saturated pentane solution at $-40\text{ }^{\circ}\text{C}$. ^1H NMR (benzene- d_6 , 600 MHz): δ 34.47 (s, 2 H), 16.33 (s, 6 H, $\text{CNCMe}_2\text{CH}_2\text{O}$), 14.90 (s, 2 H), 10.96 (s, 2 H), 9.14 (s, 1 H), -12.46 (s, 18 H, $\text{CNCMe}_2\text{CH}_2\text{O}$), -77.45 (s, 1 H), -89.01 (s, 1 H). ^{11}B NMR (benzene- d_6 , 128 MHz): δ 100.4. IR (KBr, cm^{-1}): ν 3072 (w), 3046 (w), 3012 (w), 2966

(m), 2926 (m), 2897 (m), 2869 (m), 1701 (w), 1588 (s, ν_{CN}), 1482 (m), 1459 (m), 1384 (m), 1366 (m), 1351 (m), 1271 (m), 1194 (m), 1160 (m), 1027 (m), 1008 (m), 963 (m). UV-vis (Et_2O) $\lambda_{\text{max}} = 339$ (ϵ : $3205 \text{ M}^{-1}\text{cm}^{-1}$), 439 (ϵ : $1964 \text{ M}^{-1}\text{cm}^{-1}$) 589 (ϵ : $332 \text{ M}^{-1}\text{cm}^{-1}$), 628 (ϵ : $365 \text{ M}^{-1}\text{cm}^{-1}$), 704 (ϵ : $1444 \text{ M}^{-1}\text{cm}^{-1}$). $\mu_{\text{eff}}(\text{C}_6\text{D}_6) = 4.2(7) \mu_{\text{B}}$ as determined by the Evans method. Anal. Calcd. for $\text{C}_{42}\text{H}_{58}\text{B}_2\text{CoN}_6\text{O}_6$: C, 63.17; H, 6.82; N, 7.89 Found: C, 62.71; H, 7.10; N, 8.19. Mp. 151-153°C, dec.

To^MCoCH₂SiMe₃ (2). LiCH₂SiMe₃ (0.041 g, 0.44 mmol) dissolved in pentane (1 mL) was added dropwise to a solution of To^MCoCl (0.150 g, 0.31 mmol) in tetrahydrofuran (3 mL) cooled to -78 °C. The purple reaction mixture was stirred for 15 min. at -78 °C, warmed to room temperature, and then stirred for an additional 45 min. The solvent was evaporated, and the residue was extracted with benzene. Evaporation of benzene afforded To^MCoCH₂SiMe₃ as a blue solid (0.161 g, 0.30 mmol, 97% yield). X-ray quality crystals were obtained from a saturated pentane solution at -40 °C. ¹H NMR (benzene-*d*₆, 600 MHz): δ 15.73 (s, 6 H, CNCMe₂CH₂O), 12.72 (s, 2 H, C₆H₅), 10.08 (s, 2 H, C₆H₅), 8.54 and 8.48 (s, 10 H, CH₂SiMe₃, *p*-C₆H₅), -9.58 (s, 18 H, CNCMe₂CH₂O). ¹¹B NMR (benzene-*d*₆, 128 MHz): δ 86.6. IR (KBr, cm⁻¹): ν 2966 (m), 2892 (m), 1586 (s, ν_{CN}), 1490 (m), 1462 (m), 1434 (m), 1386 (m), 1366 (m), 1275 (m), 1251 (m), 1195 (m), 1159 (m), 1020 (m), 1001 (m), 966 (m). UV-vis (Et_2O) $\lambda_{\text{max}} = 355$ (ϵ : $2228 \text{ M}^{-1}\text{cm}^{-1}$), 591 (ϵ : $374 \text{ M}^{-1}\text{cm}^{-1}$), 628 (ϵ : $448 \text{ M}^{-1}\text{cm}^{-1}$), 703 (ϵ : $1495 \text{ M}^{-1}\text{cm}^{-1}$). $\mu_{\text{eff}}(\text{C}_6\text{D}_6) = 4.9(3) \mu_{\text{B}}$ as determined by the Evans method. Anal. Calcd. for $\text{C}_{25}\text{H}_{40}\text{BCoN}_3\text{O}_3\text{Si}$: C, 56.82; H, 7.63; N, 7.95 Found: C, 56.25; H, 7.72; N, 7.54. Mp. 234-235 °C, dec.

To^MCoPh (3). Phenyllithium (1.8 M in dibutyl ether, 0.250 mL, 0.45 mmol) was added dropwise to a solution of To^MCoCl (0.151 g, 0.317 mmol) in THF (3 mL) cooled to -78

°C. The dark blue reaction mixture was stirred for 15 min. at -78 °C, warmed to room temperature, and stirred for an additional 45 min. The solvent was evaporated, and the residue was extracted with benzene. Evaporation of benzene provided $\text{To}^{\text{M}}\text{CoPh}$ as a blue solid (0.119 g, 0.230 mmol, 72.6% yield). X-ray quality crystals were obtained from saturated pentane solutions cooled to -40 °C. ^1H NMR (benzene- d_6 , 600 MHz): δ 73.95 (s, 1 H), 16.73 (s, 6 H, $\text{CNCMe}_2\text{CH}_2\text{O}$), 15.74 (s, 2 H, C_6H_5), 11.30 (s, 2 H, C_6H_5), 10.61 (s, 1 H, $p\text{-C}_6\text{H}_5$), 9.42 (s, 1 H, $p\text{-C}_6\text{H}_5$), -13.68 (s, 18 H, $\text{CNCMe}_2\text{CH}_2\text{O}$). ^{11}B NMR (benzene- d_6 , 128 MHz): δ 107.7. IR (KBr, cm^{-1}): ν 3042 (m), 2967 (m), 2927 (m), 2890 (m), 2869 (m), 1582 (s, ν_{CN}), 1494 (m), 1461 (m), 1433 (m), 1388 (m), 1368 (m), 1352 (m), 1274 (m), 1196 (m), 1159 (m), 964 (m), 951 (m). UV-vis (Et_2O): $\lambda_{\text{max}} = 330$ (ϵ : $1245 \text{ M}^{-1}\text{cm}^{-1}$), 587 (ϵ : $176 \text{ M}^{-1}\text{cm}^{-1}$), 625 (ϵ : $252 \text{ M}^{-1}\text{cm}^{-1}$), 708 (ϵ : $1333 \text{ M}^{-1}\text{cm}^{-1}$). μ_{eff} (C_6D_6) = 4.0(1) μ_{B} as determined by the Evans method. Anal. Calcd. for $\text{C}_{27}\text{H}_{34}\text{BCoN}_3\text{O}_3$: C, 62.57; H, 6.61; N, 8.11 Found: C, 63.05; H, 6.81; N, 7.75. Mp. 194-197 °C, dec.

$\text{To}^{\text{M}}\text{CoEt}$ (4). Ethyllithium (0.5 M in a mixture of benzene and cyclohexane, 0.880 mL, 0.44 mmol) was added dropwise to a solution of $\text{To}^{\text{M}}\text{CoCl}$ (0.150 g, 0.31 mmol) in THF (3 mL) cooled to -78 °C. The purple reaction mixture was stirred for 15 min. at -78 °C, warmed to room temperature, and stirred for an additional 45 min. Evaporation of volatiles, extraction of the solid residue with benzene, and evaporation of the benzene afforded $\text{To}^{\text{M}}\text{CoEt}$ as a green solid (0.114 g, 0.24 mmol, 77% yield). X-ray quality crystals were obtained from saturated pentane solutions at -40 °C. ^1H NMR (benzene- d_6 , 600 MHz): δ 15.95 (s, 2 H, C_6H_5), 14.85 (s, 6 H, $\text{CNCMe}_2\text{CH}_2\text{O}$), 11.33 (s, 2 H, C_6H_5), 9.42 (s, 1 H, $p\text{-C}_6\text{H}_5$), -14.45 (s, 18 H, $\text{CNCMe}_2\text{CH}_2\text{O}$), -31.31 (s, 1 H, CH_2CH_3). ^{11}B

NMR (benzene- d_6 , 128 MHz): δ 116.7. IR (KBr, cm^{-1}): ν 3078 (w), 3045 (w), 2967 (m), 2929 (m), 2895 (m), 2870 (m), 2837 (m), 1592 (s, ν_{CN}), 1495 (m), 1461 (m), 1434 (m), 1385 (m), 1366 (m), 1351 (m), 1268 (m), 1193 (m), 1159 (m), 1101 (w), 1017 (w), 961 (m). UV-vis ((Et₂O) λ_{max} = 382 (ϵ : 1935 $\text{M}^{-1}\text{cm}^{-1}$), 579 (ϵ : 268 $\text{M}^{-1}\text{cm}^{-1}$), 615 (ϵ : 286 $\text{M}^{-1}\text{cm}^{-1}$), 705 (ϵ : 1255 $\text{M}^{-1}\text{cm}^{-1}$). $\mu_{\text{eff}}(\text{C}_6\text{D}_6) = 4.1(6) \mu_{\text{B}}$ as determined by the Evans method. Anal. Calcd. for $\text{C}_{23}\text{H}_{34}\text{BCoN}_3\text{O}_3$: C, 58.74; H, 7.29; N, 8.94 Found: C, 58.83; H, 7.07; N, 8.64. Mp. 179-181°C, dec.

To^MCoⁿBu (5). To^MCoCl (0.155 g, 0.33 mmol) was dissolved in THF (3 mL), cooled to -78°C , and *n*-butyllithium (2.5 M in hexanes, 0.19 mL, 0.48 mmol) was added in a dropwise fashion. The dark purple reaction mixture was stirred at -78°C for 15 min., warmed to room temperature, and stirred for an additional 45 min. THF was removed *en vacuo*, the residue was extracted with benzene, and benzene was evaporated to afford To^MCoⁿBu as a dark green solid (0.100 g, 0.20 mmol, 61% yield). X-ray quality crystals were obtained from saturated pentane solutions cooled to -40°C . ¹H NMR (benzene- d_6 , 600 MHz): δ 15.91 (s, 2 H, C₆H₅), 14.88 (s, 6 H, CNCMe₂CH₂O), 14.21 (s, 2 H, (CH₂)₃CH₃), 11.34 (s, 2 H, C₆H₅), 9.47 (s, 1 H, *p*-C₆H₅), -2.67 (s, 3 H, (CH₂)₃CH₃), -14.31 (s, 18 H, CNCMe₂CH₂O). ¹¹B NMR (benzene- d_6 , 128 MHz): δ 115.0. IR (KBr, cm^{-1}): ν 3083 (w), 3047 (w), 2966 (m), 2928 (m), 2890 (m), 2871 (m), 1587 (s, ν_{CN}), 1495 (m), 1462 (m), 1434 (m), 1386 (m), 1368 (m), 1351 (m), 1271 (m), 1198 (m), 1159 (m), 1104 (w), 1025 (m), 995 (m). UV-vis (Et₂O): λ_{max} = 382 (ϵ : 1679 $\text{M}^{-1}\text{cm}^{-1}$), 576 (ϵ : 406 $\text{M}^{-1}\text{cm}^{-1}$), 613 (ϵ : 422 $\text{M}^{-1}\text{cm}^{-1}$), 705 (ϵ : 1291 $\text{M}^{-1}\text{cm}^{-1}$). $\mu_{\text{eff}}(\text{C}_6\text{D}_6) = 4.5(2) \mu_{\text{B}}$ as determined by the Evans method. Anal. Calcd. for $\text{C}_{25}\text{H}_{38}\text{BCoN}_3\text{O}_3$: C, 60.26; H, 7.69; N, 8.43 Found: C, 60.25; H, 7.37; N, 8.32. Mp. 244-246°C, dec.

Preparation of Carbonylated Complexes. As a typical procedure, $\text{To}^{\text{M}}\text{CoEt}$ (0.01 g, 0.02 mmol) was dissolved in benzene- d_6 (0.5 mL), the headspace was removed in vacuo, and then CO (1 atm) was introduced. An immediate color change from green to orange was observed. Benzene- d_6 was evaporated in vacuo to afford $\text{To}^{\text{M}}\text{Co}\{\text{C}(\text{O})\text{Et}\}\text{CO}$ as a yellow solid (0.01 g, 0.02 mmol, 95% yield). X-ray quality crystals were obtained from saturated pentane solutions cooled to $-40\text{ }^\circ\text{C}$. The other carbonylated complexes **7 – 12** were synthesized by this same procedure.

$\text{To}^{\text{M}}\text{Co}\{\text{C}(\text{O})\text{Bn}\}\text{CO}$ (7): ^1H NMR (benzene- d_6 , 600 MHz): δ 82.15, 64.43, 42.01, 26.06, 14.98, 12.63, 10.91, 9.11, 5.63, 2.78, -2.29 , -5.98 , -16.04 , -25.97 , -28.18 . ^{11}B NMR (benzene- d_6 , 128 MHz): δ 87.0. IR (KBr, cm^{-1}): ν 3076 (w), 3062 (w), 2965 (m), 2927 (m), 2894 (m), 2009 (w), 1942 (m), 1888 (m), 1717 (w), 1669 (m), 1594 (s, ν_{CN}), 1495 (m), 1460 (m), 1366 (m), 1351 (m), 1273 (m), 1195 (m), 1158 (m), 1125 (w), 1095 (w), 1069 (w), 1028 (m), 957 (m). $\mu_{\text{eff}}(\text{C}_6\text{D}_6) = 2.8(2) \mu_{\text{B}}$ as determined by the Evans method.

$\text{To}^{\text{M}}\text{Co}\{\text{C}(\text{O})\text{CH}_2\text{SiMe}_3\}\text{CO}$ (8): ^1H NMR (benzene- d_6 , 600 MHz): δ 9.56, 8.16, 7.62, 6.89, -0.09 , -0.98 . ^{11}B NMR (benzene- d_6 , 128 MHz): δ -4.7 . IR (KBr, cm^{-1}): ν 3077 (w), 3046 (w), 2967 (m), 2385 (m), 2055 (m, ν_{CO}), 1982 (m, ν_{CO}), 1938 (m, ν_{CO}), 1887 (m, ν_{CO}), 1590 (s, ν_{CN}), 1573 (m, ν_{CN}), 1556 (m, ν_{CN}), 1494 (m), 1463 (m), 1433 (m), 1388 (m), 1368 (m), 1352 (m), 1275 (m), 1251 (m), 1197 (m), 1162 (m), 1024 (m), 962 (m). UV-vis (THF): $\lambda_{\text{max}} = 669$ (ϵ : $66 \text{ M}^{-1}\text{cm}^{-1}$) and 903 (ϵ : $104 \text{ M}^{-1}\text{cm}^{-1}$) $\mu_{\text{eff}}(\text{C}_6\text{D}_6) = 2.4(2) \mu_{\text{B}}$ as determined by the Evans method.

$\text{To}^{\text{M}}\text{Co}\{\text{C}(\text{O})\text{Ph}\}\text{CO}$ (9): ^1H NMR (benzene- d_6 , 600 MHz): δ 9.76, 8.22, 7.71, 7.46, 7.16, -1.49 . ^{11}B NMR (benzene- d_6 , 128 MHz): δ -5.7 . IR (KBr, cm^{-1}): ν 3077 (w), 3044 (w), 2965 (m), 2926 (m), 2892 (m), 2853 (m), 1985 (w, ν_{CO}), 1986 (w, ν_{CO}), 1591 (s, ν_{CN}),

1557 (m), 1494 (m), 1462 (m), 1432 (m), 1415 (m), 1388 (m), 1368 (m), 1353 (m), 1279 (m), 1198 (m), 1160 (m), 1053 (m), 1025 (m), 968 (m). UV-vis (THF): $\lambda_{max} = 909$ (ϵ : $135 \text{ M}^{-1} \text{ cm}^{-1}$) $\mu_{\text{eff}}(\text{C}_6\text{D}_6) = 2.4(2) \mu_{\text{B}}$ as determined by the Evans method.

To^MCo{C(O)Et}CO (10). ¹H NMR (benzene-*d*₆, 600 MHz): δ 9.61, 8.17, 7.62, -1.18, -7.69. ¹¹B NMR (benzene-*d*₆, 128 MHz): δ -4.44. IR (KBr, cm^{-1}): ν 3080 (w), 3046 (w), 2967 (m), 2931 (m), 2890 (m), 1989 (w), 1966 (w), 1942 (w), 1886 (m), 1594 (s, ν_{CN}), 1565 (m), 1495 (m), 1465 (m), 1433 (m), 1387 (m), 1367 (m), 1352 (m), 1275 (m), 1196 (m), 1161 (m), 1075 (w), 1024 (m), 961 (m). UV-vis (THF): $\lambda_{max} = 669$ (ϵ : $102 \text{ M}^{-1} \text{ cm}^{-1}$) and 704 (ϵ : $116 \text{ M}^{-1} \text{ cm}^{-1}$) $\mu_{\text{eff}}(\text{C}_6\text{D}_6) = 2.7(2) \mu_{\text{B}}$ as determined by the Evans method.

To^MCo{C(O)ⁿBu}CO (11): ¹H NMR (benzene-*d*₆, 600 MHz): δ 9.61, 8.17, 7.63, 0.94, -1.16. ¹¹B NMR (benzene-*d*₆, 128 MHz): δ -4.9. IR (KBr, cm^{-1}): ν 3077 (w), 3046 (w), 2965 (m), 2930 (m), 2893 (m), 2873 (m), 2055 (w, ν_{CO}), 1980 (w, ν_{CO}), 1941 (m, ν_{CO}), 1887 (w, ν_{CO}), 1594 (s, ν_{CN}), 1556 (m), 1494 (m), 1463 (m), 1434 (m), 1367 (m), 1354 (m), 1276 (m), 1196 (m), 1161 (m), 1026 (m), 960 (m).

Preparation of Carboxylate Complexes. As a typical procedure, the carbonylated species **10** was generated *in situ*. The headspace was removed and O₂ (1 atm) was introduced. A color change from orange to purple was immediately visible. Benzene-*d*₆ was evaporated in vacuo to afford To^MCoO₂CEt as a purple. X-ray quality crystals were obtained for complexes **13** and **15** – **18** from a saturated pentane solution cooled to -40 °C.

To^MCo(O₂CBn) (13). ¹H NMR (benzene-*d*₆, 600 MHz): δ 49.61, 32.02, 28.01, 23.86, 23.64, 17.32, 13.17, 10.93, 9.68, -40.84. ¹¹B NMR (benzene-*d*₆, 128 MHz): δ 86.4. IR (KBr, cm^{-1}): ν 3080 (w), 3040 (w), 2964 (m), 2928 (m), 2891 (m), 1667 (m), 1591 (s,

ν_{CN}), 1517 (m), 1495 (m), 1462 (m), 1402 (m), 1367 (m), 1351 (m), 1275 (m), 1196 (m), 1160 (m), 1126 (m), 1095 (m), 1029 (m), 961 (m). UV-vis (THF): $\lambda_{\text{max}} = 663$ (ϵ : $200 \text{ M}^{-1} \text{ cm}^{-1}$). $\mu_{\text{eff}}(\text{C}_6\text{D}_6) = 4.7(2) \mu_{\text{B}}$ as determined by the Evans method. Mp. 230-232 °C.

To^MCo(O₂CCH₂SiMe₃) (14). ¹H NMR (benzene-*d*₆, 600 MHz): δ 208.77 (s, 2 H, O₂CCH₂SiMe₃), 37.30 (s, 2 H, C₆H₅), 19.31 (s, 2 H, C₆H₅), 16.20 (s, 1 H, *p*-C₆H₅), 15.92 (s, 9 H, O₂CCH₂SiMe₃), 11.34 (s, 6 H, CNCMe₂CH₂O), -49.53 (s, 18 H, CNCMe₂CH₂O). ¹¹B NMR (benzene-*d*₆, 128 MHz): δ 113.2. IR (KBr, cm⁻¹): ν 3080 (w), 3049 (w), 2965 (m), 2929 (m), 2896 (m), 2872 (m), 1595 (s, ν_{CN}), 1520, 1464 (m), 1434 (m), 1368 (m), 1354 (m), 1273 (m), 1251 (m), 1196 (m), 1162 (m), 1104 (m), 1024 (m), 958 (m). UV-vis (THF): $\lambda_{\text{max}} = 588$ (ϵ : $98 \text{ M}^{-1} \text{ cm}^{-1}$). $\mu_{\text{eff}}(\text{C}_6\text{D}_6) = 4.7(2) \mu_{\text{B}}$ as determined by the Evans method. Mp. 186-188 °C.

To^MCo(O₂CPh) (15). ¹H NMR (benzene-*d*₆, 600 MHz): δ 48.80 (s, 2 H), 31.55 (s, 2 H), 23.34 (s, 2 H), 17.16 (s, 2 H), 14.48 (s, 1 H), 13.16 (s, 6 H, CNCMe₂CH₂O), 12.83 (s, 1 H), -40.00 (s, 18 H, CNCMe₂CH₂O). ¹¹B NMR (benzene-*d*₆, 128 MHz): δ 83.6. IR (KBr, cm⁻¹): ν 3074 (w), 3045 (w), 2965 (m), 2927 (m), 2893 (m), 2870 (m), 1589 (s, ν_{CN}), 1536 (m, ν_{CN}), 1496 (m), 1462 (m), 1408 (m), 1368 (m), 1352 (m), 1273 (m), 1197 (m), 1159 (m), 1101 (m), 1069 (m), 1025 (m), 962 (m), 949 (m). UV-vis (THF): $\lambda_{\text{max}} = 587$ (ϵ : $157 \text{ M}^{-1} \text{ cm}^{-1}$). $\mu_{\text{eff}}(\text{C}_6\text{D}_6) = 4.6(2) \mu_{\text{B}}$ as determined by the Evans method. Mp. 238-240 °C.

To^MCo(O₂CEt) (16). ¹H NMR (benzene-*d*₆, 600 MHz): δ 35.16 (s, 4 H), 33.81 (s, 2 H, C₆H₅), 18.05 (s, 2 H, C₆H₅), 15.20 (s, 1 H, C₆H₅), 12.32 (s, 6 H, CNCMe₂CH₂O), -43.62 (s, 18 H, CNCMe₂CH₂O). ¹¹B NMR (benzene-*d*₆, 128 MHz): δ 95.0. IR (KBr, cm⁻¹): ν 3080 (w), 3045 (w), 2965 (m), 2932 (m), 2893 (m), 2874 (m), 1588 (s, ν_{CN}), 1544 (m,

ν_{CN}), 1466 (m), 1437 (m), 1387 (w), 1369 (m), 1352 (m), 1276 (m), 1199 (m), 1160 (m), 1074 (w), 1027 (w), 964 (m), 949 (m). UV-vis (THF): $\lambda_{\text{max}} = 584$ (ϵ : $98 \text{ M}^{-1} \text{ cm}^{-1}$). $\mu_{\text{eff}}(\text{C}_6\text{D}_6) = 4.8(2) \mu_{\text{B}}$ as determined by the Evans method. Mp. 174-176 °C.

To^MCo(O₂CⁿBu) (17). ¹H NMR (benzene-*d*₆, 600 MHz): δ 161.09 (s, 2 H, O₂CCH₂CH₂CH₂CH₃), 34.53 (s, 2 H, O₂C(CH₂)₃CH₃), 33.72 (s, 2 H, O₂C(CH₂)₃CH₃), 19.24 (s, 2 H, C₆H₅), 17.93 (s, 2 H, C₆H₅), 15.08 (s, 1 H, *p*-C₆H₅), 12.27 (s, 6 H, CNCMe₂CH₂O), 10.83 (s, 3 H, O₂C(CH₂)₃CH₃), -43.55 (s, 18 H, CNCMe₂CH₂O). ¹¹B NMR (benzene-*d*₆, 128 MHz): δ 95. IR (KBr, cm⁻¹): ν 3079 (w), 3055 (w), 2963 (m), 2930 (m), 2893 (m), 2871 (m), 1595 (s, ν_{CN}), 1540 (m, ν_{CN}), 1498 (w), 1461 (m), 1437 (m), 1385 (m), 1365 (m), 1355 (m), 1316 (w), 1274 (m), 1107 (w), 1024 (w), 956 (s). UV-vis (THF): $\lambda_{\text{max}} = 584$ (ϵ : $101 \text{ M}^{-1} \text{ cm}^{-1}$). $\mu_{\text{eff}}(\text{C}_6\text{D}_6) = 4.3(2) \mu_{\text{B}}$ as determined by the Evans method. Mp. 197-199 °C.

References

- (1) Q. Liu, H. Zhang, and A. Lei, *Angew. Chem. Int. Ed.*, **2011**, *50*, 10788-10799.
- (2) D. J. Diaz, A. K. Darko, and L. McElwee-White, *Eur. J. Org. Chem.*, **2007**, 4453-4465.
- (3) S. W. Ragsdale, *Biofactors*, **1997**, *6*, 3-11.
- (4) S. W. Ragsdale, E. Pierce, *Biochimica et Biophysica Acta*, **2008**, *1784*, 1873-1898.
- (5) S. W. Ragsdale, *Ann. N. Y. Acad. Sci.*, **2008**, *1125*, 129-136.
- (6) P. A. Lindahl, *J. Biol. Inorg. Chem.*, 2004, **9**, 516-524.

- (7) J. D. Jewson, L. M. Liable-Sands, G. P. A. Yap, A. L. Rheingold, and K. H. Theopold, *Organometallics*, **1999**, *18*, 300-305.
- (8) J. L. Kisko, T. Hascall, G. Parkin, *J. Am. Chem. Soc.*, **1998**, *120*, 10561-10562.
- (9) A. Kunishita, T. L. Gianetti, J. Arnold, *Organometallics*, **2012**, *31*, 372-380.
- (10) N. Shirasawa, T. T. Nguyet, S. Hikichi, Y. Moro-oka, M. Akita, *Organometallics*, **2001**, *20*, 3582-3598.
- (11) F. E. Jacobsen, R. M. Breece, W. K. Myers, D. L. Tierney, S. M. Cohen, *Inorg. Chem.*, **2006**, *45*, 7306-7315.
- (12) F. Lu, A. L. Rheingold, J. S. Miller, *Chem. Eur. J.*, **2013**, *19*, 14795-14797.
- (13) H. S. Ahn, T. C. Davenport, T. D. Tilley, *Chem Commun.*, **2014**, *50*, 3834-3837.
- (14) J. F. Dunne, J. Su, A. Ellern, A. D. Sadow, *Organometallics*, **2008**, *27*, 2399-2401.
- (15) R. R. Reinig, E. L. Fought, A. Ellern, T. L. Windus, and A. D. Sadow, *Chem. Commun.*, **2017**, *53*, 11020-11023.
- (16) R. R. Reinig, D. Mukherjee, Z. B. Weinstein, W. Xie, T. Albright, B. Baird, T. S. Gray, A. Ellern, G. J. Miller, A. H. Winter, S. L. Bud'ko, and A. D. Sadow, *Eur. J. Inorg. Chem.*, **2016**, 2486-2494.
- (17) S. Yoshimitsu, S. Hikichi and M. Akita, *Organometallics*, **2002**, *21*, 3762-3773.
- (18) P. J. Schebler, C. G. Riordan, I. Guzei, A. L. Rheingold, *Inorg. Chem.*, **1998**, *37*(19), 4754-4755.

- (19) J. A. DuPont, M. B. Coxey, P. J. Schebler, C. D. Incarvito, W. G. Dougherty, G. P. A. Yap, A. L. Rheingold, and C. G. Riordan, *Organometallics*, **2007**, *26*, 971-979.
- (20) N. Shirasawa, M. Akita, S. Hikichi, and Y. Moro-oka, *Chem. Comm.*, **1999**, 417-418.
- (21) R. S. Drago, *Physical methods for chemists*; 2nd ed.; Saunders College Pub.: Ft. Worth, 1992.
- (22) J. F. Dunne, D. B. Fulton, A. Ellern, A. D. Sadow, *J. Am. Chem. Soc.*, **2010**, *132*, 17680-17683.
- (23) D. Mukherjee, R. R. Thompson, A. Ellern, A. D. Sadow, *ACS Catal.*, **2011**, 698-702.
- (24) L. Yang, D. R. Powell, and R. P. Houser, *Dalton Trans.*, **2007**, 955-964.
- (25) J. P. Perdew, M. Ernzerhof, K. Burke, *J. Chem. Phys.*, **1996**, *105* (22), 9982-9985.
- (26) R. Krishnan, J. S. Binkley, R. Seeger, J. A. Pople, *J. Chem. Phys.*, **1980**, *72*, 650-654.
- (27) M. Dolg, H. Stoll, H. Preuss, R. M. Pitzer, *J. Phys. Chem.*, **1993**, *97*, 5852.
- (28) J. L. Detrich, O. M. Reinaud, A. L. Rheingold, and K. H. Theopold, *J. Am. Chem. Soc.*, **1995**, *117*, 11745-11748.
- (29) E. K. Barefield, D. H. Busch, S. M. Nelson, *Q. Rev., Chem. Soc.*, **1968**, *22*, 457-498.
- (30) J. L. Detrich, R. Konecny, W. M. Vetter, A. L. Rheingold, K. H. Theopold, *J. Am. Chem. Soc.*, **1996**, *118*, 1703-1712.

- (31) L. S. Glebov, G. A. Kliger, T. P. Popova, V. E. Shiryaeva, V. P. Ryzhikov, E. V. Marchevskaya, O. A. Lesik, S. M. Loktev, V. G. Beryezkin, *Journal of Molecular Catalysis*, **1986**, *35*, 335-348.
- (32) D. Seyferth, R. M. Weinstein, R. C. Hui, W. Wang, C. M. Archer, *J. Org. Chem.*, **1992**, *57*, 5620-5629.
- (33) G. F. Fulmer, A. J. Miller, N. H. Sherden, H. E. Gottlieb, A. Nudelman, B. M. Stoltz, J. E. Bercaw, K. I. Goldberg, *Organometallics*, **2010**, *29* (9), 2176-2179.
- (34) M. Balamurugan, M. Ramasamy, E. Suresh, M. Palaniandavar, *Dalton Trans.*, **2011**, *40*, 9413-9424.
- (35) M. Valiev, E. J. Bylaska, N. Govind, K. Kowalski, T. P. Straatsma, H. J. J. Van Dam, D. Wang, J. Nieplocha, E. Apra, T. L. Windus, W. A. Jong, *Comput. Phys. Commun.*, **2010**, *181*, 1477.
- (36) A. Klamt, G. Schüürmann, *J. Chem. Soc., Perkin Trans. 2*, **1993**, *5*, 799-805.
- (37) M. W. Schmidt, K. K. Baldrige, J. A. Boatz, S. T. Elbert, M. S. Gordon, J. H. Jensen, S. Koseki, N. Matsunaga, K. A. Nguyen, S. J. Su, T. L. Windus, M. Dupuis, J. A. Montgomery, *J. Comput. Chem.*, **1993**, *14*, 1347.

**CHAPTER 5: SYNTHESIS, CHARACTERIZATION, AND REACTIVITY OF
TRIS(OXAZOLINYL)BORATO IRON AND NICKEL COMPLEXES**

Modified from a paper to be submitted to a journal

Regina R. Reinig, Arkady Ellern, and Aaron D. Sadow*

Abstract

The reaction of FeBr₂ and thallium tris(4,4-dimethyl-2-oxazoliny)phenylborate (TlTo^M) in tetrahydrofuran (THF) provides To^MFeBr (**1**). Alternatively, FeBr₂ and 2 equiv. of TlTo^M react to give (To^M)₂Fe (**2**); however, this species is not detected in one-to-one reactions of FeBr₂ and TlTo^M. (To^M)₂Fe and FeBr₂ react in THF overnight via a comproportionation process to give To^MFeBr. Salt metathesis of **1** and KBn affords To^MFeBn (**3**) in 89% yield. Complexes **1** – **3** contain a high-spin iron(II) center characterized by the effective magnetic moments ranging from 4.9 to 5.4 μ_B determined by Evans Method. A single ¹H NMR signal assigned to the methyl groups of the To^M ligand and a single ν_{CN} band in the IR suggested tridentate coordination of the To^M ligand to iron in **1** and **3** while two ν_{CN} bands at 1604 and 1548 cm⁻¹ indicated bidentate coordination of To^M to iron in **2**. The coordination mode is supported by X-ray crystallography studies of **1** – **3** that further identify these complexes as containing a tetrahedral iron center. To^MFeBn and CO (1 atm) react to afford isolable To^MFe{C(O)Bn}(CO)₂ (**4**) as a yellow solid. Complex **4** is diamagnetic (*S* = 0), and the three distinct methyl signals in the ¹H NMR spectrum are consistent with a six-coordinate, C_s-symmetric species. This assignment is supported by its IR spectrum, which revealed intense bands at 2004 and 1935 cm⁻¹ (symmetric and asymmetric ν_{CO}), at 1680 and 1662 cm⁻¹ (acetyl rotomers, ν_{CO}), and at 1593 and 1553 cm⁻¹ (ν_{CN}). A single-

crystal X-ray diffraction study of $To^MFe\{C(O)Bn\}(CO)_2$ confirmed the spectroscopic assignments. The synthesis of To^MNiCl and To^MNiOAc is also reported; however, these complexes did not lead to any organonickel(II) complexes.

Introduction

Iron-containing compounds have attracted interest as biological mimics in order to gain further understanding of iron based proteins. In particular, iron complexes stabilized by tris(pyrazolyl)borate serve as models for oxygenation reactions due to the pyrazolyl ligands which mimic the histidine ligands which are so prevalent at the iron coordination site.¹⁻⁴ Many of these systems focus on the reactivity of the iron complexes towards O_2 in order to better understand the mechanism of iron oxygenases. While $TpFe$ compounds have been very useful in studying biological systems, a major general hindrance encountered in scorpionate chemistry is comproportionation reactions that result in, for example, Tp_2Fe .⁵ Synthetic systems oftentimes prevent this undesirable reactivity by introducing steric bulk to the ancillary ligand while biological systems rely more upon second sphere coordination environments to stabilize the metal center. The problem with stabilization of the metal center by increasing the steric bulk of the ancillary ligand is that the metal center becomes less accessible to substrates, thus potentially limiting its reactivity. Previously, we reported the synthesis and isolation of coordinatively unsaturated To^MCoCl and found that the open coordination environment provided by To^M allows for the synthesis of $(To^M)_2Co$ yet at the same time provides sufficient steric protection such that once To^MCoCl is isolated, the chloride ligand can be readily exchanged with other potentially more reactive ligands without further

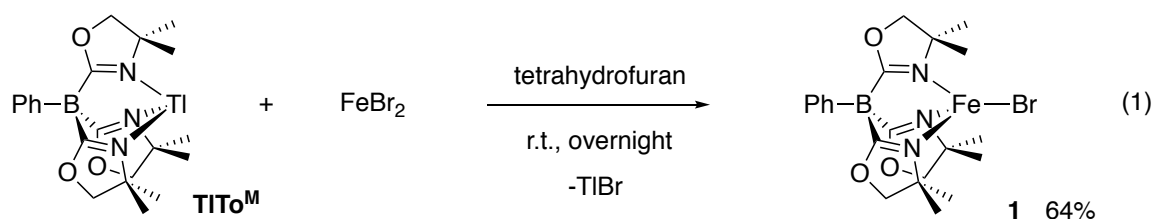
complication of $(\text{To}^{\text{M}})_2\text{Co}$.⁶ The results demonstrate To^{M} as a suitable ligand for the study of late transition metal complexes.

Of related importance is the reactivity of $\text{To}^{\text{M}}\text{CoR}$ ($\text{R} = \text{Me}, \text{Et}, \text{CH}_2\text{SiMe}_3, \text{}^n\text{Bu}, \text{Ph}, \text{Bn}$), which undergo rapid oxidative carbonylation by reaction of CO followed by O_2 to form carboxylate compounds.⁷ The carboxylate compounds can also be formed by direct insertion of CO_2 into the Co-C bond; however, the reaction is kinetically less favorable requiring up to several weeks. Thus, the results parallel biological systems, which also favor a multi-step route to acetate synthesis over direct utilization of CO_2 . The intriguing reactivity demonstrated by organocobalt(II) compounds stabilized by To^{M} in oxidative carbonylation lead us to question if analogous iron(II) alkyl compounds might also be reactive towards oxidative carbonylation or if instead the reactivity is unique to cobalt. At the same time, given TpFe complexes have shown promising reactivity as models of enzymes in oxidation reactions, the synthesis of $\text{To}^{\text{M}}\text{Fe}$ compounds could provide entryway into similar explorative studies.

Herein we report the synthesis and characterization of $\text{To}^{\text{M}}\text{FeBr}$ (**1**) and compare it to the synthesis of $\text{To}^{\text{M}}\text{CoCl}$. The independent synthesis of $(\text{To}^{\text{M}})_2\text{Fe}$ (**2**), which was expected as a side product in the synthesis of $\text{To}^{\text{M}}\text{FeBr}$, is also presented and it is shown that $(\text{To}^{\text{M}})_2\text{Fe}$ can be converted to $\text{To}^{\text{M}}\text{FeBr}$ by reaction of **2** with excess FeBr_2 . The latter reactivity explains the ease of synthesis of $\text{To}^{\text{M}}\text{FeBr}$, which contrasts with the synthetic challenges encountered in the synthesis of $\text{To}^{\text{M}}\text{CoCl}$. The utility of $\text{To}^{\text{M}}\text{FeBr}$ as a precursor to iron(II) alkyl compounds is demonstrated by the salt metathesis reaction of $\text{To}^{\text{M}}\text{FeBr}$ with KBn in THF yielding $\text{To}^{\text{M}}\text{FeBn}$ (**3**). The reactivity of **3** towards CO , O_2 , and CO_2 is studied and presented in relation to the reactivity observed for $\text{To}^{\text{M}}\text{CoBn}$.

Results and Discussion

The reaction of TITo^{M} and FeBr_2 in tetrahydrofuran at room temperature readily affords paramagnetic $\text{To}^{\text{M}}\text{FeBr}$ (**1**) as a cream colored solid (equation (1)). $\text{To}^{\text{M}}\text{FeBr}$ was characterized by a single signal in the ^{11}B NMR spectrum at 74 ppm that was significantly displaced from the region in which diamagnetic borate complexes typically appear (e.g., ^{11}B NMR signal for TITo^{M} is located at -16 ppm). The ^1H NMR spectrum of **1** contained broad, yet diagnostic resonances from 24 to -30 ppm that were assigned to the methyl (-28.9 ppm, 18 H), methylene (20.9 ppm, 6 H) and phenyl group in the To^{M} ligand on the basis of integration. The IR spectrum of **1** contained a single ν_{CN} band at 1586 cm^{-1} , which is consistent with tridentate coordination of the To^{M} ligand to iron. The $5.1(2)\ \mu_{\text{B}}$ effective magnetic moment of **1**, measured by the Evans method, characterized **1** as high-spin iron(II). This value is lower than similar tris(pyrazolyl)borate-coordinated tetrahedral iron(II) halide complexes, such as $\text{Tp}^{\text{tBu,Me}}\text{FeBr}$ ($5.4(1)\ \mu_{\text{B}}$) and $\text{Tp}^{\text{tBu}}\text{FeCl}$ ($5.7\ \mu_{\text{B}}$).⁸⁻⁹



An X-ray diffraction study confirmed tridentate coordination of the To^{M} ligand to a pseudo-tetrahedral iron center (Figure 1). The average Fe-N interatomic distance is $2.067\ \text{\AA}$ and the Fe-Br interatomic distance is $2.3517(9)\ \text{\AA}$. The Fe-N and Fe-Br interatomic distances are longer than those observed in $\text{To}^{\text{M}}\text{CoCl}$ ($\text{Co-N}_{\text{average}} = 2.055\ \text{\AA}$ and $\text{Co-Cl} = 2.206(5)\ \text{\AA}$) as would be expected on the basis of the greater ionic radii of Br

compared to Cl, and similar to other scorpionate iron(II) halide complexes. For example, in $\text{Tp}^{\text{tBu,Me}}\text{FeBr}$ the $\text{Fe-N}_{\text{average}}$ interatomic distance is 2.090 Å and the Fe-Br bond interatomic distance is 2.3604(8) Å.⁸

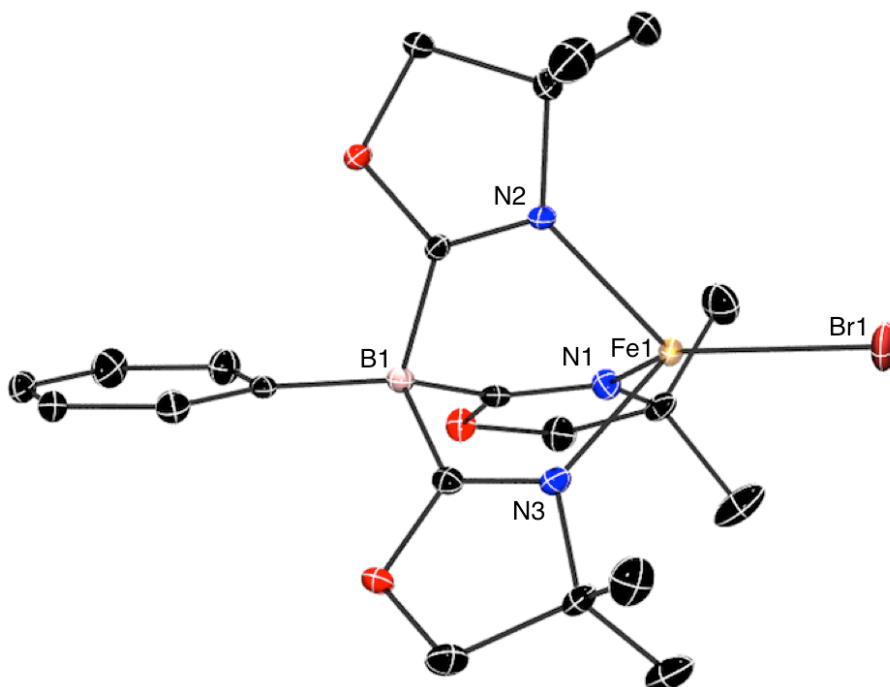
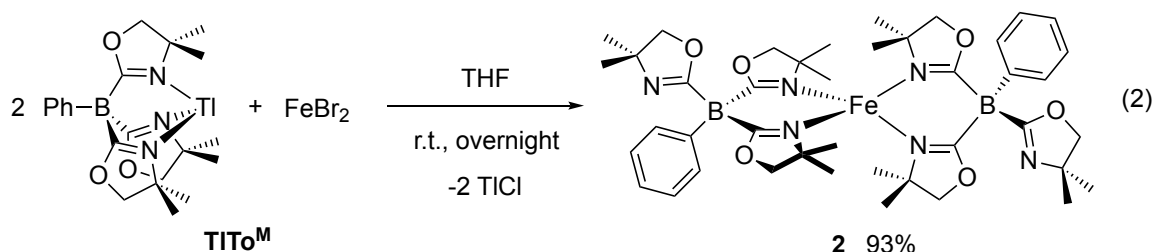


Figure 1. Thermal ellipsoid plot of $\text{To}^{\text{M}}\text{FeBr}$ (**1**) with ellipsoids at 20 % probability. Hydrogen atoms are omitted for clarity. Selected interatomic distances (Å) and angles (°): Fe1-Br1 2.3517(9), Fe1-N1 2.072(4), Fe1-N2 2.061(4), Fe1-N3 2.069(4); N1-Fe1-N2 91.4(2), N1-Fe1-N3 92.4(2), N2-Fe1-N3 90.4(2), N1-Fe1-Br1 120.4(2), N2-Fe1-Br1 129.4(1), N3-Fe1-Br1 122.8(1), B1-Fe1-Br1 174.4(2).

The synthesis of $\text{To}^{\text{M}}\text{FeBr}$ is straightforward, and the possible side product $\text{To}^{\text{M}}_2\text{Fe}$ is not detected under the conditions of equation 1. Previously, we reported the synthesis of $\text{To}^{\text{M}}\text{CoCl}$ and $\text{To}^{\text{M}}_2\text{Co}$. In the cobalt system, $\text{To}^{\text{M}}_2\text{Co}$ forms readily as a contaminant, and synthetic conditions to isolate $\text{To}^{\text{M}}\text{CoCl}$ require $\text{CoCl}_2 \cdot \text{THF}$ (rather than CoCl_2) used in excess. We sought to identify underlying chemical features responsible for the difference in selectivity for $\text{To}^{\text{M}}\text{MX}$ vs. $\text{To}^{\text{M}}_2\text{M}$ compounds. First, the independent synthesis of $(\text{To}^{\text{M}})_2\text{Fe}$ was attempted. Interestingly, $(\text{To}^{\text{M}})_2\text{Fe}$ forms as the

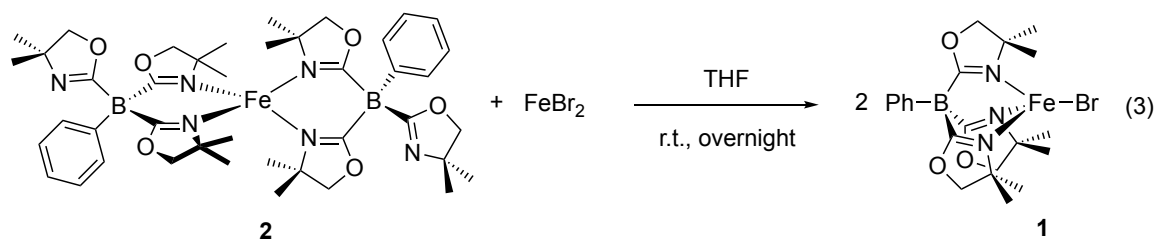
only detected product from the reaction of FeBr_2 and two equiv. of TITo^{M} in THF (equation (2)). $(\text{To}^{\text{M}})_2\text{Fe}$ (**2**) is isolated as an analytically pure white solid in excellent yield (93%).



The ^1H NMR spectrum was rather unusual and contained peaks in the diamagnetic region as well as the expected paramagnetic signals. Given the selective synthesis of $\text{To}^{\text{M}}\text{FeBr}$ above, we considered a possible interpretation of the apparent diamagnetic signals in the ^1H NMR spectrum that compound **2** was in fact a mixture of $\text{To}^{\text{M}}\text{FeBr}$ and TITo^{M} . Several data eliminate that possibility. First, the chemical shifts of the diamagnetic signals and those of TITo^{M} were distinct. Moreover, mixtures of TITo^{M} and $(\text{To}^{\text{M}})_2\text{Fe}$ gave ^1H NMR spectra that contained two sets of diamagnetic signals, with one set matching the shifts expected for TITo^{M} (1.03 ($\text{CNCMe}_2\text{CH}_2\text{O}$) and 3.41 ($\text{CNCMe}_2\text{CH}_2\text{O}$) ppm) and the other corresponding to the resonances observed in isolated $(\text{To}^{\text{M}})_2\text{Fe}$ (1.02 and 2.96 ppm). The ^{11}B NMR spectrum of $(\text{To}^{\text{M}})_2\text{Fe}$ contained a characteristic signal at -122 ppm, and this signal was distinct from the downfield ^{11}B NMR signal in samples of $\text{To}^{\text{M}}\text{FeBr}$ and the diamagnetic signal of TITo^{M} (^{11}B NMR: -16 ppm). Nonetheless, the ^{11}B NMR is clearly affected by the high spin Fe(II) center. Finally, the effective magnetic moment for **2** of $4.9(2) \mu_{\text{B}}$, measured in solution by the Evans method, is consistent with high spin Fe(II) . If the signals were in fact due to

TlTo^M then the effective magnetic moment would be expected to be much lower due to the lower than expected concentration of the paramagnetic To^MFe species. The reason for the distinct diamagnetic signals intermixed with paramagnetic signals is currently not understood, but it can be concluded that paramagnetic (To^M)₂Fe is analytically and spectroscopically pure despite these diamagnetic signals. The infrared spectrum of **2** suggested bidentate coordination of the To^M ligands to iron with two ν_{CN} bands appearing at 1604 and 1548 cm⁻¹ similar to the stretching frequencies observed for (To^M)₂Co (ν_{CN} = 1602 and 1554 cm⁻¹).

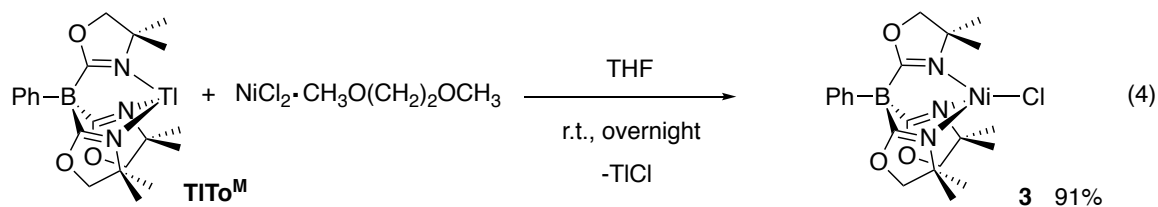
The independent synthesis of (To^M)₂Fe from reaction of TlTo^M and FeBr₂ in THF at room temperature indicates that (To^M)₂Fe is indeed a viable side product under the reaction conditions adopted for the synthesis of To^MFeBr. Thus, the results suggest that a thermodynamic difference may be playing a role in the facile synthesis of To^MFeBr. To explore this possibility, FeBr₂ and (To^M)₂Fe were allowed to react in THF. Upon stirring overnight, NMR analysis confirmed the complete conversion of (To^M)₂Fe to To^MFeBr. The reaction was found to occur in other solvents as well, such as toluene, but in these more nonpolar solvents the reaction requires heating at 60°C for several days. Thus, it appears that the reason FeBr₂ is an effective precursor for the synthesis of To^MFeBr is that while it allows for the formation of (To^M)₂Fe, (To^M)₂Fe in turn readily reacts with FeBr₂ in THF to form the desired To^MFeBr.



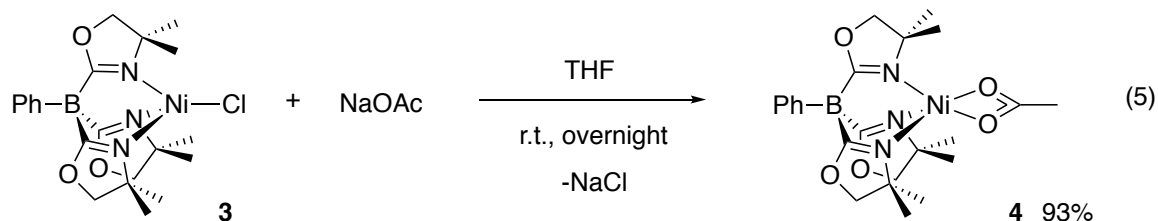
The observed transformation of $(\text{To}^{\text{M}})_2\text{Fe}$ to $\text{To}^{\text{M}}\text{FeBr}$ is particularly unexpected given in the analogous cobalt system, $(\text{To}^{\text{M}})_2\text{Co}$ occurs readily if conditions are not used that kinetically favor instead the synthesis of $\text{To}^{\text{M}}\text{CoCl}$. In comparison, the analogous Tp_2Fe complexes are reported to be stable and in fact present a challenge when attempting to synthesize heteroleptic Fe compounds. For instance, the synthesis of TpFeR (R = alkyl or aryl) is complicated by the strong tendency of these latter compounds to disproportionate to form Tp_2Fe .¹ Perhaps one reason for the increased favorability of Tp_2Fe versus $\text{To}^{\text{M}}_2\text{Fe}$ is that Tp_2Fe forms as an octahedral complex whereas $(\text{To}^{\text{M}})_2\text{Fe}$ maintains a tetrahedral geometry with each To^{M} ligand bound in a bidentate fashion. The coordinatively unsaturated $(\text{To}^{\text{M}})_2\text{Fe}$ could explain its enhanced reactivity compared with Tp_2Fe . Importantly, this change in coordination environment indicates that the slightly more sterically hindered To^{M} versus Tp^{Me_2} concluded from earlier studies of solid angles is significant enough to cause this change in preferential geometry.¹⁰

Synthesis of $\text{To}^{\text{M}}\text{NiCl}$ (**3**) was similarly achieved by the reaction of TiTo^{M} and $\text{NiCl}_2 \cdot \text{DME}$ (DME = dimethoxyethane) in THF. This reaction can be performed on a multi-gram scale, with respect to TiTo^{M} , affording $\text{To}^{\text{M}}\text{NiCl}$ as a pink crystalline solid in over 90% yield (equation (4)). An X-band EPR spectrum of **3** collected at 10K showed no signal. This result is in accord with literature reports of other nickel(II) complexes in a tetrahedral geometry which are EPR silent due to large zero-field splitting parameters.¹¹ The UV-Vis spectrum of **1** displayed λ_{max} at 310 (ϵ : $233 \text{ M}^{-1}\text{cm}^{-1}$), 478 (ϵ : $355 \text{ M}^{-1}\text{cm}^{-1}$), 817 (ϵ : $84 \text{ M}^{-1}\text{cm}^{-1}$), and 925 nm (ϵ : $115 \text{ M}^{-1}\text{cm}^{-1}$), which is similar to that reported for

tris(pyrazolyl)borate nickel(II) halide complexes (e.g. $\text{Ni}^{\text{II}}(\text{Cl})(\text{Tp}^{\text{Me}_2\text{Br}})$ in CH_2Cl_2 $\lambda_{\text{max}} = 481$ ($\epsilon: 360 \text{ M}^{-1}\text{cm}^{-1}$), 801 ($\epsilon: 105 \text{ M}^{-1}\text{cm}^{-1}$), and 900 nm ($\epsilon: 120 \text{ M}^{-1}\text{cm}^{-1}$)).¹²

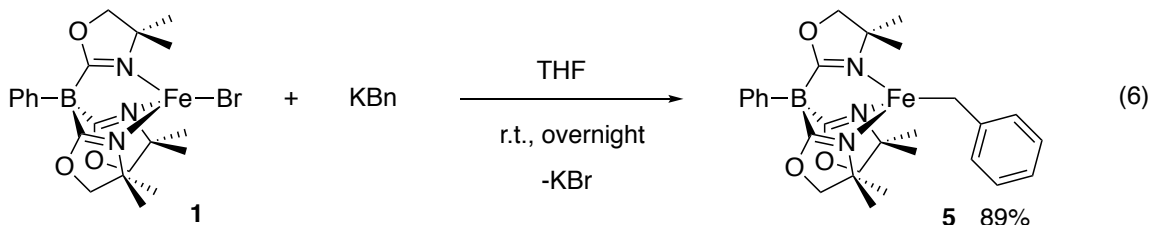


Salt metathesis reaction of $\text{To}^{\text{M}}\text{NiCl}$ with NaOAc proceeds readily in THF at room temperature overnight. $\text{To}^{\text{M}}\text{NiOAc}$ was isolated as a bright green solid (equation (5)). Single X-ray quality crystals of $\text{To}^{\text{M}}\text{NiOAc}$ grown from a saturated pentane solution at $-40 \text{ }^\circ\text{C}$ showed a tetrahedral geometry around the nickel center. However, despite attempts to form alkylated products $\text{To}^{\text{M}}\text{NiR}$ ($\text{R} = \text{Me}, \text{CH}_2\text{SiMe}_3, \text{or Bn}$), no nickel(II) alkyls could be isolated and instead decomposition occurred.



In contrast, $\text{To}^{\text{M}}\text{FeBr}$ reacts with KBn to form $\text{To}^{\text{M}}\text{FeBn}$ (**5**) as a yellow solid (equation (6)). Complex **5** was characterized by a single signal at -225 ppm in the ^{11}B NMR spectrum which was the most downfield resonance observed for the iron(II) complexes reported here. As in $\text{To}^{\text{M}}\text{FeBr}$, the methyl and methylene signals of the oxazoline group in the To^{M} ligand were equivalent in the ^1H NMR spectrum supporting tridentate coordination. The signal corresponding to the methyl resonances is shifted even further upfield (-56.35 ppm) relative to **1** (-30 ppm). The infrared spectrum (KBr) of **5** contained several notable features. Instead of a single ν_{CN} signal observed as expected for tridentate coordination of To^{M} to iron, two ν_{CN} signals were observed at

1586 and 1552 cm^{-1} . Given no ν_{CN} signals appear at higher intensity than 1600 cm^{-1} , the three oxazoline rings are clearly coordinated to iron. However, the presence of two rather than one ν_{CN} band indicates that the oxazoline rings are not bound to iron in an equivalent manner. In addition, a distinct band at 1701 cm^{-1} was evident.



X-ray quality crystals of **5** revealed a tetrahedral iron center with the Fe-C interatomic distance of 2.067(3) Å only slightly longer than the analogous Co-C interatomic distance of 2.023(2) Å in $\text{To}^{\text{M}}\text{CoBn}$ and similar to other organoiron compounds (e.g. $\text{Tp}^{\text{iPr}}\text{Fe}-\text{CH}_2\text{C}_6\text{H}_4\text{Me}-p$ Fe-C 2.05(1) Å (Figure 2)).¹³ The B-Fe-C angle was nearly linear (170°) but the benzyl ligand deviated further from linearity than in $\text{To}^{\text{M}}\text{FeBr}$ where B-Fe-Br measures 174°.

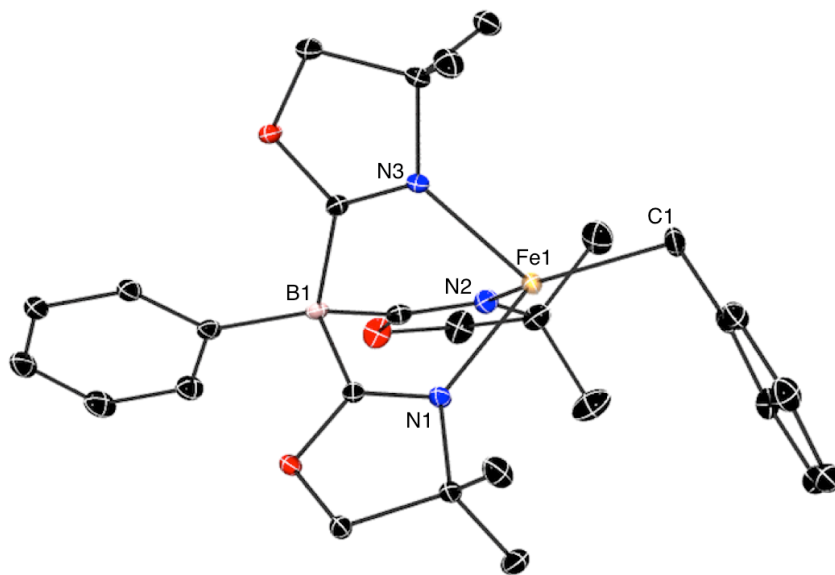
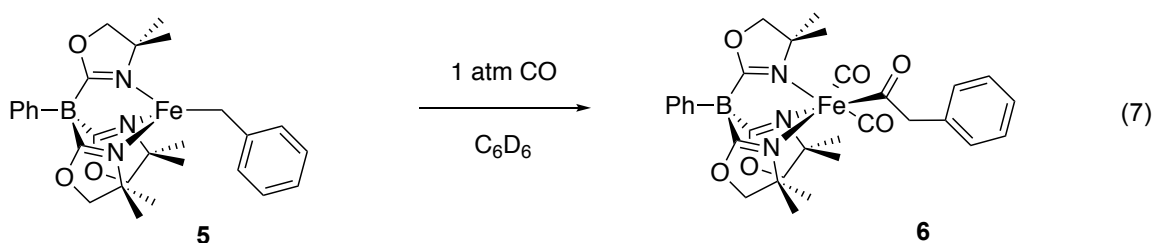


Figure 2. Thermal ellipsoid plot of $\text{To}^{\text{M}}\text{FeBn}$ (**5**) with ellipsoids at 20 % probability. Hydrogen atoms are omitted for clarity. Selected interatomic distances (Å) and angles (°): Fe1-C1 2.067(3), Fe1-N1 2.073(2), Fe1-N2 2.096(3), Fe1-N3 2.092(2); N1-Fe1-N2 90.0(1), N1-Fe1-N3 90.3(1), N2-Fe1-N3 88.6(1), N1-Fe1-C1 134.8(1), N2-Fe1-C1 121.6(1), N3-Fe1-C1 119.2(1), B1-Fe1-C1 170.0(1).

To^MFeBn reacts readily with CO to form To^MFe{C(O)Bn}(CO)₂ (**6**); upon exposure of a solution of **5** to CO (atm) the solution maintains its yellow color but if allowed to stand a precipitate settles out (equation (7)). NMR spectroscopy analysis of the product revealed a new ¹¹B NMR signal at -28 ppm and diamagnetic signals in the ¹H NMR that can be assigned to an octahedral iron(II) configuration with three distinct signals visible for the methyl groups of the oxazoline ring. The absence of any paramagnetic signals in the ¹H NMR spectrum suggests that species **6** is low-spin iron(II). The IR spectrum of **6** contained two equally intense signals at 2004 and 1935 cm⁻¹ and two weaker signals at 1680 and 1662 cm⁻¹. The two higher energy bands are assigned as two terminal CO ligands coordinated to iron and the two lower energy bands suggest the presence of an acyl ligand that exists as two rotamers. In combination with the two coordinated CO ligands and acyl ligand, the IR spectrum indicates that all of the oxazoline rings of the To^M ligand are coordinated to iron with two ν_{CN} signals observed at 1593 and 1553 cm⁻¹ as explained by To^M occupying a combination of equatorial and axial coordination sites.



Finally, X-ray crystallography confirmed the octahedral structural assignment of **6** (Figure 3). The reaction of To^MFeBn with CO to form To^MFe{C(O)Bn}(CO)₂ is not unprecedented given similar carbonylated TpFe complexes have been isolated (e.g. HBpz₃Fe{C(O)Me}(CO)₂ and *t*-BuTp^{*i*-Pr}Fe{C(O)Me}(CO)₂).¹⁴⁻¹⁵ The Fe–C interatomic distances measure 1.753(7) and 1.753(6) Å for the carbonyl groups and 1.984(6) Å for

the acetyl moiety. These interatomic distances are similar to related compounds. For example, in $\text{HBpz}_3\text{Fe}\{\text{C}(\text{O})\text{Me}\}(\text{CO})_2$ the Fe–C interatomic distances are 1.758(6) and 1.771(5) Å for the carbonyl groups and 1.968(5) Å for the acetyl group. Similarly, as in $\text{HBpz}_3\text{Fe}\{\text{C}(\text{O})\text{Me}\}(\text{CO})_2$ where the longest Fe–N interatomic distance (2.082(4) Å) lies trans to the acetyl group, the Fe–N interatomic distance (2.097(4) Å) trans to the acetyl group is longer than the Fe–N interatomic distances (2.028(4) and 2.047(4) Å) which are trans to the carbonyls.

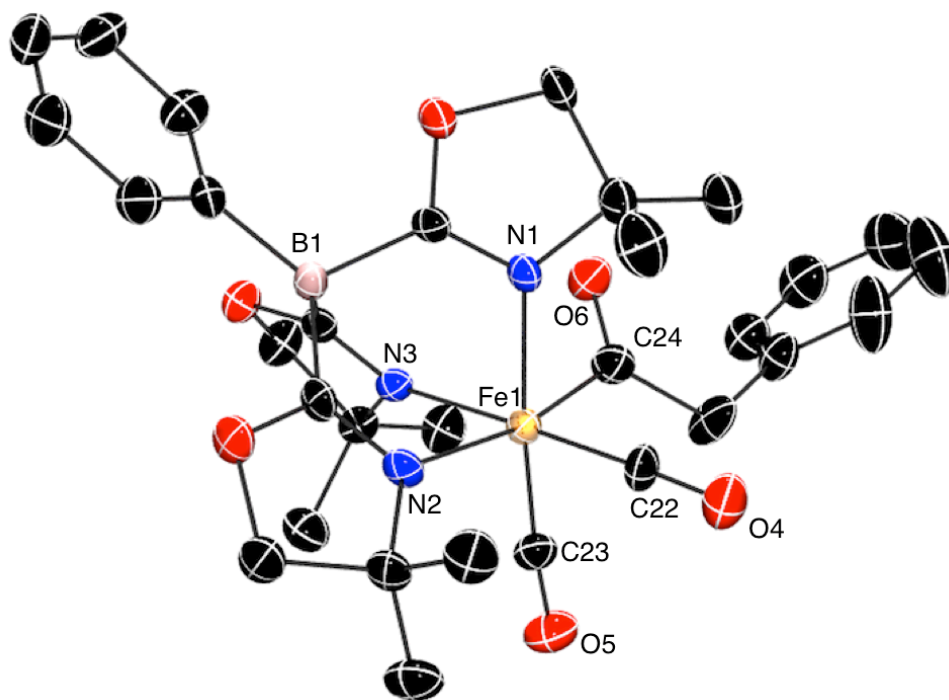


Figure 3. Thermal ellipsoid plot of $\text{To}^{\text{M}}\text{Fe}\{\text{C}(\text{=O})\text{Bn}\}(\text{CO})_2$ (**6**) with ellipsoids at 20 % probability. Hydrogen atoms are omitted for clarity. Selected interatomic distances (Å) and angles (°): Fe1–C22 1.753(6), Fe1–C23 1.753(7), Fe1–C24 1.984(6), Fe1–N1 2.028(4), Fe1–N2 2.097(4), Fe1–N3 2.047(4), C22–O4 1.159(7), C23–O5 1.155(7), C24–O6 1.228(7); N2–Fe1–C22 97.6(2), C22–Fe1–C24 91.1(3), C24–Fe1–N3 86.8(2), N3–Fe1–N2 84.9(2), N1–Fe1–C23 174.7(2).

$\text{To}^{\text{M}}\text{Fe}\{\text{C}(\text{O})\text{Bn}\}(\text{CO})_2$ and O_2 reacts to form a species that has a ^{11}B signal indistinguishable from **6** (−18 ppm) as well as similar signals in the ^1H NMR at 1 and 3 ppm; however, an identifying feature in the ^1H NMR at 10 ppm indicates a new product has formed. The ^1H signal at 10 ppm typically signifies formation of HTo^{M} ; however the ^1H signals of the new species are shifted slightly upfield in comparison with the signals reported for HTo^{M} . In addition, if authentic HTo^{M} is added to a benzene- d_6 solution of the new species, the signals corresponding to the new species as well as a separate set of signals for HTo^{M} are observed further ruling out HTo^{M} as the product. The UV-Vis supports conversion of **6** to a new iron containing species with the characteristic broad band at 800 nm disappearing upon addition of O_2 to **6**. The only absorption in the UV-Vis for the new species is a broad tailing absorption from 200 to 500 nm. Loss of the carbonyl and acetyl function groups in **4** is confirmed by IR spectroscopy where in the carbonyl and acetyl region only one weak band at 1700 cm^{-1} was observed for the new species. The direct reaction of $\text{To}^{\text{M}}\text{FeBn}$ and O_2 forms the same product as the reaction of **4** with O_2 as evidenced by matching signals in the ^1H NMR and ^{11}B NMR spectra. The unexpected similarity between these two reactions suggests that the oxidative carbonylation to form carboxylate compounds, as found in the cobalt(II) alkyl system, does not occur in the analogous iron(II) alkyl complexes. Support for this conclusion was further gained by reaction of $\text{To}^{\text{M}}\text{FeBn}$ with CO_2 to provide a product that was characterized by a new major signal at −24.27 ppm assigned to the methyl groups on the oxazoline ring on the basis of integration and a ^{11}B signal at 35 ppm. The product is presumably $\text{To}^{\text{M}}\text{FeO}_2\text{CBn}$ and supports that this carboxylate compound is not forming in the reaction of $\text{To}^{\text{M}}\text{FeBn}$ with CO followed by O_2 .

Conclusion

In synthesizing $\text{To}^{\text{M}}\text{FeBr}$, several striking differences with regards to cobalt were discovered. Primarily, solvent-free FeBr_2 readily provides spectroscopically and analytically pure $\text{To}^{\text{M}}\text{FeBr}$ whereas a solvent adduct of the cobalt chloride starting material, $\text{CoCl}_2 \cdot \text{THF}$ (THF = tetrahydrofuran), is required in order to effectively promote salt metathesis reaction with TiTo^{M} and to avoid formation of $(\text{To}^{\text{M}})_2\text{Co}$. Interrelated to this first observation was the discovery that $(\text{To}^{\text{M}})_2\text{Fe}$ also serves as precursor to $\text{To}^{\text{M}}\text{FeBr}$. Thus, reaction of $(\text{To}^{\text{M}})_2\text{Fe}$ with FeBr_2 in THF at room temperature affords **1** in THF. $\text{To}^{\text{M}}\text{NiCl}$ is also isolable and serves as precursor to $\text{To}^{\text{M}}\text{NiOAc}$; however, organonickel compounds could not be isolated. Complex **1** readily undergoes salt metathesis reaction with KBn to provide $\text{To}^{\text{M}}\text{FeBn}$. Like similar TpFeBn complexes, **5** reacts with CO to form a dicarbonyl acyl species. We are currently working to synthesize alternative iron(II) alkyl complexes supported by To^{M} to more fully understand the reactivity of this class of organometallic compounds.

Experimental Section

General Procedures. All reactions were performed using standard Schlenk techniques under argon or in a glovebox under an inert atmosphere of nitrogen. Benzene and tetrahydrofuran were dried and deoxygenated using an IT PureSolv system. Benzene- d_6 was degassed with freeze-pump-thaw cycles, heated to reflux over a Na/K alloy, and then vacuum transferred. ^1H and ^{11}B NMR spectra were collected on a Bruker Avance III 600 spectrometer. ^{11}B NMR spectra were referenced to an external sample of $\text{BF}_3 \cdot \text{Et}_2\text{O}$. Infrared spectra were measured on a Bruker Vertex 80 FTIR spectrometer. UV-Vis spectra were recorded on an Agilent 8453 UV-vis spectrophotometer. The electron

paramagnetic resonance (EPR) spectra were obtained with an X-band Elexsys 580 FT-EPR spectrometer in continuous-wave mode. Elemental analyses were performed using a Perkin-Elmer 2400 Series II CHN/S. Single crystal X-ray diffraction data was collected on an APEX II.

To^MFeBr (1). Tl[To^M] (0.200 g, 0.341 mmol) was dissolved in tetrahydrofuran (3 mL) and added to a suspension of FeBr₂ (0.081 g, 0.38 mmol) in tetrahydrofuran (10 mL). The cloudy white solution was stirred overnight and the solvent evaporated. The product was extracted using benzene and isolated *in vacuo* to afford To^MFeBr as a cream colored solid (0.113 g, 0.218 mmol, 63.9%). X-ray quality crystals were obtained from pentane at -40 °C. ¹H NMR (benzene-*d*₆, 600 MHz): δ 24.36 (s, 2 H, C₆H₅), 20.09 (s, 6 H, CNCMe₂CH₂O), 14.48 (s, 2 H, C₆H₅), 11.97 (s, 1 H, *p*-C₆H₅), -28.93 (s, 18 H, CNCMe₂CH₂O). ¹¹B NMR (benzene-*d*₆, 128 MHz): δ 74. IR (KBr, cm⁻¹): ν 2965 (m), 2929 (w), 2897 (w), 2870 (w), 1586 (s, ν_{CN}), 1496 (w), 1461 (m), 1434 (w), 1387 (m), 1368 (m), 1351 (m), 1270 (s), 1191 (s), 1161 (m), 1099 (w), 1017 (w), 982 (w), 956 (s). UV-vis (THF) λ_{max} = 312 (ε: 597 M⁻¹cm⁻¹). μ_{eff}(C₆D₆) = 5.1(2) μ_B as determined by the Evans method. Anal. Calcd. for C₂₁H₂₉BBrFeN₃O₃: C, 48.69; H, 5.64; N, 8.11 Found: C, 48.42; H, 5.68; N, 8.00. Mp.238-241.

(To^M)₂Fe (2). Tl[To^M] (0.200 g, 0.341 mmol) was dissolved in tetrahydrofuran (3 mL) and added to a suspension of FeBr₂ (0.037 g, 0.17 mmol) in tetrahydrofuran (10 mL). The cloudy white solution was stirred overnight and the solvent evaporated. The product was extracted using benzene and isolated *in vacuo* to afford To^MFeBr as a white colored solid (0.130 g, 0.158 mmol, 93.2%). X-ray quality crystals were obtained from pentane at -40 °C. ¹H NMR (benzene-*d*₆, 600 MHz): δ 20.16, 17.78, 16.59, 16.56, 8.05, 7.16, 7.05,

6.22, 5.16, 4.11, 2.96, 1.02, -0.04. ^{11}B NMR (benzene- d_6 , 128 MHz): δ -122. IR (KBr, cm^{-1}): ν 3069 (w), 3046 (w), 2966 (m), 2930 (m), 2881 (m), 1604 (m, ν_{CN}), 1548 (s, ν_{CN}), 1491 (w), 1463 (m), 1433 (w), 1370 (m), 1281 (m), 1250 (m), 1197 (m), 1151 (m), 1107 (w), 1027 (w), 1001 (m), 966 (m). UV-vis (Et_2O) $\lambda_{\text{max}} = 304$ (ϵ : $156 \text{ M}^{-1}\text{cm}^{-1}$), 581 (ϵ : $388 \text{ M}^{-1}\text{cm}^{-1}$), 617 (ϵ : $424 \text{ M}^{-1}\text{cm}^{-1}$), 697 (ϵ : $1078 \text{ M}^{-1}\text{cm}^{-1}$). $\mu_{\text{eff}}(\text{C}_6\text{D}_6) = 4.9(2) \mu_{\text{B}}$ as determined by the Evans method. Anal. Calcd. for $\text{C}_{42}\text{H}_{58}\text{B}_2\text{FeN}_6\text{O}_6$: C, 61.49; H, 7.13; N, 10.24 Found: C, 61.35; H, 7.15; N, 10.05. Mp. 217–219°C, dec.

To^MNiCl (3). TiTo^{M} (3.89 g, 6.64 mmol) dissolved in tetrahydrofuran (400 mL) was added to $\text{NiCl}_2 \cdot \text{DME}$ (1.45 g, 6.60 mmol) and the mixture was stirred for 18 hours at room temperature. Tetrahydrofuran was removed *in vacuo* and the product extracted with methylene chloride (200 mL). Evaporation of methylene chloride afforded $\text{To}^{\text{M}}\text{NiCl}$ as a pink solid (2.86 g, 6.00 mmol, 91%). Recrystallization from pentane gave analytically pure $\text{To}^{\text{M}}\text{NiCl}$. ^1H NMR (benzene- d_6 , 600 MHz): δ 16.94 (s, 6 H, $\text{CNCMe}_2\text{CH}_2\text{O}$), 7.59 and 7.49 (4 H, C_6H_5), 6.73 (s, 1 H, C_6H_5), -0.93 (s, 18 H, $\text{CNCMe}_2\text{CH}_2\text{O}$). ^{11}B NMR (benzene- d_6 , 128 MHz): δ -17. IR (KBr, cm^{-1}): ν 2966 (m), 2933 (m), 2899 (m), 2861 (m), 1600 (s, ν_{CN}), 1463 (m), 1388 (m), 1369 (m), 1353 (m), 1276 (m), 1195 (m), 1167 (m), 955 (m). UV-vis (THF): λ_{max} 310 nm (ϵ : $233 \text{ M}^{-1}\text{cm}^{-1}$), 478 nm (ϵ : $355 \text{ M}^{-1}\text{cm}^{-1}$), 817 nm (ϵ : $84 \text{ M}^{-1}\text{cm}^{-1}$), 925 nm (ϵ : $115 \text{ M}^{-1}\text{cm}^{-1}$). Evans method: $\mu_{\text{eff}}(\text{C}_6\text{D}_6) = 3.3(1) \mu_{\text{B}}$. Anal. Calcd. for $\text{C}_{23}\text{H}_{32}\text{BNiN}_3\text{O}_5$: C, 52.94; H, 6.14; N, 8.82 Found: C, 52.88; H, 6.11; N, 8.85. Mp. 267-267 °C.

To^MNiOAc (4). $\text{To}^{\text{M}}\text{NiCl}$ (0.051 g, 0.107 mmol) dissolved in tetrahydrofuran (5 mL) was added to NaOAc (0.009 g, 0.110 mmol) and the mixture was stirred for 18 hours at room temperature. The reaction mixture was filtered and the solvent evaporated to afford

To^MNiOAc as a yellow solid (0.050 g, 0.100 mmol, 93%). Recrystallization from pentane gave analytically pure To^MNiOAc. ¹H NMR (benzene-*d*₆, 600 MHz): δ 91.01 (s, 3 H, CoO₂CCH₃), 13.28 (s, 6 H, CNCMe₂CH₂O), 8.25 (s, 2 H, C₆H₅), 7.72 (s, 2 H, C₆H₅), 6.96 (s, 1 H, *p*-C₆H₅), and -1.51 (s, 18 H, CNCMe₂CH₂O). ¹¹B NMR (benzene-*d*₆, 128 MHz): δ -5.9. IR (KBr, cm⁻¹): ν 2964 (m), 2928 (m), 2891 (m), 2853 (m), 1602 (s, ν_{CN}), 1535 (m), 1463 (m), 1387 (m), 1366 (m), 1353 (m), 1274 (m), 1198 (m), 1163 (m), 959 (m). UV-vis (CH₂Cl₂): λ_{max} 422 nm (ε: 233 M⁻¹cm⁻¹), 704 nm (ε: 75 M⁻¹cm⁻¹), 874 nm (ε: 63 M⁻¹cm⁻¹). Evans method: μ_{eff} (C₆D₆) = 3.1(3) μ_B. Anal. Calcd. for C₂₃H₃₂BNiN₃O₅: C, 55.25; H, 6.45; N, 8.40 Found: C, 55.03; H, 6.62; N, 8.34. Mp. 181-183 °C.

To^MFeBn (5). KBn (0.030 mg, 0.23 mmol) was dissolved in THF (3 mL) and added dropwise to a THF solution (10 mL) of To^MFeBr (0.100 g, 0.19 mmol). The yellow solution was stirred for 30 min. at room temperature. The solvent was removed *in vacuo* and filtered with toluene to provide To^MFeBn as a yellow solid (0.090 g, 0.17 mmol, 89% yield). ¹H NMR (benzene-*d*₆, 600 MHz): δ 41.70 (s, 2 H), 41.02 (s, 2 H), 21.42 (s, 2 H), -17.44 (s, 1 H), 13.60 (s, 7 H, CNCMe₂CH₂O), -17.61 (s, 1 H), -56.35 (s, 18 H, CNCMe₂CH₂O), -63.08 (s, 1 H). ¹¹B NMR (benzene-*d*₆, 128 MHz): δ -225. IR (KBr, cm⁻¹): ν 3070 (w), 3048 (w), 2966 (m), 2928 (m), 2896 (w), 2871 (m), 1701 (m), 1586 (s, ν_{CN}), 1552 (m, ν_{CN}), 1493 (m), 1460 (m), 1433 (w), 1388 (m), 1367 (m), 1275 (m), 1198 (s), 1158 (m), 1027 (w), 1005 (m), 969 (s). UV-vis (THF) λ_{max} = 395 (ε: 1739 M⁻¹cm⁻¹). μ_{eff}(C₆D₆) = 5.4(2) μ_B as determined by the Evans method. Mp. 218-220 °C.

To^MFe{C(O)Bn}(CO)₂ (6). To^MFeBn (0.01 g, 0.02 mmol) was dissolved in benzene-*d*₆ (0.5 mL), the headspace was removed *in vacuo*, and then CO (1 atm) was introduced.

Benzene- d_6 was evaporated *in vacuo* to afford $\text{To}^{\text{M}}\text{Fe}\{\text{C}(\text{O})\text{Bn}\}(\text{CO})_2$ as a yellow solid (0.01 g, 0.02 mmol, 91% yield). X-ray quality crystals were obtained from pentane cooled to $-40\text{ }^\circ\text{C}$. ^1H NMR (benzene- d_6 , 600 MHz): δ 8.31, 8.30, 7.51, 7.33, 7.25, 7.22, 7.13, 7.11, 7.00, 4.48, 3.49, 3.41, 3.36, 1.15, 0.94, 0.87. ^{11}B NMR (benzene- d_6 , 128 MHz): δ -18 . IR (KBr, cm^{-1}): ν 3078 (w), 3041 (w), 3000 (m), 2969 (m), 2931 (m), 2881 (m), 2004 (s, ν_{CO}), 1935 (s, ν_{CO}), 1680 (m, $\nu_{\text{C=O}}$), 1662 (m, $\nu_{\text{C=O}}$), 1593 (s, ν_{CN}), 1553 (m, ν_{CN}), 1495 (w), 1460 (m), 1388 (w), 1369 (m), 1355 (m), 1284 (m), 1248 (m), 1199 (s), 1156 (m), 1070 (w), 1028 (w), 993 (m), 970 (s). UV-vis (THF) $\lambda_{\text{max}} = 776$ (ϵ : $92\text{ M}^{-1}\text{cm}^{-1}$).

References

- (1) M. Wagner, C. Limberg, and B. Zimer, *Eur. J. Inorg. Chem.*, **2008**, 3970-3976.
- (2) M. P. Mehn, K. Fujisawa, E. L. Hegg, and L. Que Jr., *J. Am. Chem. Soc.*, **2003**, *125*, 7828-7842.
- (3) M. Sallmann, B. Braun, and C. Limberg, *Chem. Commun.*, **2015**, *51*, 6787-6787.
- (4) T. Tietz, C. Limberg, R. Stöber, and B. Ziemer, *Chem. Eur. J.*, **2011**, *17*, 10010-10020.
- (5) E. Becker, S. Pavlik, and K. Kirchner, in *Advances in Organometallic Chemistry*, ed. Pedro J. Pérez, **2008**, pp. 155-197.
- (6) R. R. Reinig, D. Mukherjee, Z. B. Weinstein, W. Xie, T. Albright, B. Baird, T. S. Gray, A. Ellern, G. J. Miller, A. H. Winter, S. L. Bud'ko and A. D. Sadow, *Eur. J. Inorg. Chem.*, **2016**, 2486-2494.

- (7) R. R. Reinig, E. L. Fought, A. Ellern, T. L. Windus, and A. D. Sadow, *Chem. Comm.*, **2017**, *53*, 11020-11023.
- (8) F. A. Jové, C. Pariya, M. Scoble, G. P. A. Yap, and K. H. Theopold, *Chem. Eur. J.*, **2011**, *17*, 1310-1318.
- (9) I. B. Gorrell, G. Parkin, *Inorganic Chemistry*, **1990**, *29* (13), 2452-2456.
- (10) K. Wu, D. Mukherjee, A. Ellern, and A. D. Sadow, *New J. Chem.*, **2011**, *35*, 2169-2178.
- (11) H. R. Jiménez, J. Salgado, J. M. Moratal, and I. Morgenstern-Badarau, *Inorg. Chem.*, **1996**, *35* (10), 2737-3741.
- (12) S. Hikichi, K. Hanaue, T. Fujimura, H. Okuda, J. Nakazawa, Y. Ohzu, C. Kobayashi, and M. Akita, *Dalton Trans.*, **2013**, *42*, 3346-3356.
- (13) M. Akita, S. Nobuhiko, S. Hikichi, and Y. Moro-oka, *Chem. Commun.*, **1998**, 973-974.
- (14) F. A. Cotton, B. A. Frenz, and A. Shaver, *Inorganica Chimica Acta*, **1973**, *7* (1), 161-169.
- (15) O. Graziani, L. Toupet, M. Tilset, and J. Hamon, *Inorganica Chimica Acta*, **2007**, *360*, 3083-3090.

**CHAPTER 6: EFFECTS OF BIRADICAL DEUTERATION ON THE
PERFORMANCE OF DNP: TOWARDS BETTER PERFORMING POLARIZING
AGENTS**

Modified from *Physical Chemistry Chemical Physics* **2016**, 18, 65-69. [‡] Copyright ©

2016 Owner Societies.

Frédéric A. Perras, Regina R. Reinig, Igor I. Slowing, Aaron D. Sadow* and Marek Pruski*

Department of Chemistry, U.S. DOE Ames Laboratory, Iowa State University, Ames IA

50011-3111

Abstract

We study the effects of the deuteration of biradical polarizing agents on the efficiency of dynamic nuclear polarization (DNP) via the cross-effect. To this end, we synthesized a series of bTbK and TOTAPol biradicals with systematically increased deuterium substitution. The deuteration increases the radical's relaxation time, thus contributing to a higher saturation factor and larger DNP enhancement, and reduces the pool of protons within the so-called spin diffusion barrier. Notably, we report that full or partial deuteration leads to improved DNP enhancement factors in standard samples, but also slows down the build-up of hyperpolarization. Improvements in DNP enhancement factors of up to 70% and time savings of up to 38% are obtained upon full deuteration. It is foreseen that this approach may be applied to other DNP polarizing agents thus enabling further sensitivity improvements.

*Other Author's contributions

Frédéric A. Perras: Responsible for measuring the DNP enhancements for each of the biradicals studied.

Introduction

Dynamic nuclear polarization (DNP) is the most widely applicable hyperpolarization technique to enhance the sensitivity of nuclear magnetic resonance (NMR) experiments. In most DNP solid-state (SS)NMR applications, a sample is placed in contact with a source of unpaired electrons (usually an exogenous radical polarization agent) and is irradiated, at low temperature (<110 K), with high power microwaves near the electron Larmor frequency.¹ Electron polarization can then be transferred to the nuclei by a series of mechanisms, the cross-effect generally being the most efficient. The cross-effect is a process involving three coupled spins: two electrons and one nucleus.²⁻⁴

Large strides have been made in recent years towards the improvement of DNP for solids. Specifically, the development of stable high-power microwave sources (gyrotrons), and advances in probe technology for low temperature magic angle spinning (MAS) have enabled the application of DNP SSNMR to high magnetic field strengths (49.4 T).⁵⁻¹² Another important line of inquiry, of relevance here, concerns the development of polarizing agents capable of generating larger NMR enhancement factors (ϵ) and operating at higher temperatures. A notable breakthrough was reached by Hu *et al.* who demonstrated that the cross-effect condition was easier to satisfy by tethering two nitroxide radicals together in a single biradical molecule.^{13,14} Matsuki *et al.* then showed

that further improvement could be obtained by using a rigid linker, thus fixing the relative orientation of the two electrons' g tensors.^{15,16} Most recently, Zagdoun *et al.* demonstrated that even larger enhancements may be obtained by using a biradical with a high molecular weight.¹⁷⁻¹⁹ It was hypothesized that the lessened molecular motions in these compounds slow the electrons' relaxation, thus enabling a higher electron saturation factor, and a larger DNP enhancement.^{17,20} These breakthroughs may be combined, thus multiplying the improvements available from each approach, as is the case for the TEKPol biradical.²⁰ Note that such efforts may not be beneficial for DNP experiments performed at liquid helium temperatures, where the electron relaxation times can become much longer.²¹

Instead of hindering the molecular motions that are responsible for the electrons' relaxation, the size of the interactions contributing to relaxation may also be lessened. Given that dipolar coupling to protons, particularly those in rapidly rotating methyl groups, is a leading cause of electron relaxation under the DNP conditions, these interactions may be reduced by a factor of 6.5 by simply perdeuterating the polarizing agent.^{22,23} Perdeuteration also eliminates the ¹H spins that are nearest to the radical. These nuclei possess short relaxation times and thus become a polarization sink. Since spin diffusion from these nuclei to the bulk is also slowed by the presence of pseudocontact shifts, they are said to be within the so-called spin diffusion barrier.²⁴⁻²⁶ As a result of deuteration, less electron polarization will be spent repolarizing these rapidly relaxing ¹H spins. It is important to note that the use of deuterated solvent, or sample, is also known to lead to an increase in DNP enhancement factor.²⁷⁻²⁹

Results and Discussion

We have prepared four versions of the benchmark organic soluble polarizing agent bTbK¹⁵ using reagents at natural abundance (bTbK-d0), a deuterated pentaerythritol linker (bTbK-d8), deuterated nitroxides (bTbK-d32), as well as perdeuterated reagents (bTbK-d40), see Figure 1.

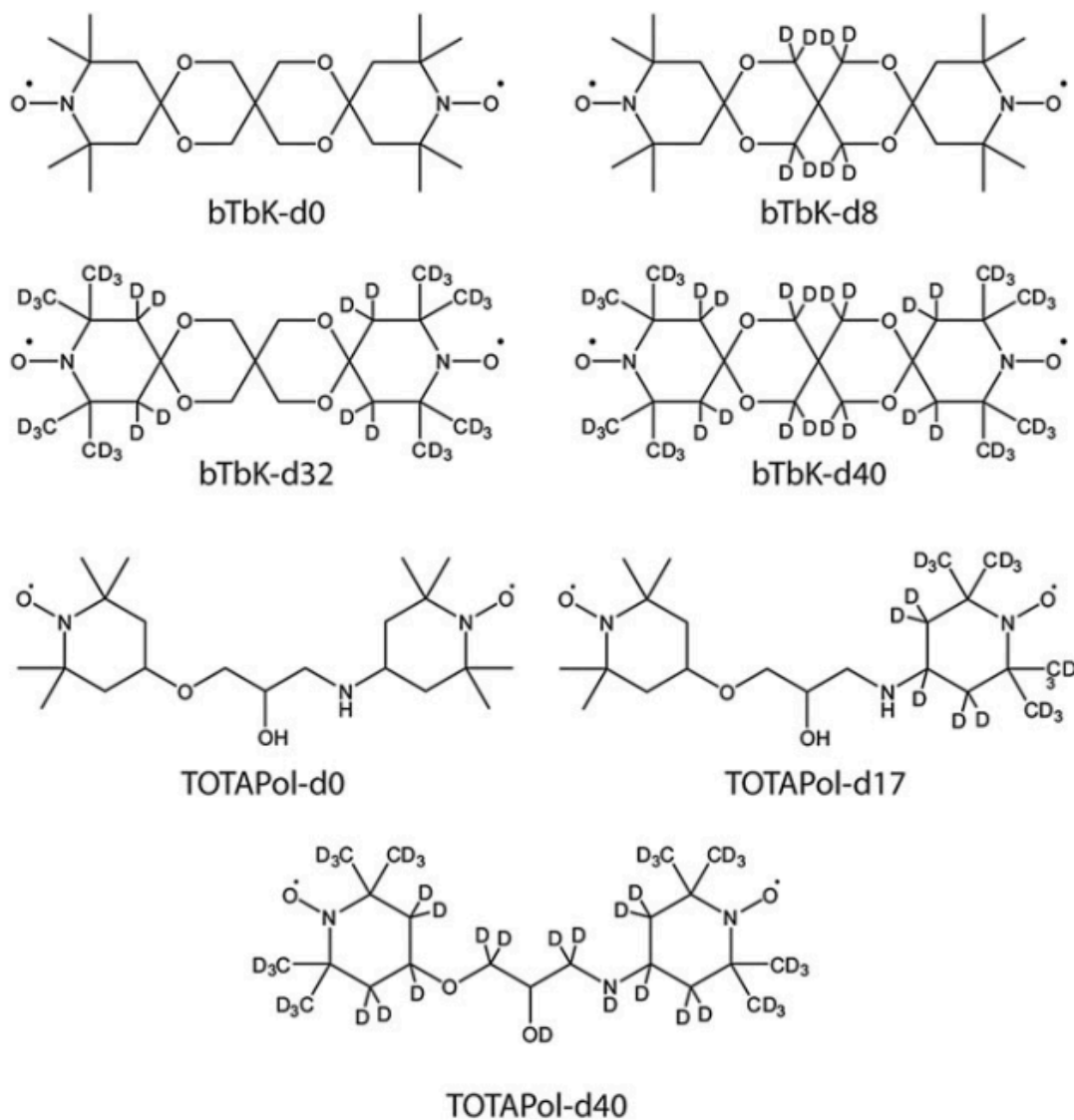


Figure 1. Biradical polarizing agents used in this study.

All isotopologues of bTbK were dissolved in a 96 : 4 tetrachloroethane (TCE) : methanol- d_4 (CD_3OD) solvent mixture to form a 16 mM solution, and 20 mL of this solution was pipetted into 3.2 mm sapphire rotors. The solutions were degassed by repeatedly inserting and ejecting the sample, as previously described,^{19,30} until the DNP enhancement reached a plateau. As shown in Figure 2 and Table 1, the maximum achievable DNP enhancements at 109 K, using a constant microwave power near 30 W, progressively increase with the level of deuteration, from 53 in the protonated bTbK to 91 in the fully perdeuterated version. This corresponds to a 70% increase in DNP enhancement by simply deuterating the polarizing agent.

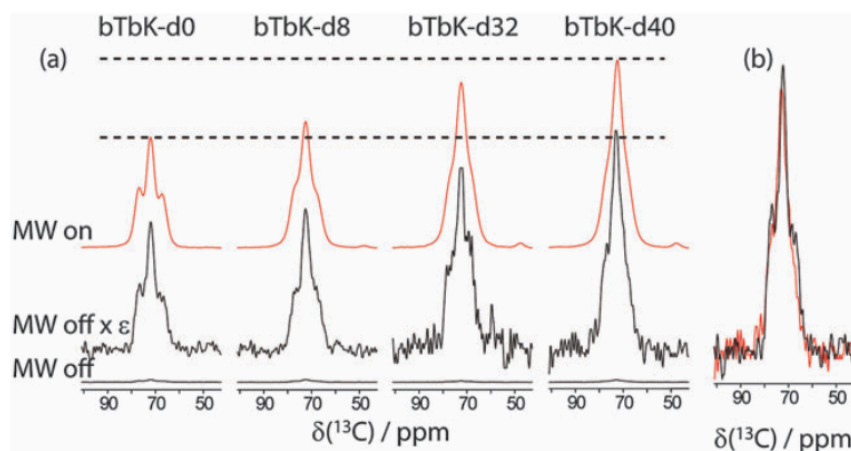


Figure 2. (a) DNP enhancement of 16 mM 96:4 TCE: CD_3OD solutions of bTbK- d_n radicals. The ‘MW off’ spectrum is shown on the bottom along with this same spectrum scaled by the enhancement factor listed in Table 1. The ‘MW on’ spectrum is shown on the top of the figure and dashed lines highlight the relative intensities of the spectra acquired using bTbK-d0 and bTbK-d40. A comparison of ‘MW off’ spectra of equal volume solutions of the non- (black) and perdeuterated (red) biradicals is shown in (b) highlighting the minute difference of depolarization for both radicals.

Table 1 DNP performance of various deuterated biradicals

Polarizing agent ^a	Solvent ^b	$\epsilon_{C,CP}$ ^c	T_{DNP} ^d /s	$e^2/T_{DNP}/s^{-1}$	T_{1e} ^e /μs
bTbK	96 : 4 TCE : CD ₃ OD	53	3.5	800	35
bTbK-d8		59	3.9	890	62
bTbK-d32		78	5.8	1050	87
bTbK-d40		91	7.8	1060	121
TOTAPol-d0	60 : 30 : 10	67	8.5	530	120
TOTAPol-d17	glycerol-d8 : D ₂ O : H ₂ O	85	11.0	660	131
TOTAPol-d40		83	23.5	290	153
TOTAPol-d0	60 : 40 glycerol : H ₂ O	39	6.1	250	124
TOTAPol-d17		51	8.6	300	128
TOTAPol-d40		59	10.1	344	153

^a Note that the true deuteration level of the TOTAPol biradicals in solution will differ as there are 2 exchangeable protons. ^b The concentrations used were of 16 mM and 10 mM for the bTbK and TOTAPol radicals, respectively. ^c To reduce unnecessary human errors, the enhancement factors were measured by integrating the ¹³C CPMAS signals with the microwaves turned on and off. The uncertainties of the enhancement factors are then on the order of ±5%. ^d The proton T_1 values were approximately equal to T_{DNP} . ^e The T_{1e} values were measured at 9 GHz.

Surprisingly, the deuteration of the linker, containing only 8 hydrogen atoms, was particularly important, leading to a comparable improvement in enhancement per atom than the deuteration of the TEMPO moiety (1.4–2.1% vs. 1.5–1.7% higher enhancement per hydrogen atom). As shown in Table 1, this increase in DNP enhancement is also accompanied by an increase in the DNP buildup time (T_{DNP}) from 3.5 s in the nonlabeled compound to 7.8 s in the perdeuterated compound. Because the signal to noise increases linearly as a function of the square of the number of scans, the relative sensitivity per unit of time (e^2/T_{DNP}) is still 30% higher when using the perdeuterated radical. ¹³C and ²⁹Si DNP-enhanced NMR experiments performed on 3-(3-phenylureido)propyl-functionalized mesoporous silica nanoparticles (PUP-MSNs) in fact demonstrate that larger enhancement factors can also be obtained on solid samples of interest, although in PUP-MSN the relative sensitivity per unit of time remains

approximately the same. As can be seen in Figure 2b and 3b, the extent of the signal loss, thought to be related to both blanking and MAS-induced depolarization, does not increase by a measurable amount for the deuterated biradicals.³¹

To confirm that this is indeed a generally applicable strategy for improving the effectiveness of other DNP polarization agents we have also synthesized and tested deuterated versions of the hydrophilic TOTAPol biradical.^{1b} Natural abundance (TOTAPol-d0), perdeuterated (TOTAPol-d40), as well as a biradical with deuterium labeling on only the amine-terminated nitroxide (TOTAPol-d17) were prepared, see Figure 1. These radicals were then dissolved in 60:30:10 glycerol-*d*₈:D₂O:H₂O (the so-called ‘DNP juice’) at a concentration of 10 mM as well as in a deuterium-free 60 : 40 mixture of glycerol and H₂O.³² The DNP enhancement measurements on these solutions were performed following the protocol described for the bTbK radicals.

As shown in Figure 3a and Table 1, the DNP enhancement increases upon deuteration of TOTAPol from 67 to 85 for the d0 and d17 derivatives, respectively, when using DNP juice. The fully deuterated biradicals, TOTAPol-d40, yields the same enhancement as partly-deuterated TOTAPol-d17, within uncertainty in the estimates (5%). Since the DNP build-up time increases from 8.5 to 11.0 and 23.5 s upon deuteration, the sensitivity per time is affected accordingly; the reason for this will be expanded later in the text. As was expected, however, the enhancement increases steadily from 39 to 51 and 59 for the d0, d17, and d40 derivatives, respectively, when using the fully protonated solvent. The enhancement factor for TOTAPol then increases by 50% upon perdeuteration and the sensitivity per unit of time increases by 38%.

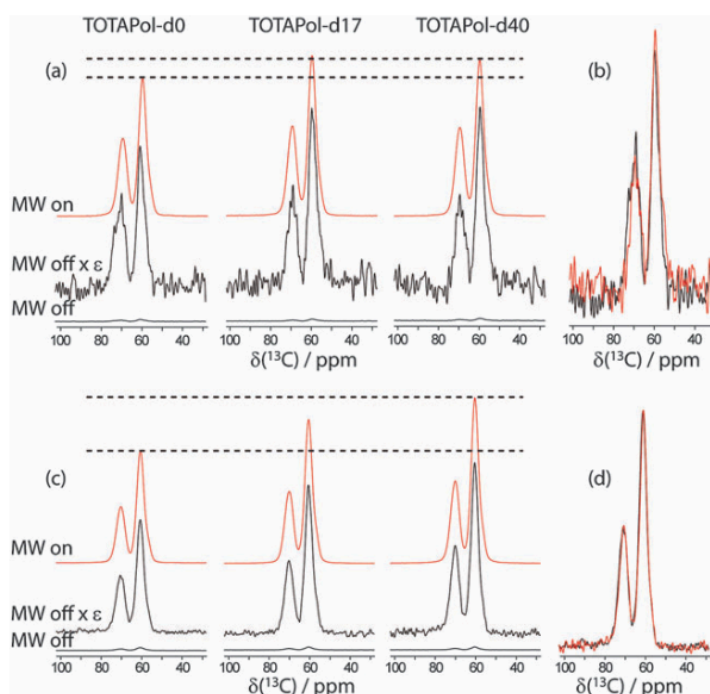


Figure 3. DNP enhancement of 10 mM 60:30:10 glycerol-d8: D₂O: H₂O (a) and 60:40 glycerol:H₂O (c) solutions of various TOTAPol radicals. The ‘MW off’ spectrum is shown on the bottom along with this same spectrum scaled by the enhancement factor listed in Table 1. The ‘MW on’ spectrum scaled by the enhancement factor listed in Table 1. The ‘MW on’ spectrum is shown on the top of the figure and dashed lines highlight the relative intensities of the spectra acquired using TOTAPol-d0 and TOTAPol-d40. A comparison of ‘MW off’ spectra of equal-volume solutions of the non- (black) and perdeuterated (red) biradicals is shown in (b and d) highlighting the minute difference of depolarization for both radicals.

Using a model spin system consisting of two electrons and one nucleus, Thurber and Tycko have shown theoretically that long T_{1e} values prevent the loss of magnetization between the MAS-induced frequency crossing events that lead to cross-effect polarization transfer.²⁶ The subsequent investigation of a series of functionalized nitroxide biradicals by Zagdoun *et al.*¹⁹ confirmed that electron relaxation properties were highly correlated with the DNP enhancements. Thus, both theoretical and experimental studies of the cross effect under MAS demonstrate that longer T_{1e} relaxation times of the electrons generally lead to higher enhancement factors;^{17,33,34} as was mentioned earlier,

this was the main motivation for the synthesis of the perdeuterated biradicals by the present authors. As can be seen from the plots shown in Figure 4, the T_{1e} and ϵ values indeed increase linearly as the biradical polarizing agents are progressively deuterated. The deuteration of the solvent, on the other hand, does not lead to an increase of T_{1e} .³⁵ We also note that, for bTbK, the observed increase in DNP enhancement is in agreement with the numerical calculations of Mance *et al.* for the increase in T_{1e} that we observed.³³ However, for TOTAPol, the modest increase in T_{1e} does not appear to fully explain the observed 50% increase in DNP enhancement factor.³³ This may be the result of the use of a much lower magnetic field for the EPR measurements (9 vs. 263 GHz). Another plausible mechanism contributing to an increase in ϵ values would be that, as mentioned earlier, there is a diminished loss of polarization within the so-called spin diffusion barrier when perdeuterated radicals are used.²⁴ The elimination of ^1H spins within the spin diffusion barrier also, unfortunately, has the effect of increasing the ^1H DNP build-up time due to the reduced efficiency of DNP-assisted spin diffusion (see Table 1).³⁶ Hovav and coworkers demonstrated that the rate at which hyperpolarization is transferred to the bulk nuclei depends on the strength of the dipolar coupling between the core nuclei and the electron and depends very little on the dipolar coupling between the bulk nuclei. The deuteration of the radicals then reduces the dipolar coupling between the core nuclei and the electrons and essentially slows down the spin diffusion of hyperpolarization to the bulk. In extreme cases when deuterated solvents are used this can lead to particularly long T_{DNP} values and a loss of sensitivity.

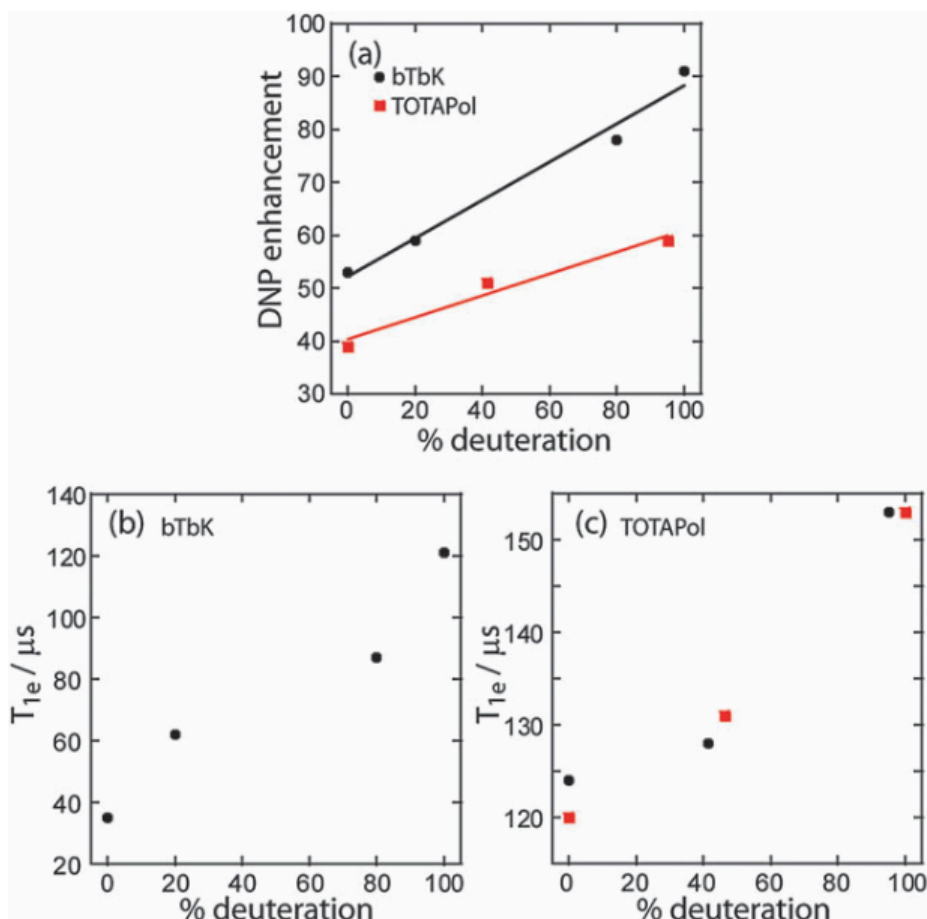


Figure 4. (a) The DNP enhancement factors of various bTbK and TOTAPol radicals are plotted as a function of the deuteration level of the molecule. The linear fits correspond to $e = 52.1 + 0.36 D$ for bTbK and $e = 40.2 + 0.21 D$, where D corresponds to the % deuteration of the molecule. The correlation between the deuteration levels of a biradical and the T_{1e} values are plotted in (b) and (c) for bTbK and TOTAPol, respectively. In (c) the black circles correspond to the use of fully protonated solvent whereas the red squares correspond to the data acquired when using a 90% deuterated solvent.

Conclusion

In conclusion, we have explored a simple approach for improving the DNP enhancement afforded by biradical polarizing agents. Indeed, using the bTbK and TOTAPol biradicals, an increase in DNP enhancement factors of up to 70%, and an

improved sensitivity per unit of time of up to 38% can be obtained by simply perdeuterating the polarizing agent. The deuteration of biradicals increases their T_{1e} values, thus improving the saturation factors upon continuous wave microwave irradiation, and consequently contributing to higher enhancement factors. The use of deuterated polarizing agents also reduces the number of ^1H spins within the spin diffusion barrier, which has the effects of reducing the polarization loss, but also leads to slower DNP-assisted spin diffusion and longer build-up times.³⁶ The perdeuteration, or partial deuteration, of the current state-of-the-art polarizing agents (AMUPol¹⁸ and TEKPol¹⁹), which can already yield enhancement factors over 200 at 105 K, is likely to yield the next generation of biradicals giving enhancement factors well over 300; we are actively exploring this avenue. The results of this study may also help in understanding the mechanisms of the cross effect in DNP of solids, particularly with respect to the polarization of remote spins.

Experimental Section

EPR Spectroscopy. The T_{1e} measurements were performed on an X-band Elexsys 580 FT- EPR spectrometer by using an inversion recovery method at a temperature of 100 K. The $\pi/2$ and π pulse durations used for the relaxation measurements were 16 ns and 32 ns, respectively. As had been previously described,³⁷ the relaxation process in these samples is not monoexponential and is better represented by a stretched exponential function:

$$I(t) = I_0 + I_1 e^{-\left(\frac{t}{T_{1e}^*}\right)^\beta}$$

In the expression above, I_0 is the initial intensity, I_1 is a proportionality constant, T_{1e}^* is a

decay constant, and β is the stretching parameter. The T_{1e} values mentioned in the text are in fact the mean T_{1e} values, which correspond to the first moment of the stretched exponential decay. These are calculated as:

$$\langle T_{1e} \rangle = \frac{T_{1e}^*}{\beta} \Gamma\left(\frac{1}{\beta}\right).$$

The T_{1e}^* and β fitting parameters are listed in Table 2 below.

Table 2. Fitting parameters for the T_{1e} measurements of the radicals described in the text.

polarizing agent	solvent	$T_{1e}^* / \mu\text{s}$	β	$\langle T_{1e} \rangle / \mu\text{s}$
bTbK	96:4	26.8	0.76	35
bTbK-d8	TCE : CD ₃ OD	40.8	0.66	62
bTbK-d32		46.8	0.54	87
bTbK-d40		69.4	0.57	121
TOTAPol-d0	60:30:10	71.8	0.60	120
TOTAPol-d17	glycerol-d8 : H ₂ O	90.7	0.69	131
TOTAPol-d40	D ₂ O : H ₂ O	111.3	0.73	153
TOTAPol-d0	60:40 glycerol : H ₂ O	76.50	0.62	124
TOTAPol-d17		86.5	0.67	128
TOTAPol-d40		103.3	0.68	153

General Procedure: All deuterated chemicals were purchased from C/D/N Isotopes Inc. with the exception of pentaerythritol-d12, which was purchased from Cambridge Isotope Laboratories, Inc. Acetonitrile was dried by heating to reflux over calcium hydride followed by distillation. All other chemicals were used as received from suppliers. ¹H and ¹³C{¹H} NMR spectra were collected on a Bruker AVII 600 spectrometer. Infrared spectra were measured on a Bruker Vertex 80 FTIR spectrometer. Accurate mass measurements were achieved using an Agilent QTOF 6540 mass spectrometer.

Experimental Procedures:

Preparation of the diamine 2,2,4,4,14,14,16,16-octamethyl-7,11,18,21-tetraoxa-3,15-diazatrispiro[5.2.2.5¹².2⁹.2⁶]henicosane followed a combination of the methods

previously reported by Matsuki and Griffin and later by Thankamony, Lafon, and Polshettiwar.^{38,39} Synthesis of the bTbK series followed the method reported by Matsuki and Griffin.³⁸ Synthesis of the epoxide precursor to TOTAPOL followed the procedure reported by Zhang whereas the synthesis of TOTAPOL from the epoxide followed the procedure reported by Song and Griffin.^{40,41} All of the syntheses were performed on a significantly smaller scale than what was previously reported. While the reactions proved to be scalable, the yields of the diamines were variable and this is attributed to the low scale of these reactions. The conditions for the deuterated syntheses were never optimized due to the cost of the isotopically labeled starting materials and the nature of the DNP experiments, which only require milligram quantities of the polarizing agent.

Synthesis of 2,2,4,4,14,14,16,16-octamethyl-7,11,18,21-tetraoxa-3,15-diazatrispiro-[5.2.2.5¹².2⁹.2⁶]hencosane.

Pentaerythritol (0.237 g, 1.60 mmol), 2,2,6,6-tetramethyl-4-piperidone (0.500 g, 3.22 mmol) and *p*-toluenesulfonic acid (0.730 g, 3.84 mmol) were mixed together in toluene (15 mL) and heated to reflux for 12 hours in a Dean-Stark trap. The solution was cooled to room temperature and then washed with 2.0 M NaOH solution (2 × 10 mL) and brine (1 × 10 mL). The organic layer was dried over Na₂SO₄ and filtered, and the solvent was removed under vacuum. Recrystallization from diethyl ether afforded white crystals (0.418 g, 1.02 mmol, 64%). The ¹H and ¹³C{¹H} NMR spectra match the reported literature values.³⁹ ¹H NMR (600 MHz, CDCl₃): δ 3.76 (s, 8 H), 1.68 (s, 8 H), 1.21 (s, 24 H). ¹³C{¹H} NMR (150 MHz, CDCl₃): δ 99.65, 63.56, 51.18, 43.08, 32.64, 32.24. IR (KBr, cm⁻¹): ν 3337, 2954, 2919, 2856, 1487, 1461, 1445, 1420, 1377, 1356, 1311, 1245,

1193, 1164, 1113, 1079, 1036, 1021, 979. Mp. 134-135 °C. ESI-MS: m/z Calcd. for $C_{23}H_{42}N_2O_4$ $[M+H]^+$: 411.32; Found: 411.3224.

Synthesis of 2,2,4,4,14,14,16,16-octamethyl-7,11,18,21-tetraoxa-3,15-diazatrispiro[5.2.2.5¹².2⁹.2⁶]henicosane-8,8,10,10,19,19,20,20-d8 (diamine-d8).

Pentaerythritol-d12 (0.237 g, 1.60 mmol), 2,2,6,6-tetramethyl-4-piperidone (0.500 g, 3.22 mmol) and *p*-toluenesulfonic acid (0.730 g, 3.84 mmol) were mixed together in toluene (15 mL) and heated to reflux for 12 hours in a Dean-Stark apparatus with azeotropic removal of water. The solution was cooled to room temperature and then washed with 2.0 M NaOH solution (2 × 10 mL) and brine (1 × 10 mL). The organic layer was dried over Na₂SO₄ and filtered, and the solvent was removed under vacuum. Recrystallization from diethyl ether afforded white crystals (0.105 g, 0.25 mmol, 16%). ¹H NMR (600 MHz, CDCl₃): δ 1.67 (s, 8 H), 1.21 (s, 24 H). ¹³C{¹H} NMR (150 MHz, CDCl₃): δ 99.56, 62.76 (br), 51.14, 43.11, 32.25, 31.95. IR (KBr, cm⁻¹): ν 3553, 3499, 3021, 2927, 2864, 2229, 2095, 1652, 1488, 1448, 1424, 1375, 1362, 1314, 1240, 1200, 1155, 1086, 1034, 1018, 1001, 955. Mp. 131-133 °C. ESI-MS: m/z Calcd. for $C_{23}H_{34}D_8N_2O_4$ $[M+H]^+$: 419.37; Found: 420.3782.

Synthesis of 2,2,4,4,14,14,16,16-octakis(methyl-d3)-7,11,18,21-tetraoxa-3,15-diazatrispiro[5.2.2.5¹².2⁹.2⁶]henicosane-1,1,5,5,13,13,17,17-d8 (diamine-d32).

Pentaerythritol (0.197 g, 1.45 mmol), 4-oxo-2,2,6,6-tetramethylpiperidine-d17 (0.500 g, 2.90 mmol) and *p*-toluenesulfonic acid (0.662 g, 3.48 mmol) were mixed together in toluene (15 mL) following the procedure described for the unlabeled or partially labeled diamine described above to afford 0.489 g (1.10 mmol, 76%) of diamine-d32. ¹H NMR (600 MHz, CDCl₃): δ 3.76 (s, 8 H). ¹³C{¹H} NMR (150 MHz, CDCl₃): δ 99.62, 63.57,

50.62, 43.00, 42.60, 32.62, 31.15 (br). IR (KBr, cm^{-1}): ν 3553, 3499, 2949, 2870, 2253, 2214, 2123, 2061, 1652, 1473, 1381, 1351, 1261, 1194, 1166, 1086, 1067, 907. Mp. 114-116 °C. ESI-MS: m/z Calcd. for $\text{C}_{23}\text{H}_{10}\text{D}_{32}\text{N}_2\text{O}_4$ $[\text{M}+\text{H}]^+$: 442.79; Found: 439.4974. The experimentally measured molecular mass distribution indicates there is a small amount of proton exchange occurring and a fraction of the diamine-d32 contains a decreased level of deuteration. This proton exchange occurs at the acidic methylene position of the TEMPO moiety via the enolization of 4-oxo-2,2,6,6-tetramethylpiperidine-d17, and this position provides a small signal in the ^1H NMR spectrum.

Synthesis of 2,2,4,4,14,14,16,16-octakis(methyl-d3)-7,11,18,21-tetraoxa-3,15-diazatrispiro[5.2.2.5¹².2⁹.2⁶]henicosane-1,1,5,5,8,8,10,10,13,13,17,17,19,19,20,20-d16 (diamine-d40).

Pentaerythritol-d12 (0.107 g, 0.72 mmol), 4-oxo-2,2,6,6-tetramethylpiperidine-d17 (0.250 g, 1.45 mmol), and *p*-toluenesulfonic acid (0.360 g, 1.89 mmol) were allowed to react following the procedure described above to provide tan colored crystals of diamine-d40 (0.127 g, 0.28 mmol, 39%). $^{13}\text{C}\{^1\text{H}\}$ NMR (150 MHz, CDCl_3): δ 99.48, 62.69 (br), 50.59, 42.98, 42.58 (br), 31.89, 31.16 (br). IR (KBr, cm^{-1}): ν 3551, 3497, 2961, 2927, 2850, 2214, 2096, 2070, 1654, 1472, 1454, 1349, 1316, 1286, 1263, 1238, 1196, 1175, 1154, 1103, 1071, 1040, 1024, 950. Mp. 112-115 °C. ESI-MS: m/z Calcd. for $\text{C}_{23}\text{H}_2\text{D}_{40}\text{N}_2\text{O}_4$ $[\text{M}+\text{H}]^+$: 450.84; Found: 448.5544. As observed for diamine-d32, the experimentally measured molecular mass indicates there is proton exchange occurring resulting in a decreased level of deuteration.

Synthesis of bTbK-d0.

A mixture of the diamine-d0 (0.107 g, 0.261 mmol), sodium tungstate dehydrate (0.010 g, 0.030 mmol), and methanol (10 mL) was cooled to 0 °C. Hydrogen peroxide solution (30% in water, 128 µL, 1.28 mmol) was added in a dropwise fashion. The reaction mixture was allowed to warm to room temperature and was stirred for 20 hours. Potassium carbonate (~0.3 g) was added, and the mixture was filtered. The filtrate was dried over magnesium sulfate, the volatiles were evaporated, and the product was purified by silica gel chromatography (hexanes:ethyl acetate = 4:5) to afford bTbK as an orange colored solid (0.076 g, 0.172 mmol, 66%). IR (KBr, cm^{-1}): ν 2976, 2935, 2864, 1471, 1453, 1377, 1344, 1243, 1191, 1167, 1110, 1085, 1024, 1008. Mp. 167-169 °C. ESI-MS: m/z Calcd. for $\text{C}_{23}\text{H}_{40}\text{N}_2\text{O}_6^{2+}$ $[\text{M}+\text{H}]^+$: 441.58; Found: 441.2953.

Synthesis of bTbK-d8.

The procedure described for bTbK-d0 was used with a mixture of the diamine-d8 (0.058 g, 0.138 mmol), sodium tungstate dihydrate (0.023 mg, 0.070 mmol), and methanol (0.9 mL) to afford bTbK-d8 as an orange colored solid (0.031 g, 0.068 mmol, 57%). IR (KBr, cm^{-1}): ν 3566, 3318, 2935, 2870, 2235, 2099, 1728, 1633, 1476, 1363, 1346, 1239, 1195, 1094, 1034, 999. Mp. 174-176 °C. ESI-MS: m/z Calcd. for $\text{C}_{23}\text{H}_{32}\text{D}_8\text{N}_2\text{O}_6^{2+}$ $[\text{M}+\text{H}]^+$: 449.63; Found: 450.3528.

Synthesis of bTbK-d32.

The procedure described for bTbK-d0 was used with a mixture of the diamine-d32 (0.100 g, 0.225 mmol), sodium tungstate dihydrate (0.009 mg, 0.027 mmol), and methanol (10 mL) to afford bTbK-d32 as an orange colored solid (0.039 g, 0.082 mmol, 36%). IR (KBr, cm^{-1}): ν 2982, 2933, 2865, 2228, 1462, 1386, 1355, 1252, 1199, 1181, 1168, 1067,

1054. Mp. 163-165 °C. ESI-MS: m/z Calcd. for $C_{23}H_8D_{32}N_2O_6^{2+}$ $[M+H]^+$: 473.78; Found: 469.4709.

Synthesis of bTbK-d40.

The procedure described for bTbK-d0 was used with a mixture of the diamine-d40 (0.050 g, 0.110 mmol), sodium tungstate dihydrate (0.018 mg, 0.055 mmol), and methanol (0.75 mL) to afford bTbK-d40 as an orange colored solid (0.031 g, 0.065 mmol, 59%). IR (KBr, cm^{-1}): ν 3564, 3488, 3317, 2963, 2935, 2241, 2228, 1743, 1353, 1329, 1299, 1261, 1236, 1186, 1139, 1094, 1076, 1042, 1021. Mp. 158-161 °C. ESI-MS: m/z Calcd. for $C_{23}D_{40}N_2O_6^{2+}$ $[M+H]^+$: 481.83; Found: 478.5280.

Synthesis of 4-(2,3-Epoxypropoxy)-2,2,6,6-tetramethyl-1-piperidin-1-oxyl (epoxide-d0).

Epichlorohydrin (2.25 mL, 28.7 mmol), 4-hydroxy-TEMPO (0.250 g, 1.45 mmol) and tetrabutylammonium hydrogen sulfate (0.029 g, 0.085 mmol) were added to a 90% w/w aqueous NaOH solution (0.232 g NaOH/0.263 mL H_2O). The mixture was stirred at 30 °C for 4 hours, at which point the mixture was poured into ice water and the product was extracted with diethyl ether (3×10 mL). The organic layer was washed with brine solution, dried over Na_2SO_4 , and concentrated in vacuo. The product was purified by silica gel chromatography (hexanes:ethyl acetate = 4:5) to obtain a red oil (0.119 g, 0.521 mmol, 36%). The infrared spectrum of the product matched the literature report.⁴⁰ IR (KBr, cm^{-1}): ν 2976, 2938, 2869, 1635, 1465, 1378, 1363, 1245, 1179, 1096. ESI-MS: m/z Calcd. for $C_{12}H_{22}NO_3^+$ $[M+H]^+$: 229.16; Found: 229.1676.

Synthesis of 1-(2,2,6,6-Tetramethyl-1-oxy-4-piperidinyl)oxy-3-(2,2,6,6-tetramethyl-1-oxy-4-piperidinyl)amino-propan-2-ol (TOTAPol-d0).

Under an inert atmosphere of nitrogen, the epoxide-d0 (0.100 g, 0.438 mmol) and LiClO₄ (0.047 g, 0.442 mmol) were dissolved in acetonitrile (0.8 mL). A solution of 4-amino-TEMPO (0.074 g, 0.432 mmol) dissolved in acetonitrile (0.2 mL) was added in a dropwise fashion. The solution was stirred overnight, concentrated, and purified by silica gel chromatography (hexanes:ethyl acetate = 4:5) to obtain a red solid (0.084 g, 0.210 mmol, 49%). The infrared spectrum of the product matched the literature report.⁴⁰ IR (KBr, cm⁻¹): ν 3424, 2976, 2938, 2867, 1635, 1466, 1364, 1244, 1179, 1112, 1089. ESI-MS: m/z Calcd. for C₂₁H₄₁N₃O₄²⁺ [M+H]⁺: 400.32; Found: 400.3169.

Synthesis of 4-(2,3-Epoxypropoxy)-2,2,6,6-tetramethyl-1-piperidin-1-oxyl (epoxide-d22).

Epichlorohydrin-d₅ (1.0 g, 10.3 mmol), 4-hydroxy-TEMPO-d₁₇ (0.122 g, 0.644 mmol) and tetrabutylammonium hydrogen sulfate (0.013 g, 0.038 mmol) were added to a 90% w/w aqueous NaOH solution (0.101 g NaOH/0.117 mL H₂O). The mixture was stirred at 30°C for 4 hours, at which point the mixture was poured into ice water and the product was extracted with diethyl ether (3 × 10 mL). The organic layer was washed with brine solution, dried over Na₂SO₄, and concentrated in vacuo. The product was purified by silica gel chromatography (hexanes:ethyl acetate = 4:5) to obtain a red oil (0.086 g, 0.343 mmol, 53%). ESI-MS: m/z Calcd. for C₁₂D₂₂NO₃[•] [M+H]⁺: 251.30; Found: 251.3057.

Synthesis of 1-(2,2,6,6-Tetramethyl-1-oxy-4-piperidinyl)oxy-3-(2,2,6,6-tetramethyl-1-oxy-4-piperidinyl)amino-propan-2-ol (TOTAPol-d17).

Under an inert atmosphere of nitrogen, the epoxide-d0 (0.045 g, 0.197 mmol) and LiClO₄ (0.021 g, 0.197 mmol) were dissolved in acetonitrile (0.3 mL). A solution of 4-amino-TEMPO-d₁₇ (0.038 g, 0.202 mmol) dissolved in acetonitrile (0.1 mL) was added in a dropwise fashion. The solution was stirred overnight, concentrated, and purified by silica gel chromatography (hexanes:ethyl acetate = 4:5) to obtain a red solid (0.018 g, 0.043 mmol, 22%). IR (KBr, cm⁻¹): ν 3435, 2975, 2922, 2851, 2235, 1632, 1467, 1383, 1367, 1261, 1178, 1099, 1054. ESI-MS: m/z Calcd. for C₂₁H₂₄D₁₇N₃O₄²⁺ [M+H]⁺: 417.42; Found: 417.4241.

Synthesis of 1-(2,2,6,6-Tetramethyl-1-oxy-4-piperidinyl)oxy-3-(2,2,6,6-tetramethyl-1-oxy-4-piperidinyl)amino-propan-2-ol (TOTAPol-d40).

Under an inert atmosphere of nitrogen, the epoxide-d22 (0.047 g, 0.188 mmol) and LiClO₄ (0.020 g, 0.188 mmol) were dissolved in acetonitrile (0.3 mL). A solution of 4-amino-TEMPO-d₁₇ (0.035 g, 0.186 mmol) dissolved in acetonitrile (0.5 mL) was added in a dropwise fashion. The solution was stirred overnight, concentrated, and purified by silica gel chromatography (hexanes:ethyl acetate = 4:5) to obtain a red solid (0.042 g, 0.095 mmol, 51%). IR (KBr, cm⁻¹): ν 3437, 2962, 2929, 2768, 2232, 2107, 1735, 1630, 1436, 1368, 1257, 1180, 1109, 1054. ESI-MS: m/z Calcd. for C₂₁HD₄₀N₃O₄²⁺ [M+H]⁺: 440.82; Found: 439.5619.

References

- (1) T. Maly, G. T. Debelouchina, V. S. Bajaj, K.-N. Hu, C.-G. Joo, M. L. Mak-Jurkauskas, J. R. Sirigiri, P. C. A. van der Wel, J. Herzfeld, R. J. Temkin and R. G. Griffin, *J. Chem. Phys.*, **2008**, *128*, 052211.
- (2) C. F. Hwang and D. A. Hill, *Phys. Rev. Lett.*, **1967**, *19*, 1011–1014.
- (3) Ü. Akbey, W. T. Franks, A. Linden, M. Orwick-Rydmark, S. Lange and H. Oschkinat, *Top. Curr. Chem.*, **2013**, *338*, 181–228.
- (4) K. Michaelis, T.-C. Ong, M. K. Kiesewetter, D. K. Frantz, J. J. Walish, E. Ravera, C. Luchinat, T. M. Swager and R. G. Griffin, *Isr. J. Chem.*, **2014**, *54*, 207–221.
- (5) L. R. Becerra, G. J. Gerfen, R. J. Temkin, D. J. Singel and R. G. Griffin, *Phys. Rev. Lett.*, **1993**, *71*, 3561–3564.
- (6) M. Rosay, J. C. Lansing, K. C. Haddad, W. W. Bachovchin, J. Herzfeld, R. J. Temkin and R. G. Griffin, *J. Am. Chem. Soc.*, **2003**, *125*, 13626–13627.
- (7) A. B. Barnes, M. L. Mak-Jurkauskas, Y. Matsuki, V. S. Bajaj, P. C. A. van der Wel, R. DeRocher, J. Bryant, J. R. Sirigiri, R. J. Temkin, J. Lugtenburg, J. Herzfeld and R. G. Griffin, *J. Magn. Reson.*, **2009**, *198*, 261–270.
- (8) M. Rosay, L. Tometich, S. Pawsey, R. Bader, R. Schauwecker, M. Blank, P. M. Borchard, S. R. Cauffman, K. L. Felch, R. T. Weber, R. J. Temkin, R. G. Griffin and W. E. Maas, *Phys. Chem. Chem. Phys.*, **2010**, *12*, 5850–5860.
- (9) Y. Matsuki, H. Takahashi, K. Ueda, T. Idehara, I. Ogawa, M. Toda, H. Akutsu and T. Fujiwara, *Phys. Chem. Chem. Phys.*, **2010**, *12*, 5799.
- (10) A. B. Barnes, E. Markhasin, E. Daviso, V. K. Michaelis, E. A. Nanni, S. K.

- Jawla, E. L. Mena, R. DeRocher, A. Thakkar, P. P. Woskov, J. Herzfeld, R. J. Temkin and R. G. Griffin, *J. Magn. Reson.*, **2012**, *224*, 1.
- (11) K. J. Pike, T. F. Kemp, H. Takahashi, R. Day, A. P. Howes, E. V. Kryukov, J. F. Macdonald, A. E. C. Collis, D. R. Bolton, R. J. Wylde, M. Orwick, K. Kosuga, A. J. Clark, T. Idehara, A. Watts, G. M. Smith, M. E. Newton, R. Dupree and M. E. Smith, *J. Magn. Reson.*, **2012**, *215*, 1.
- (12) T. Idehara, Y. Tatematsu, Y. Yamaguchi, E. M. Khutoryan, A. N. Kuleshov, K. Ueda, Y. Matsuki and T. Fujiwara, *J. Infrared, Millimeter, Terahertz Waves*, **2015**, *36*, 613.
- (13) K.-N. Hu, H.-h. Yu, T. M. Swager and R. G. Griffin, *J. Am. Chem. Soc.*, **2004**, *126*, 10844–10845.
- (14) C. Song, K.-N. Hu, C.-G. Joo, T. M. Swager and R. G. Griffin, *J. Am. Chem. Soc.*, **2006**, *128*, 11385–11390.
- (15) Y. Matsuki, T. Maly, O. Ouari, H. Karoui, F. Le Moigne, E. Rizzato, S. Lyubenova, J. Herzfeld, T. Prisner, P. Tordo and R. G. Griffin, *Angew. Chem., Int. Ed.*, **2009**, *48*, 4996–5000.
- (16) M. K. Kiesewetter, B. Corzilius, A. A. Smith, R. G. Griffin and T. M. Swager, *J. Am. Chem. Soc.*, **2012**, *134*, 4537–4540.
- (17) A. Zagdoun, G. Casano, O. Ouari, G. Lapadula, A. J. Rossini, M. Lelli, M. Baffert, D. Gajan, L. Veyre, W. E. Maas, M. Rosay, R. T. Weber, C. Thieuleux, C. Coperet, A. Lesage, P. Tordo and L. Emsley, *J. Am. Chem. Soc.*, **2012**, *134*, 2284–2291.
- (18) C. Sauvé, M. Rosay, G. Casano, F. Aussenac, R. T. Weber, O. Ouari and P.

- Tordo, *Angew. Chem., Int. Ed.*, **2013**, *52*, 10858–10861.
- (19) A. Zagdoun, G. Casano, O. Ouari, M. Schwarzwalder, A. J. Rossini, F. Aussenac, M. Yulikov, G. Jeschke, C. Cop´eret, A. Lesage, P. Tordo and L. Emsley, *J. Am. Chem. Soc.*, **2013**, *135*, 12790–12797
- (20) V. Kathirvelu, C. Smith, C. Parks, M. A. Mannan, Y. Miura, K. Takeshita, S. S. Eaton and G. R. Eaton, *Chem. Commun.*, **2009**, 454–456.
- (21) L. Lumata, M. E. Merritt, C. R. Malloy, A. D. Sherry and Z. Kovacs, *J. Phys. Chem. A*, **2012**, *116*, 5129–5138.
- (22) B. van den Brandt, E. I. Bunyatova, P. Hautle and J. A. Konter, *Nucl. Instrum. Methods Phys. Res., Sect. A*, **2004**, *526*, 53–55.
- (23) L. Lumata, A. K. Jindal, M. E. Merritt, C. R. Malloy, A. D. Sherry and Z. Kovacs, *J. Am. Chem. Soc.*, **2011**, *133*, 8673–8680.
- (24) C. Ramanathan, *Appl. Magn. Reson.*, **2008**, *34*, 409–421.
- (25) A. A. Smith, B. Corzilius, A. B. Barnes, T. Maly and R. G. Griffin, *J. Chem. Phys.*, **2012**, *136*, 015101.
- (26) K. R. Thurber and R. Tycko, *J. Chem. Phys.*, **2012**, *137*, 084508.
- (27) A. Kagawa, Y. Murokawa, K. Takeda and M. Kitagawa, *J. Magn. Reson.*, **2009**, *197*, 9–13.
- (28) ˘. Akbey, W. T. Franks, A. Linden, S. Lange, R. G. Griffin, B.- J. van Rossum and H. Oschkinat, *Angew. Chem., Int. Ed.*, **2010**, *49*, 7803–7806.
- (29) L. Lumata, M. E. Merritt and Z. Kovacs, *Phys. Chem. Chem. Phys.*, **2013**, *15*, 7032.
- (30) D. J. Kubicki, A. J. Rossini, A. Porea, A. Zagdoun, O. Ouari, P. Tordo, F.

- Engelke, A. Lesage and L. Emsley, *J. Am. Chem. Soc.*, **2014**, *136*, 15711–15718.
- (31) F. Mentink-Vigier, S. Paul, D. Lee, A. Feintuch, S. Hediger, S. Vega and G. De Paëpe, *Phys. Chem. Chem. Phys.*, **2015**, *17*, 21824–21836.
- (32) G. J. Gerfen, L. R. Becerra, D. A. Hall, R. G. Griffin, R. J. Temkin and D. J. Singel, *J. Chem. Phys.*, **1995**, *102*, 9494–9497.
- (33) D. Mance, P. Gast, M. Huber, M. Baldus and K. L. Ivanov, *J. Chem. Phys.*, **2015**, *142*, 234201.
- (34) F. Mentink-Vigier, U. Akbey, H. Oschkinat, S. Vega and A. Feintuch, *J. Magn. Reson.*, **2015**, *258*, 102.
- (35) A. Volkov, C. Codkter, T. Bund, H. Paulsen and G. Jeschke, *Biophys. J.*, **2009**, *96*, 1124.
- (36) Y. Hovav, A. Feintuch and S. Vega, *J. Chem. Phys.*, **2011**, *134*, 074509.
- (37) A. Zagdoun, G. Casano, O. Ouari, M. Schwarzwälder, A. J. Rossini, F. Aussenac, M. Yulikov, G. Jeschke, C. Copéret, A. Lesage, P. Tordo, and L. Emsley, *J. Am. Chem. Soc.*, **2013**, *135*, 12790.
- (38) Y. Matsuki, T. Maly, O. Ouari, H. Karoui, F. Le Moigne, E. Rizzato, S. Lyubenova, J. Herzfeld, T. Prisner, P. Tordo, and R. G. Griffin, *Angew. Chem. Int. Ed.*, **2009**, *48*, 4996-5000.
- (39) A. Thankamony, C. Lion, F. Pourpoint, B. Singh, A. Linde, D. Carnevale, G. Bodenhausen, H. Vezin, O. Lafon, and V. Polshettiwar, *Angew. Chem. Int. Ed.*, **2015**, *54*, 2190.
- (40) Z. P. Zhang, M. Z. Rong, and M. Q. Zhang, *Polymer*, **2014**, *55*, 3936-3943.

- (41) C. Song, K.-N. Hu, C.-G. Joo, T. Swager, and R. G. Griffin, *J. Am. Chem. Soc.*, **2006**, *128*, 11385.

CHAPTER 7: CONCLUSION

General Conclusions

Research based on the iron triad consisting of iron, cobalt, and nickel is of particular interest given these metal's usefulness in both commercial and biological applications. In addition, they have the benefit of being relatively abundant in the earth's crust compared with other metals. This thesis demonstrates To^M as a suitable ancillary ligand for isolation and study of iron, cobalt, and nickel complexes.

Synthesis of paramagnetic $To^M MX$ ($M, X = Fe, Br; Co, Cl; Ni, Cl$) was achieved by reaction of $TlTo^M$ with the corresponding metal halide. The synthesis of $To^M CoCl$ was the most challenging requiring careful control of reaction conditions to exclude formation of the side products $(To^M)_2Co$ and $HTo^M CoCl_2$. The synthesis of $To^M FeBr$ and $To^M NiCl$ was more straightforward and formed selectively under various reaction conditions. $(To^M)_2Ni$ was not identified even in attempted independent syntheses. On the other hand, $(To^M)_2Fe$ can be readily independently synthesized. Interestingly, $(To^M)_2Fe$ reacts with $FeBr_2$ to form $To^M FeBr$.

$To^M CoCl$ reacts with $NaOAc$ to provide $To^M CoOAc$. The catalytic activity of $To^M CoOAc$ in oxidation of hydrocarbons was studied using cyclohexane as the substrate and *m*CPBA as the oxidant and found to be selective towards cyclohexanol over the over-oxidized products of cyclohexane and ϵ -caprolactone.

Organometallic cobalt(II) and iron(II) complexes were found to be accessible through salt metathesis reactions $To^M CoCl$ and $To^M FeBr$ and alkyllithium or benzyl

potassium. Reactions involving Grignard reagents instead resulted in transmetalation. $\text{To}^{\text{M}}\text{CoR}$ ($\text{R} = \text{Me}, \text{Et}, \text{}^t\text{Bu}, \text{CH}_2\text{SiMe}_3, \text{Bn}, \text{and Ph}$) were found to react with CO followed by O_2 to form the corresponding carboxylate compounds. The oxidative carbonylation reactivity observed for these cobalt(II) alkyl complexes was found to be unique to cobalt, thus, similar reactivity was not observed for $\text{To}^{\text{M}}\text{FeBn}$. $\text{To}^{\text{M}}\text{FeBn}$ reacts with CO to form low-spin, diamagnetic $\text{To}^{\text{M}}\text{Fe}\{\text{C}(\text{O})\text{Bn}\}(\text{CO})_2$ as a yellow solid.

Lastly, deuterated biradicals were synthesized and found to result in a larger DNP enhancement as a result of the radical's longer relaxation time. Consequently, the results suggest that deuteration of biradicals is a promising approach to achieving larger DNP enhancements and thus increase the sensitivity of nuclear magnetic resonance (NMR) experiments.